Application of the relativistic random-phase and distorted wave impulse approximations to quasielastic proton-nucleus scattering

by

David Douglas van Niekerk

Dissertation presented for the degree of Doctor of Philosophy in Physics at Stellenbosch University

Department of Physics
Stellenbosch University
Private Bag X1, Matieland 7602, South Africa

Promoter: Dr B. I. S. van der Ventel

Co-promoter: Prof. G. C. Hillhouse

December 2010

Declaration

By submitting this dissertation electronically, I declare that the entirety of the work contained therein is my own, original work, and that I have not previously in its entirety or in part submitted it for obtaining any qualification.

December 2010

Abstract

In this dissertation a fully relativistic model for polarized inclusive quasielastic proton-nucleus scattering is developed. Using a standard relativistic impulse approximation (RIA) treatment of quasielastic scattering and a two-body SPVAT form of the current operator, it is shown how the behaviour of projectile and target can be decoupled. Subsequently, different models for projectile and target can be adopted and combined to examine a variety of relativistic effects.

The most simplistic model of the target is provided by a mean-field nuclear matter approximation to the relativistic meson-nucleon model, quantum hadrodynamics (QHD). Here relativistic effects manifest as an effective mass, which is lower than the free mass, of the constituent nucleons. This model is improved upon by including many-body correlations through medium-modification of meson propagators in the relativistic random-phase approximation (RPA).

Since it is generally accepted that the strong nuclear force and the extended range of the nuclear potential lead to distortion effects on the projectile and ejectile (seen as a modulation of the wave functions), our formalism is geared towards the use of relativistic distorted waves (RDWIA). The distorted waves are written as partial wave expansions and are solutions to the Dirac equation with potentials. The inclusion of distortions, however, greatly increases the computational burden and we show how a number of analytical and numerical techniques can be used to facilitate the process of calculation. It is also shown how the standard relativistic plane wave treatment (RPWIA) can, instead, be easily employed to obtain a baseline for determining the impact of distortions.

A calculation is performed for the reaction $^{40}\mathrm{Ca}(\vec{p},\vec{p}\,')$ at a beam energy of 500 MeV. Here it is found that the effect of correlations on the RPWIA calculation can be seen as a quenching of the cross section that is expected to become more pronounced at lower energies or for higher density targets. A RDWIA calculation shows additional reduction and if target correlations are included this effect is enhanced. To our knowledge this is the first calculation that attempts to include both these effects (RPA and RDWIA) in the context of quasielastic proton-nucleus scattering.

Samevatting

In hierdie proefskrif word 'n ten volle relatiwistiese model vir die berekening van inklusiewe kwasi-elastiese proton-kern verstrooiing daargestel. Deur gebruik te maak van 'n standaard relatiwistiese impulsbenadering (RIA) vir kwasi-elastiese verstrooiing asook 'n twee-deeltjie-SPVAT-vorm vir die stroom-operator, word daar gewys hoedat die gedrag van die projektiel en teiken ontkoppel kan word. Verskillende modelle kan dus vir die projektiel en teiken gebruik word om 'n verskeidenheid relatiwistiese effekte te bestudeer.

Die mees simplistiese model vir die teiken word verskaf deur 'n gemiddelde-veld kernmateriaal-benadering tot die relatiwistiese meson-nukleon-model, kwantum-hadrodinamika (QHD). In hierdie model manifesteer relatiwistiese effekte as 'n effektiewe massa, wat kleiner is as die vrye massa, van nukleone in die kern. Hierdie model word verbeter deur die inagneming van veeldeeltjie korrelasies deur medium-gewysigde meson-propagators in die relatiwistiese ewekansige-fase-benadering (RPA).

Aangesien dit algemeen aanvaar word dat die sterk-wisselwerking en die reikwydte van die kernpotensiaal aanleiding gee tot vervormingseffekte op die projektiel en ejektiel (gesien as die modulasie van golffunksies), is ons model optimaal geformuleer om gebruik te maak van relatiwistiese vervormde golwe (RDWIA). Die vervormde golwe word geskryf as parsiële-golf uitbreidings en dien as oplossings vir die Dirac-vergelyking met potensiale. Insluiting van vervormings vermeerder egter die berekeningslas geweldig en ons toon hoedat 'n aantal analitiese en numeriese tegnieke gebruik kan word om die proses te vergemaklik. Daar word ook aangetoon hoe die standaard- relatiwistiese-vlakgolf-benadering (RPWIA), in plaas van vevormde golwe, maklik gebruik kan word om 'n verwysingspunt vir die meting van die effek van vervormings te bepaal.

'n Berekening vir die reaksie $^{40}\mathrm{Ca}(\vec{p},\vec{p}\,')$ teen 'n projektiel-energie van 500 MeV word getoon. Hier word dit gevind dat die effek van korrelasies op die RPWIA-berekening gesien kan word as 'n verlaging van die kansvlak. Daar word verwag dat hierdie effek duideliker sal word by laer energieë en hoër kerndigthede. 'n RDWIA-berekening word getoon wat daarop dui dat addisionele verlaging in die kansvlak voorkom en indien korrelasies hier ingesluit word, word hierdie effek vergroot. Sover ons kennis strek, is hierdie die eerste berekening wat poog om beide hierdie effekte (RPA en RDWIA) in die konteks van kwasi-elastiese proton-kern verstrooiing in te sluit.

Acknowledgements

I would like to express my sincere gratitude to the following people whose contributions have made this work possible:

- Dr Brandon van der Ventel, my promoter and academic mentor, for patience and much guidance,
- Prof. C. J. Horowitz and Gang Shen at the Nuclear Theory Centre, Indiana University Bloomington,
- the Fulbright Program for the opportunity to visit Indiana University Bloomington,
- Profs F. G. Scholtz and K. K. Müller-Nedebock as well as the Institute of Theoretical Physics at Stellenbosch University for financial support,
- Hannes Kriel and Nortin Titus for many productive discussions and
- my family and friends for support and encouragement.

The financial assistance of the National Research Foundation (NRF) towards this research is hereby acknowledged. Opinions expressed and conclusions arrived at, are those of the author and are not necessarily to be attributed to the NRF.

Contents

List of Figures

List of Tables

Chapter 1

Introduction

With newly commissioned radioactive beam facilities such as RIKEN in Japan, GSI-FAIR in Germany and FRIB in the United States, where the goal is to extend the nuclear landscape up to the driplines, many changes are expected to be observed in the structure of exotic nuclei. However, understanding these changes is tied to our understanding of the reactions which will be used to probe them, such as elastic and inelastic proton-nucleus scattering.

In contrast to elastic collisions which are only sensitive to scalar and vector (isoscalar) pieces of the nucleon-nucleon (NN) scattering amplitudes, inelastic reactions are sensitive to all [1]. When results are compared to those of free NN scattering, inelastic scattering spin observables and cross sections can shed new light on nuclear structure since changes in scattering observables are likely due to changes in the collective response of the target or from a medium-modification of the free NN interaction [2]. Among these, quasifree elastic (or quasielastic) scattering, a single-step surface peaked reaction whereby a projectile interacts with a single bound nucleon in the target nucleus, is considered to be the dominant mechanism for nuclear excitation at moderate momentum transfers ($1 \leq q \leq 2$ fm^{-1}) and energies between 100 and 500 MeV [3]. Details of nuclear structure and excited states are unimportant for quasielastic scattering and compared to elastic scattering it offers a wider range of spin observables [4, 5].

Quasielastic scattering manifests itself in the cross section as a peak close to the excitation energy of free NN scattering with a width ascribable to the Fermi motion of the target nucleons. The centroid of the quasielastic peak also moves according to NN energy and momentum conservation and the peak position and width do not vary significantly with target mass confirming that the reaction mechanism is dominated by a single-step process [3, 6]. Multiple scattering events are expected to be less than 10% at the quasielastic peak. On the high-energy-loss side, however, between the peak and the appearance of resonances, this effect can play an important role affecting the strength observed in the cross section as well as the the spin observables [1, 6, 7].

It has been established that inclusive spectra for targets with mass numbers less than 60 and laboratory scattering angles less than 25° exhibit clear quasielastic peaks that become more pronounced with increasing beam energy and broadens and drops with an increase in the angle [8, 9]. Typical spectra are shown in Figs 1.1 and 1.2.

1.1 Relativistic Impulse Approximation

A central feature of many models of quasielastic and elastic scattering, whether it be lepton or hadron induced, is the impulse approximation (IA) where the in-medium amplitudes are replaced with free on-shell NN amplitudes. This approximation is increasingly accurate for beam energies much larger than the binding energies of the target nucleons. Historically the amplitudes for proton-nucleus scattering have been determined, amongst others, by means of fits to scattering data based on one-boson-exchange models, known as IA1 [10, 11] or IA2 [12–16], or multiple Yukawa-type meson-exchanges in the first-order Born approximation as is the case in the Love-Franey and Horowitz–Love-Franey models [17].

Traditionally nuclear physics calculations were done using the Schrödinger equation with central and spin-orbit potentials. These included calculations for elastic [18] and quasielastic proton scattering [6, 19] as well as quasielastic electron scattering [20], amongst others. However, since the pioneering work of Clark and collaborators [21–25] as well as that of McNeil, Shepard and Wallace [10, 11] it has been shown that a formalism based on the Dirac equation offers an attractive alternative to the traditional Schrödinger equation-based approach. This is referred to as the relativistic impulse approximation (RIA). Apart from its computational successes, the RIA also offers a number of conceptually attractive feautures. Due to their intrinsically relativistic nature RIA models can be made Lorentz covariant allowing for reliable extrapolation to extreme conditions of density, temperature or momentum transfer. In addition, the natural occurance of spin as well as the direct relation of the microscopic scalar and vector optical potentials (and therefore the Schrödinger equivalent central and spin-orbit potentials) to the Lorentz properties of the mesons mediating the strong nuclear force [26] make a relativistic formalism conceptually more satisfying. Virtual negative energy projectile states, only present in relativistic models, can contribute significantly to the proton-nucleus scattering process leading to good agreement between theoretical predictions of spin observables and experimental observations [18, 27, 28]. Even in the context of relativistic models, however, a too simplistic impulse approximation model can fail. For elastic scattering RIA calculations, based on IA1, provide an excellent description at 500 MeV and above [4, 11, 29] but appears to be inadequate at lower energies ($T_{\rm lab} < 400$ MeV). At these energies Pauli-blocking, binding energy, target nucleon correlations and an explicit non-local treatment of NN exchange, due to reduced NN relative momentum and increased effective interaction, can start to play an important role [17, 18, 29]. Ref. [26] predicts that this effect will become especially enhanced below 200 MeV and indeed below 100 MeV this is seen as a divergence of the scalar and vector optical potentials from the RIA which become much larger than the phenomenological ones [17]. At too high energies ($T_{\rm lab} \approx 1$ GeV) on the other hand meson production becomes possible, leading to the excitation of resonances in the target nucleons [6]. For nucleon-nucleus interaction the complexity of projectile-nucleon interaction could also lead to significant modification of the interaction in the nuclear medium [30].

1.2 Relativistic Plane Wave Impulse Approximation

The most simplistic RIA model makes use of plane waves for the projectile and treats the nuclear target as a free Fermi gas. Since no modification is made to the free NN interaction or the collective response of the target, no important deviations of spin observables are expected when compared

to free NN scattering [2].

A more realistic RPWIA model was developed by Horowitz and collaborators [1, 4, 29]. Here strong optical scalar and time-like vector components of mean-fields in the medium enhance the lower components of the Dirac nucleon wave functions of the projectile and target nucleons through effective masses (M^*) as derived in relativistic mean-field theory [31]. The use of M^* for the projectile, derived by means of an eikonal estimate for the average nuclear density, can be viewed as an effective means of incorporating distortions [32]. This model is expected to be a reasonably accurate approximation due to the fact that at the momentum transfers and excitation energies of interest, details of nuclear structure are unimportant and the properties of nuclear matter are probed [3]. It has been suggested that relativistic effects in elastic scattering are primarily due to the projectile, not the target but early calculations of quasielastic scattering observables have shown that both can contribute [1, 27].

M^* of the projectile has been calculated using a Woods-Saxon form of the scalar field [4], an optical potential arising from a self-consistent Hartree calculation [33] and a phenomenological Dirac optical potential formula [34]. In Ref. [33] it was found that spin observables can be very sensitive to the value of the effective mass.

Ref. [1] presents cross sections and spin observables for quasielastic proton scattering from ^{40}Ca, ^{208}Pb and ^{12}C at energies from 300 to 800 MeV and their accurate prediction of the analyzing power has been regarded as positive confirmation of relativistic effects. They find that the spin-orbit interaction is not affected by the effective mass and recommend that a full distorted wave (DWIA) calculation be done to estimate this effect. They also recommend a random-phase approximation (RPA) calculation to investigate particle-hole and particle-anitparticle correlations in the nuclear target. The change in the nucleon mass due to the presence of the scalar mean-field leads to a shift in the position of the quasielastic peak $\omega = \mathfrak{q}^2/2M^*$, as well as a broadening of the width $\Delta\omega = |\mathfrak{q}|k_F/M^*$ compared to the free Fermi gas results and the uncorrelated response of a target therefore accounts for most of the experimentally observed features [2, 32]. In Ref. [19] it was found that the magnitude of the analyzing power for ^{54}Fe$(\vec{p},\vec{p}\,')$ is accurately reproduced but the slope as a function of energy is not. Overall the RPWIA has had mixed success in describing complete sets of spin observables [3, 35].

1.3 Relativistic Distorted Wave Impulse Approximation

Distortions of the projectile wave function through the NN interaction could play a role in quasielastic nucleon-nucleus scattering due to the range of the nuclear potential. Strong projectile-nucleon interaction leads to distortions in incoming and outgoing wave functions and localizes the scattering in the region of the nuclear surface [30]. In the context of nonrelativistic models the PWIA reproduces fairly well the position and width of the quasielastic peaks but overestimates the overall magnitude. DWIA have been seen to provide the correct normalization [6]. Since spin observables are in effect ratios of polarized double differential cross sections they are, however, not expected to be significantly modified by distortions [32]. Nevertheless, as the incident energy is lowered and the target mass increased the effect of distortions is expected to become more pronounced [3]. Nonrelativistic calculations suggest that distortion effects can noticeably affect the shape and position of the quasielastic peak [36]. Although hard scattering may occur at the center of the quasielastic peak, distortions may play a role off the peak affecting spin observables

and changing the slope of a spin observable with respect to excitation energy [1] and full relativistic DWIA calculations could be used to investigate this.

In contrast to the RPWIA model of Horowitz and Murdock [4] where relativistic effects are included via the effective nucleon masses, RDWIA incorporates these effects by generating the projectile and ejectile wave functions as solutions of the Dirac equation with relativistic potentials. Ref. [4] presents one of the first calculations for quasielastic proton-nucleus scattering in ^{208}Pb using the RDWIA treated in an eikonal formalism. They find a consistent decrease in spin observables but due to a lack of data for different nuclei they are unable to separate effective mass effects from multiple scattering corrections which are expected to play a greater role in heavier nuclei.

1.4 Relativistic Mean-Field theory

The lowest-order relativistic response of the nucleus which takes the interaction among nucleons within the nucleus into account is the relativistic mean-field or Hartree approximation of the Walecka ($\sigma\omega$) model [31] (see Appendix B for a more complete discussion). The nucleus is modelled as a Fermi gas of nucleons where the interaction is mediated by the exchange of scalar and vector isoscalar mesons. Subsequent models have included effects from isovector mesons. This interaction is modelled in nuclear matter (and therefore is more applicable to heavier nuclei) which leads to constant potentials that only affect the mass of the nucleons. The response is therefore indentical to that of a free Fermi gas except for the effective mass which is generally smaller than the free nucleon mass. Using phenomenological coupling parameters this model reproduces the Fermi momentum and binding energy of nuclear matter quite well. It provides a relativistic saturation mechanism of nuclear matter and naturally predicts the spin-orbit interaction [31, 37]. It has also been shown that many phenomena in finite nuclei (ground state rms radii, charge densities, neutron densities, quadropole deformations, and spin-orbit splittings) can be explained as a relativistic effect in this framework [38–40].

In relativistic theories of nuclear structure polarization of the core consists of particle-hole excitations as well as nucleon-antinucleon excitations known as vacuum polarization [41]. Mean-field theory (MFT) calculations use parameters and meson fields which saturate nuclear matter neglecting vacuum effects in the response whereas relativistic Hartree approximation (RHA) calculations use smaller mean fields and include vacuum effects [42]. Coupling constants and the scalar mass are determined by fitting nuclear matter properties at saturation. This produces a dynamical shift in the nucleon mass brought about by the scalar field. In RHA the fitting is done by explicitly including the effect of the mass shift on the antinucleons in the Dirac sea. This results in different masses and couplings for MFT and RHA. The mass difference between RHA and MFT is important because it affects the position and width of the quasielastic peak [41]. The RHA response of the nucleus also contains a renormalized vacuum contribution. Vacuum effects are expected to become more important in heavier nuclei since the smaller effective mass of the nucleon leads to easier virtual excitation of nucleon-antinucleon pairs across the reduced mass gap [41, 42]. Even though RHA may be conceptually more complete, the role of vacuum polarization in effective hadronic field theories is currently being revisited [38, 39, 43–45]. Serot [40] feels that inclusion of vacuum effects is essential to maintain the completeness of the Dirac basis which plays a crucial role in field theory but the current description of the vacuum by summing simple baryon

loops is inadequate. Horowitz [46] has also suggested that some of the differences between MFT and RHA calculations may not be due to the inclusion of vacuum effects but rather the different effective masses and meson couplings.

1.5 Relativistic Random-Phase Approximation

The interaction of a nucleon with the many-body medium of the nucleus can excite particle-hole and particle-antiparticle pairs and in a dense system these excitations can propagate via the interactions of the constituents [47]. It is therefore important to study the effect of these correlations which are not explicitly included in the mean-field description since the dynamical effects thereof play a role in scattering [48]. The random-phase approximation (RPA) improves on the simple single particle response by including the effects of long-range coherence among particle-hole (and nucleon-antinucleon) excitations by iterating lowest-order (uncorrelated) polarizations to infinite order [49, 50].

The relatvistic RPA has been quite successful in the calculation of electromagnetic responses of nuclei [30, 41, 42, 48, 51–53] where it has consistently been shown to be in better agreement with experimental data than the lowest-order (Hartree) response (both in nuclear matter and finite nucleus calculations). In general it has been noted that RPA correlations shifts strength downwards due to the attractive particle-hole interactions [46].

Ref. [2] examines spin observables for quasielastic $(\vec{p},\vec{n})$ scattering in the RPWIA. Nuclear response functions are calculated in an isovector RPA to the Walecka model. They find better agreement with data for all spin observables calculated in relativistic RPA when compared to the Hartree approximation as well as Fermi gas (free mass) RPA. A calculation that includes both distortions as well as RPA is suggested for further improvement of theoretical predictions.

1.6 Our model

The model we present has been formulated to describe inclusive quasielastic nucleon-nucleus scattering and we apply it specifically to proton-induced reactions. As discussed above, the quasielastic nature of the process leads to the assumption that the many-body interaction can be modelled by a two-body current operator in the impulse approximation. We make use of the IA1 (SPVAT) representation of the NN amplitudes as presented in Ref. [14]. Despite not incorporating Pauli blocking and binding energy corrections, this parametrization is expected to be adequate for the relatively low density of the nuclear surface where quasielastic scattering is assumed to be localized [32]. This form of the amplitudes has been succesfully employed in impulse approximation descriptions of both elastic [18, 28] and quasielastic scattering [1, 4].

An important feature of the model is the separation of the projectile/ejectile and target behaviours into two separate and independent, so-called hadronic and polarization tensors. Different models for these two components can therefore be evaluated systematically so as to determine their individual effects on theoretical predictions. Since a central aim of this project is to study the effect of distortions due to the projectile and ejectile nucleons, both the RPWIA and RDWIA are used in turn to determine the projectile tensor. The distorted waves are written as partial wave expansions and are solutions to the Dirac equation with scalar, time-like vector and Coulomb potentials.

The response of the target is calculated in MFT where vacuum effects are neglected. We make use of the Walecka model (QHD-I) where ground state (bulk) properties are determined by isoscalar mesons [38]. The isovector ρ-meson enters only in isospin-asymmetric situations in a lowest-order MFT description [39] and we therefore perform our example calculation for ^{40}Ca. Subsequently the effects of residual isoscalar particle-hole correlations are investigated by means of RPA. Ref. [38] notes that a consistent treatment of excited states in the Hartree approximation constrains only isoscalar particle-hole correlations significantly. Isovector RPA (as discussed in Ref. [2]) applied to the present model is a subject of future work and we restrict our calculation to $(\vec{p}, \vec{p}\,')$ reactions where we can demonstrate the effect of isoscalar RPA. Parameters of the model (masses of mesons and coupling constants) are determined from the ground state properties of ^{40}Ca [33, 37].

1.7 Quasielastic proton-nucleus scattering studies at Stellenbosch University

The study of quasielastic proton-nucleus scattering has been a subject of intense investigation for a number of years by the Nuclear Theory Group at the Department of Physics at Stellenbosch University. Amongst other factors, it is due to the close proximity of the 200 MeV proton accelerator facility iThemba Labs (formerly known as the National Accelerator Center) to Stellenbosch University and the resulting possibility to measure spin observables such as A_y and D_{nn}. Within the relativistic framework the group investigated in a series of papers [33, 54–58] the following aspects of quasielastic proton-nucleus scattering:

- self-consistent calculation of the projectile and ejectile effective masses,
- sensitivities of complete sets spin observables to different five-term parametrizations of the NN interaction,
- new meson-exchange parameters for the relativistic NN amplitudes,
- medium modifications of the NN interaction and the effect on $(\vec{p}, \vec{p}\,')$ and $(\vec{p}, \vec{n})$ complete sets of spin observables and
- the replacement of the ambiguous five-term parametrization of the NN interaction matrix by a general Lorentz invariant representation.

One of the most important findings was that the well-known "quenching effect" of the analyzing power (first observed in Ref. [1]) is not so pronounced when the general Lorentz invariant representation is used for the NN scattering matrix [57]. All calculations above, however, were done using the plane wave approximation for the projectile and ejectile wave functions. This dissertation (together with the PhD project of N. P. Titus in the Nuclear Theory Group) presents the first steps in doing away with this assumption by explicitly including nuclear distortion effects. The work of N. P. Titus focusses on the eikonal approximation, whereas here we use the full partial wave expansion of the wave functions and include RPA corrections. The increase in numerical burden cannot be overstated. Indeed, this has hampered progress in the relativistic distorted wave formalism for many years for quasielastic proton nucleus scattering. Advances in computing power has, however, now made the project feasible and for the numerical calculations we made use of the powerful fitting and interpolation capabilities of the Matlab computing package as well as cluster

computing using the Fortran programming language. This has made it possible to, for the first time (together with the work of N. P. Titus), produce results for the relativistic distorted wave formalism for quasielastic proton-nucleus scattering.

1.8 Organization of dissertation

Chapter 2 presents the theoretical framework of our model. Firstly, a general derivation of the cross section is provided. This is followed by a short discussion on the amplitudes. Section 2.5 presents the formalism for the hadronic tensor both in terms of plane waves and distorted waves. Section 2.6 shows the derivation of the lowest-order polarization tensor as well as the RPA correction.

In Chapter 3 the numerical implementation and certain related features of our model are discussed. Subsequently, results are presented for plane wave and distorted wave calculations with and without RPA corrections.

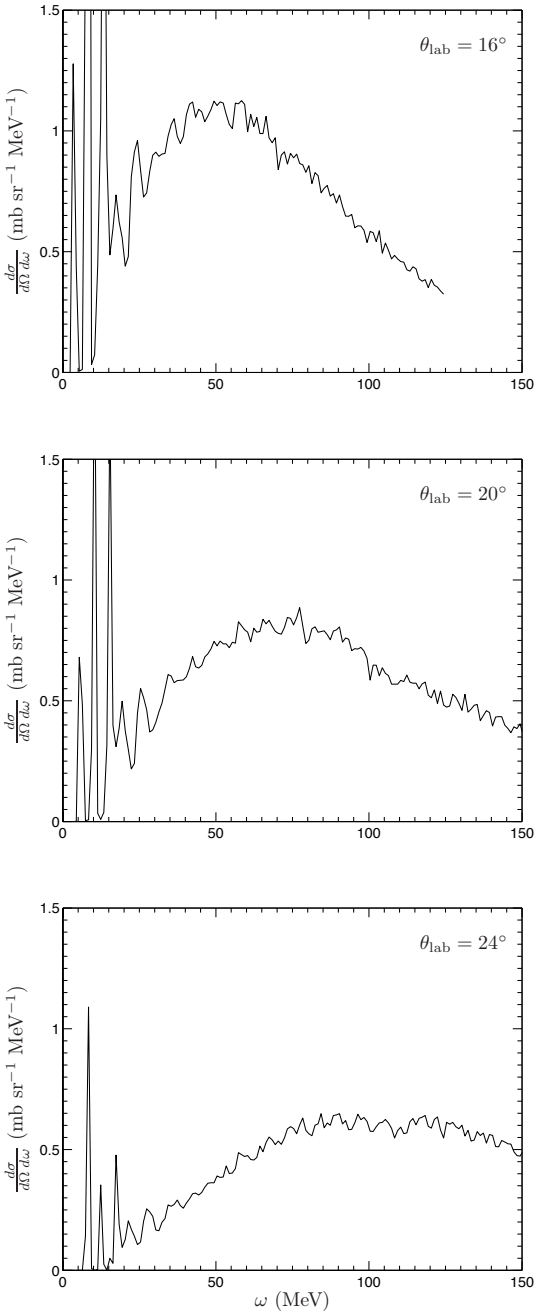

Figure 1.1: Double differential cross sections for inclusive ^{12}C(p, p') scattering as a function of energy transferred to the nucleus for incident proton energy ($T_{\rm lab}$) of 400 MeV. Laboratory scattering angles are indicated on figures. Data are from Ref. [59].

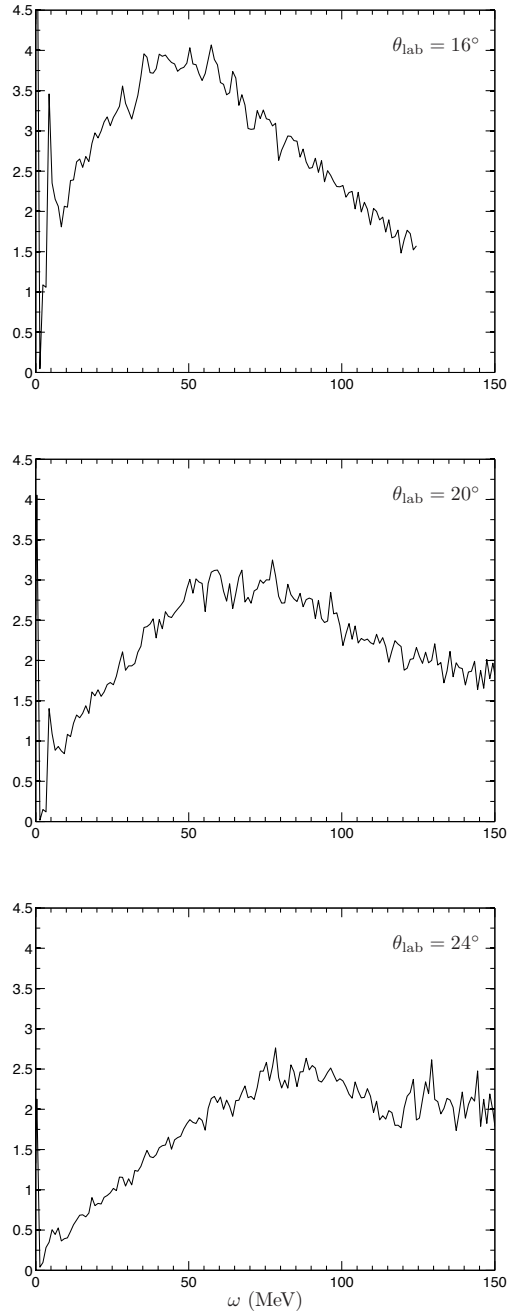

Figure 1.2: Double differential cross sections for inclusive ^{208}Pb(p, p') scattering as a function of energy transferred to the nucleus for incident proton energy ($T_{\rm lab}$) of 400 MeV. Laboratory scattering angles are indicated on figures. Data are from Ref. [59].

Chapter 2

Formalism

2.1 Introduction

Consider the inclusive quasielastic reaction between an incident proton and a nucleus X resulting in a recoil nucleus X$'$ and a nucleon:

$$\text{proton} + \text{X} \rightarrow \text{nucleon} + \text{X}'.$$

This reaction can be represented by the diagram in Fig. 2.1.

The differential cross section for ths reaction is [60]

$$d\sigma = \frac{1}{|\mathbf{v}_1 - \mathbf{v}_2|} \left(\frac{M^2}{E(\mathbf{k})E(\mathbf{k}')} \right) (2\pi)^4 \delta(k + K - k' - K') \frac{d^3k'}{(2\pi)^3} \frac{d^3K'}{(2\pi)^3} |\mathcal{M}|^2, \tag{2.1}$$

where $\mathbf{v}_1$ and $\mathbf{v}_2$ are the velocities of the projectile and target nucleus respectively, k and k' are the asymptotic four-momenta of the projectile and ejectile nucleons, K and K' are the asymptotic four-momenta of the target and residual nucleus, M the free nucleon mass and $\mathcal{M}$ the transiton matrix element.

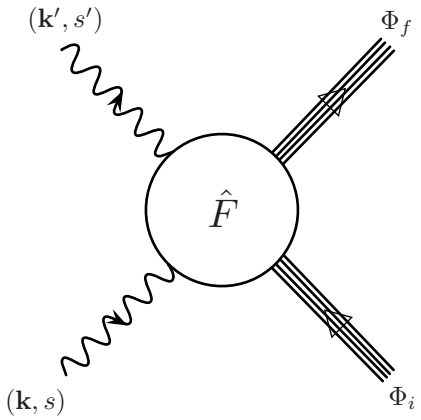

Figure 2.1: Diagrammatic representation of quasielastic nucleon-nucleus scattering. $(\mathbf{k}, s)$ $[(\mathbf{k}', s')]$ represents the asymptotic momenta and spin projection of the initial [final] nucleon, Φ_i (Φ_f) the initial (final) states of the nucleus and $\hat{F}$ the NN interaction matrix.

2.2 Kinematics

The integration over $\mathbf{K}'$ can be performed if the delta function is written as

$$(2\pi)^4\delta(k+K-k'-K') = (2\pi)^3\delta(\mathbf{k}+\mathbf{K}-\mathbf{k}'-\mathbf{K}')(2\pi)\delta\left(E(\mathbf{k})+E(\mathbf{K})-E(\mathbf{k}')-E(\mathbf{K}')\right). \quad (2.2)$$

Using the fact that

$$d^3k' = \mathbf{k}'^2\, d|\mathbf{k}'|\, d\Omega_{k'} = |\mathbf{k}'|\, E(\mathbf{k}')\, dE(\mathbf{k}')\, d\Omega_{k'}, \quad (2.3)$$

Eq. (2.1) is written as

$$d\sigma = \frac{M^2}{(2\pi)^2|\mathbf{v}_1-\mathbf{v}_2|\, E(\mathbf{k})}\delta\left(\omega+E(\mathbf{K})-E(\mathbf{K}')\right)\, |\mathbf{k}'|\, |\mathcal{M}|^2\, dE(\mathbf{k}')\, d\Omega_{k'}, \quad (2.4)$$

where the energy transfer is defined as

$$\omega = E(\mathbf{k}) - E(\mathbf{k}'). \quad (2.5)$$

Eq. (2.1) is valid in any reference frame. For the present calculation, however, we make use of the center-of-mass frame since this is the traditional reference frame used in distorted wave calculations. The proton-nucleus center-of-mass frame is defined by

$$\mathbf{k}+\mathbf{K} = \mathbf{k}'+\mathbf{K}'. \quad (2.6)$$

This means that the four-momenta are given by

$$k = (E(\mathbf{k}), \mathbf{k}), \quad (2.7)$$

$$K = (E(\mathbf{K}), -\mathbf{k}), \quad (2.8)$$

$$k' = (E(\mathbf{k}'), \mathbf{k}'), \quad (2.9)$$

$$K' = (E(\mathbf{K}'), -\mathbf{k}'). \quad (2.10)$$

The velocity-dependent factor can be eliminated using [61]

$$\begin{aligned}|\mathbf{v}_1-\mathbf{v}_2|\, E(\mathbf{k})\, E(\mathbf{K}) &= \left[(k\cdot K)^2 - M^2M_{\text{target}}^2\right]^{1/2} \\ &= |\mathbf{k}|\left[E(\mathbf{k})+E(\mathbf{K})\right], \end{aligned} \quad (2.11)$$

where use was made of Eqs (2.7) to (2.10). The differential cross section can now be written as

$$\frac{d\sigma}{dE'\, d\Omega'} = \mathcal{K}\,\delta\left(\omega+E(\mathbf{K})-E(\mathbf{K}')\right)\, |\mathcal{M}|^2, \quad (2.12)$$

where

$$\mathcal{K} = \frac{M^2|\mathbf{k}'|E(\mathbf{K})}{4\pi^2|\mathbf{k}|\left[E(\mathbf{k})+E(\mathbf{K})\right]}$$

$$= \frac{M^2|\mathbf{k}'|\left(\mathbf{k}^2+M^2_{\text{target}}\right)^{1/2}}{4\pi^2|\mathbf{k}|\left[\left(\mathbf{k}^2+M^2\right)^{1/2}+\left(\mathbf{k}^2+M^2_{\text{target}}\right)^{1/2}\right]}. \tag{2.13}$$

Since we are interested in inclusive scattering, the cross section has to be summed over all final nuclear states. This results in the following expression for the polarized double differential cross section:

$$\frac{d\sigma}{dE'\,d\Omega'} = \mathcal{K}\sum_n |\mathcal{M}|^2\delta\left(\omega-(E_n-E_0)\right)$$

$$= -\frac{1}{\pi}\mathcal{K}\,\text{Im}\left\{\sum_n |\mathcal{M}|^2\frac{1}{\omega-(E_n-E_0)+i\epsilon}\right\}, \tag{2.14}$$

where we have used the Cauchy Principal Value theorem to write

$$\delta\left(\omega-(E_n-E_0)\right) = -\frac{1}{\pi}\text{Im}\left\{\frac{1}{\omega-(E_n-E_0)+i\epsilon}\right\}. \tag{2.15}$$

Clearly Eq. (2.13) and therefore Eq. (2.14) requires explicit knowledge of the projectile's momentum $\mathbf{k}$. This is provided by choosing the incident momentum along the $\hat{z}$-axis and determining its magnitude from

$$|\mathbf{k}| = \sqrt{E(\mathbf{k})^2-M^2}, \tag{2.16}$$

where the projectile energy is determined using [29]

$$E(\mathbf{k}) = \frac{M^2+M_{\text{target}}(M+T_{\text{lab}})}{\left[(M+M_{\text{target}})^2+2M_{\text{target}}T_{\text{lab}}\right]^{1/2}}. \tag{2.17}$$

For further calculation the ejectile momentum $\mathbf{k}'$ and the ejectile energy are also required. The latter is calculated using Eq. (2.5) and the former by specifying the vector components in terms of

$$|\mathbf{k}'| = \sqrt{E(\mathbf{k}')^2-M^2} \tag{2.18}$$

and the center-of-mass scattering angle θ_{cm} (see Fig. 2.2) as

$$k'_x = |\mathbf{k}'|\sin\theta_{\text{cm}}, \tag{2.19}$$

$$k'_y = 0, \tag{2.20}$$

$$k'_z = |\mathbf{k}'|\cos\theta_{\text{cm}}. \tag{2.21}$$

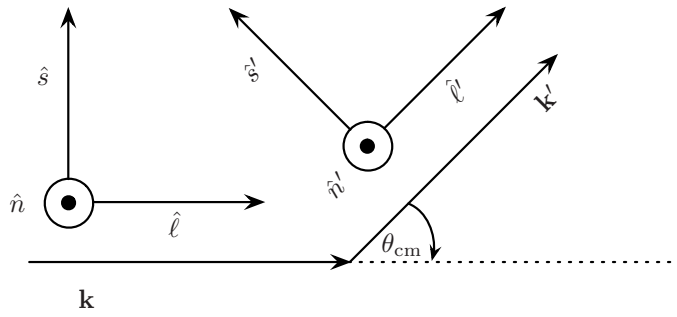

Figure 2.2: Centre-of-mass kinematics for the scattering process.

2.3 Transition matrix element

As is generally the case, the dynamics of the scattering process is contained in the transition matrix element. For our model we adopt the notation used in Ref. [62] and write it as

$$\mathcal{M} = \int d^4x\, d^4x' \prod_{m=1}^{A} d^4y_m \prod_{n=1}^{A} d^4y'_n \left[\bar{\psi}^{(-)}(x', \mathbf{k}', \hat{i}', s') \otimes \bar{\Phi}_f(y'_1, ...y'_n, ...y'_A)\right]$$
$$\times \hat{F}_{\rm many}(x, x', \{y\}, \{y'\}) \left[\psi^{(+)}(x, \mathbf{k}, \hat{i}, s) \otimes \Phi_i(y_1, ...y_m, ...y_A)\right], \tag{2.22}$$

where

- $\otimes$ denotes the Kronecker product,
- $\psi^{(+)}(x, \mathbf{k}, \hat{i}, s)$ is the relativistic distorted wave function of the projectile with outgoing boundary conditions [indicated by superscript $(+)$], asymptotic three-momentum $\mathbf{k}$ in the proton-nucleus centre-of-mass system, spin projection s along an arbitrary quantization axis $\hat{i}$ in the rest frame of the projectile,
- $\psi^{(-)}(x', \mathbf{k}', \hat{i}', s')$ is the relativistic distorted wave function of the ejectile with incoming boundary conditions [indicated by superscript $(-)$], asymptotic three-momentum $\mathbf{k}'$ in the proton-nucleus centre-of-mass system, spin projection s' along an arbitrary quantization axis $\hat{i}'$ in the rest frame of the ejectile,
- $\Phi_i(y_1, ...y_i, ...y_A)$ is the many-body ground state of the target nucleus which depends on all A constituent nucleons,
- $\Phi_f(y'_1, ...y'_j, ...y'_A)$ is the many-body ground state of the recoil nucleus which depends on all A constituent nucleons,
- $\hat{F}_{\rm many}$ is the many-body operator that connects the inital and final states.

Since we model the scattering as a quasielastic process where the interaction takes place between the projectile and a single nucleon inside the target nucleus we approximate the many-body operator as

$$\hat{F}_{\rm many}(x, x', \{y\}, \{y'\}) = \sum_{i=1}^{A} \langle x' y'_i | \hat{F} | x y_i \rangle \prod_{j=1, i\neq j}^{A} \delta(y'_j - y_j), \tag{2.23}$$

where $\hat{F}$ is a two-body operator. With this approximation the transition matrix element becomes

$$\mathcal{M} = \sum_{i=1}^{A} \int d^4x\, d^4x'\, d^4y_i\, d^4y_i' \prod_{j=1, i\neq j}^{A} d^4y_j \left[\bar{\psi}^{(-)}(x', \mathbf{k}', \hat{i}', s') \otimes \bar{\Phi}_f(y_1, ...y_i', ...y_A)\right]$$

$$\times \langle x' y_i' | \hat{F} | x y_i \rangle \left[\psi^{(+)}(x, \mathbf{k}, \hat{i}, s) \otimes \Phi_i(y_1, ...y_i, ...y_A)\right], \tag{2.24}$$

where use was made of the fact that

$$\int \sum_{i}^{A} \prod_{m}^{A} d^4y_m \prod_{n}^{A} d^4y_n' \prod_{j\neq i}^{A} \delta(y_j' - y_j) \equiv \int \sum_{i}^{A} d^4y_i\, d^4y_i' \prod_{j\neq i}^{A} d^4y_j. \tag{2.25}$$

If we insert a complete set of eigenstates defined by

$$1 = \int \frac{d^4p}{(2\pi)^4} |p\rangle\langle p|, \tag{2.26}$$

we obtain

$$\mathcal{M} = \sum_{i=1}^{A} \int d^4x\, d^4x'\, d^4y_i\, d^4y_i' \prod_{j=1, j\neq i}^{A} d^4y_j \, \frac{d^4p}{(2\pi)^4} \frac{d^4p'}{(2\pi)^4} \frac{d^4p_i}{(2\pi)^4} \frac{d^4p_i'}{(2\pi)^4}$$

$$\times e^{ip\cdot x} e^{-ip'\cdot x'} e^{ip_i\cdot y_i} e^{-ip_i'\cdot y_i'} \left[\bar{\psi}^{(-)}(x', \mathbf{k}', \hat{i}', s') \otimes \bar{\Phi}_f(y_1, ...y_i', ...y_A)\right]$$

$$\times \langle p' p_i' | \hat{F} | p\, p_i \rangle \left[\psi^{(+)}(x, \mathbf{k}, \hat{i}, s) \otimes \Phi_i(y_1, ...y_i, ...y_A)\right], \tag{2.27}$$

where we have used

$$\langle x | p \rangle = e^{-ip\cdot x}. \tag{2.28}$$

If we assume that the time-dependence of the wave functions is given by

$$\psi^{(+)}(x, \mathbf{k}, \hat{i}, s) = e^{-iE(\mathbf{k})x_0} \psi^{(+)}(\mathbf{x}, \mathbf{k}, \hat{i}, s), \tag{2.29}$$

$$\bar{\psi}^{(-)}(x', \mathbf{k}', \hat{i}', s') = e^{iE(\mathbf{k}')x_0} \bar{\psi}^{(-)}(\mathbf{x}', \mathbf{k}', \hat{i}', s'), \tag{2.30}$$

$$\Phi_i(y_1, ...y_i, ...y_A) = \left[\prod_{m=1, m\neq i}^{A} e^{-iK_{m,0}y_{m,0}}\right] e^{-iK_{i,0}y_{i,0}} \Phi_i(\mathbf{y}_1, ...\mathbf{y}_i, ...\mathbf{y}_A), \tag{2.31}$$

$$\bar{\Phi}_f(y_1, ...y_i', ...y_A) = \left[\prod_{n=1, n\neq i}^{A} e^{iK'_{n,0}y_{n,0}}\right] e^{iK'_{i,0}y'_{i,0}} \bar{\Phi}_f(\mathbf{y}_1, ...\mathbf{y}_i', ...\mathbf{y}_A), \tag{2.32}$$

we can perform the integration over the time-like components to obtain

$$\mathcal{M} = \sum_{i=1}^{A} \Delta_i \int d^3x\, d^3x'\, d^3y_i\, d^3y_i' \prod_{j=1,j\neq i}^{A} d^3y_j \frac{d^3p}{(2\pi)^3}\frac{d^3p'}{(2\pi)^3}\frac{d^3p_i}{(2\pi)^3}\frac{d^3p_i'}{(2\pi)^3}$$
$$\times e^{-i\mathbf{p}\cdot\mathbf{x}} e^{i\mathbf{p}'\cdot\mathbf{x}'} e^{-i\mathbf{p}_i\cdot\mathbf{y}_i} e^{i\mathbf{p}_i'\cdot\mathbf{y}_i'} \left[\bar{\psi}^{(-)}(\mathbf{x}',\mathbf{k}',\hat{i}',s') \otimes \bar{\Phi}_f(\mathbf{y}_1,...\mathbf{y}_i',...\mathbf{y}_A)\right]$$
$$\times \langle \mathbf{p}'\mathbf{p}_i'|\hat{F}|\mathbf{p}\,\mathbf{p}_i\rangle \left[\psi^{(+)}(\mathbf{x},\mathbf{k},\hat{i},s) \otimes \Phi_i(\mathbf{y}_1,...\mathbf{y}_i,...\mathbf{y}_A)\right], \tag{2.33}$$

with

$$\Delta_i = \int \prod_{j=1,j\neq i}^{A} dy_{j,0} \left\{ \prod_{m=1,m\neq i}^{A} e^{-iK_{m,0}y_{m,0}} \prod_{n=1,n\neq i}^{A} e^{iK'_{n,0}y_{n,0}} \right\}$$
$$= \int \prod_{j=1,j\neq i}^{A} dy_{j,0}\, e^{-iK_{j,0}y_{j,0}} e^{iK'_{j,0}y_{j,0}}$$
$$= \prod_{j=1,j\neq i}^{A} \delta(K'_{j,0} - K_{j,0}). \tag{2.34}$$

The energies of the spectator nucleons present here in the product of delta functions can be integrated out. To proceed, a specific representation for the operator $\hat{F}$ has to be chosen. We use

$$\langle \mathbf{p}'\mathbf{p}_i'|\hat{F}|\mathbf{p}\,\mathbf{p}_i\rangle = (2\pi)^3\delta(\mathbf{p}+\mathbf{p}_i-\mathbf{p}'-\mathbf{p}_i') \sum_{L=S}^{T} F_L(\mathbf{p},\mathbf{p}_i,\mathbf{p}',\mathbf{p}_i')(\lambda^L \otimes \lambda_L). \tag{2.35}$$

This is the well-known SPVAT form which has been successfully employed in elastic [10, 11, 29], quasielastic [1, 55] and inelastic proton-nucleus scattering [62, 63], where $\lambda^L \in \left\{I_4, \gamma^5, \gamma^\mu, \gamma^5\gamma^\mu, \sigma^{\mu\nu}\right\}$, i.e. $L = S, P, V, A, T$, and F_L is the complex NN amplitude. In the impulse approximation the interaction between two nucleons in the nuclear medium is assumed to be identical to the free-space interaction. This means that the NN interaction is fully determined by two-nucleon data. Note that three-momentum conservation is explicitly enforced. In the expression for λ^L we adopt the conventions of Ref. [60].

Substitution of this expression for $\hat{F}$ into Eq. (2.33) and subsequent integration over $\mathbf{p}_i'$ results in

$$\mathcal{M} = \sum_{i=1}^{A}\sum_{L=S}^{T} \int d^3x\, d^3x'\, d^3y_i\, d^3y_i' \prod_{j=1,j\neq i}^{A} d^3y_j \frac{d^3p}{(2\pi)^3}\frac{d^3p'}{(2\pi)^3}\frac{d^3p_i}{(2\pi)^3}$$
$$\times e^{i\mathbf{p}\cdot(\mathbf{y}_i'-\mathbf{x})} e^{i\mathbf{p}'\cdot(\mathbf{x}'-\mathbf{y}_i')} e^{i\mathbf{p}_i\cdot(\mathbf{y}_i'-\mathbf{y}_i)} F_L(\mathbf{p},\mathbf{p}_i,\mathbf{p}')$$
$$\times \left[\bar{\psi}^{(-)}(\mathbf{x}',\mathbf{k}',\hat{i}',s')\lambda^L\psi^{(+)}(\mathbf{x},\mathbf{k},\hat{i},s)\right]$$
$$\times \left[\bar{\Phi}_f(\mathbf{y}_1,...\mathbf{y}_i',...\mathbf{y}_A)\lambda_L\Phi_i(\mathbf{y}_1,...\mathbf{y}_i,...\mathbf{y}_A)\right]. \tag{2.36}$$

We make the additional approximation that the NN amplitudes are evaluated at the asymptotic momenta (equivalent to a zero-range approximation as presented in Refs [3, 64])

$$F_L(\mathbf{p}, \mathbf{p}_i, \mathbf{p}') \rightarrow F_L(\mathbf{k}, \mathbf{K}_i, \mathbf{k}'). \tag{2.37}$$

The remaining integrals over the momenta $\mathbf{p}$, $\mathbf{p}'$ and $\mathbf{p}_i$ can now be performed and results in the delta functions $\delta(\mathbf{y}'_i - \mathbf{x})\delta(\mathbf{x}' - \mathbf{y}'_i)\delta(\mathbf{y}'_i - \mathbf{y}_i)$. Performing the integral over $\mathbf{y}'_i$ results in

$$\mathcal{M} = \sum_{i=1}^{A}\sum_{L=S}^{T}\int d^3x\, d^3x'\, d^3y_i \prod_{j=1,j\neq i}^{A} d^3y_j\, F_L(\mathbf{k}, \mathbf{K}_i, \mathbf{k}') \left[\bar{\psi}^{(-)}(\mathbf{x}', \mathbf{k}', \hat{i}', s')\lambda^L\psi^{(+)}(\mathbf{x}, \mathbf{k}, \hat{i}, s)\right]$$

$$\times \left[\bar{\Phi}_f(\mathbf{y}_1, ...\mathbf{y}_i, ...\mathbf{y}_A)\lambda_L\Phi_i(\mathbf{y}_1, ...\mathbf{y}_i, ...\mathbf{y}_A)\right] \delta(\mathbf{y}_i - \mathbf{x})\delta(\mathbf{x}' - \mathbf{y}_i). \tag{2.38}$$

An additional approximation is that the many-body operator, λ_L, has a simple one-body form. If we define the initial and final nuclear states in terms of Slater determinants as

$$\Phi_i = \frac{1}{\sqrt{A!}} \det\left[\phi_n^{(i)}(\mathbf{y}_k)\right]_{n=1..A,\, k=1..A}, \tag{2.39}$$

$$\Phi_f = \frac{1}{\sqrt{A!}} \det\left[\phi_m^{(f)}(\mathbf{y}_k)\right]_{m=1..A,\, k=1..A}, \tag{2.40}$$

the action of the operator λ_L, which only sees the i^{th} particle, can be written as

$$\int \prod_{j=1,j\neq i}^{A} d^3y_j\, \bar{\Phi}_f\lambda_L^{(i)}\Phi_i = \frac{1}{A!}\sum_{m=1}^{A}\sum_{n=1}^{A}(-1)^{2+m+n}$$

$$\times \int \prod_{j=1,j\neq i}^{A} d^3y_j\, \overline{\det\left[\phi_{g\neq m}^{(f)}(\mathbf{y}_{k\neq i})\right]} \det\left[\phi_{h\neq n}^{(i)}(\mathbf{y}_{\ell\neq i})\right]$$

$$\times \bar{\phi}_m^{(f)}(\mathbf{y}_i)\lambda_L^{(i)}\phi_n^{(i)}(\mathbf{y}_i). \tag{2.41}$$

Since the inital and final nuclear states differ only by a single one-particle state, say state number 1, this becomes

$$\int \prod_{j=1,j\neq i}^{A} d^3y_j\, \bar{\Phi}_f\lambda_L^{(i)}\Phi_i = \frac{(A-1)!}{A!}\sum_{m=1}^{A}\sum_{n=1}^{A}\delta_{m1}\delta_{n1}\,\bar{\phi}_m^{(f)}(\mathbf{y}_i)\lambda_L^{(i)}\phi_n^{(i)}(\mathbf{y}_i)$$

$$= \frac{1}{A}\bar{\phi}_1^{(f)}(\mathbf{y}_i)\lambda_L^{(i)}\phi_1^{(i)}(\mathbf{y}_i)$$

$$= \frac{1}{A}\langle\Phi_f|\hat{\bar{\phi}}(\mathbf{y}_i)\lambda_L\hat{\phi}(\mathbf{y}_i)|\Phi_i\rangle, \tag{2.42}$$

where $\hat{\phi}$ is the Heisenberg field operator. Substitution of this expression into Eq. (2.38) and subsequent integration over $\mathbf{y}_i$ and $\mathbf{x}'$ results in

$$\mathcal{M} = \sum_{i=1}^{A} \frac{1}{A} \sum_{L=S}^{T} \int d^3x\, F_L(\mathbf{k}, \mathbf{K}_i, \mathbf{k}') \left[\bar{\psi}^{(-)}(\mathbf{x}, \mathbf{k}', \hat{i}', s')\lambda^L \psi^{(+)}(\mathbf{x}, \mathbf{k}, \hat{i}, s)\right] \langle \Phi_f | \hat{\bar{\phi}}(\mathbf{x}) \lambda_L \hat{\phi}(\mathbf{x}) | \Phi_i \rangle$$

$$= \sum_{L=S}^{T} \int d^3x\, F_L(\mathbf{k}, \mathbf{K}, \mathbf{k}') \left[\bar{\psi}^{(-)}(\mathbf{x}, \mathbf{k}', \hat{i}', s')\lambda^L \psi^{(+)}(\mathbf{x}, \mathbf{k}, \hat{i}, s)\right] \langle \Phi_f | \hat{\bar{\phi}}(\mathbf{x}) \lambda_L \hat{\phi}(\mathbf{x}) | \Phi_i \rangle. \quad (2.43)$$

Substitution of Eq. (2.43) into Eq. (2.14) results in

$$\frac{d\sigma}{dE'\, d\Omega'} = -\frac{1}{\pi} \mathcal{K}\, \mathrm{Im} \left\{ \sum_{L,L'=S}^{T} F_L(\mathbf{k}, \mathbf{K}, \mathbf{k}') F^*_{L'}(\mathbf{k}, \mathbf{K}, \mathbf{k}') \int d^3x\, d^3y\, H^{LL'}(\mathbf{x}, \mathbf{y}) \Pi_{LL'}(\mathbf{x}, \mathbf{y}, \omega) \right\}, \quad (2.44)$$

where we have defined the following:

- $H^{LL'}(\mathbf{x}, \mathbf{y})$ is the projectile tensor:

$$H^{LL'}(\mathbf{x}, \mathbf{y}) = \left[\bar{\psi}^{(-)}(\mathbf{x}, \mathbf{k}', \hat{i}', s')\lambda^L \psi^{(+)}(\mathbf{x}, \mathbf{k}, \hat{i}, s)\right] \left[\bar{\psi}^{(+)}(\mathbf{y}, \mathbf{k}, \hat{i}, s)\overline{\lambda^{L'}} \psi^{(-)}(\mathbf{y}, \mathbf{k}', \hat{i}', s')\right]. \quad (2.45)$$

- $\Pi_{LL'}(\mathbf{x}, \mathbf{y}, \omega)$ is the response of the nucleus defined as the polarization tensor:

$$\Pi_{LL'}(\mathbf{x}, \mathbf{y}, \omega) = \sum_n \left[\frac{\langle n | \hat{\bar{\phi}}(\mathbf{x}) \lambda_L \hat{\phi}(\mathbf{x}) | 0 \rangle \langle 0 | \hat{\bar{\phi}}(\mathbf{y}) \overline{\lambda_{L'}} \hat{\phi}(\mathbf{y}) | n \rangle}{\omega - (E_n - E_0) + i\epsilon} \right.$$

$$\left. + \frac{\langle n | \hat{\bar{\phi}}(\mathbf{y}) \overline{\lambda_{L'}} \hat{\phi}(\mathbf{y}) | 0 \rangle \langle 0 | \hat{\bar{\phi}}(\mathbf{x}) \lambda_L \hat{\phi}(\mathbf{x}) | n \rangle}{\omega + (E_n - E_0) - i\epsilon} \right], \quad (2.46)$$

  where

  - the second term in Eq. (2.46) has been added to write the result in terms of a time-ordered product as shown in Section 2.6. This can be done since the energy transfered to the nucleus is always positive and the contribution of this term to the cross section is therefore zero,
  - $|0\rangle$ is the initial interacting many-body ground state (initial state of the nucleus) and $|n\rangle$ similarly the final state. Both are eigenstates of the full Hamilton operator,
  - since we consider only single-particle field operators, we take into account only one-particle-one-hole excitations,
  - $\overline{\lambda_{L'}} = \gamma^0 \lambda^\dagger_{L'} \gamma^0$.

As shown in Section 2.6.2 in the nuclear matter approximation the polarization tensor can be written as

$$\Pi_{LL'}(\mathbf{x}, \mathbf{y}, \omega) = \int \frac{d^3q}{(2\pi)^3} e^{-i\mathbf{q}\cdot(\mathbf{x}-\mathbf{y})} \Pi_{LL'}(\mathbf{q}, \omega), \quad (2.47)$$

which results in

$$\frac{d\sigma}{dE'\,d\Omega'} = -\frac{1}{\pi}\mathcal{K}\,\mathrm{Im}\left\{\sum_{L,L'=S}^{T} F_L(\mathbf{k},\mathbf{K},\mathbf{k}')F^*_{L'}(\mathbf{k},\mathbf{K},\mathbf{k}')\int\frac{d^3q}{(2\pi)^3}\,H^{LL'}(\mathbf{q})\,\Pi_{LL'}(\mathbf{q},\omega)\right\}, \quad (2.48)$$

where

$$\begin{aligned} H^{LL'}(\mathbf{q}) &= \int d^3x\,d^3y\,e^{-i\mathbf{q}\cdot(\mathbf{x}-\mathbf{y})}H^{LL'}(\mathbf{x},\mathbf{y}) \\ &= \int d^3x\,e^{-i\mathbf{q}\cdot\mathbf{x}}\left[\bar{\psi}^{(-)}(\mathbf{x},\mathbf{k}',\hat{i}',s')\lambda^L\psi^{(+)}(\mathbf{x},\mathbf{k},\hat{i},s)\right] \\ &\quad\times\int d^3y\,e^{i\mathbf{q}\cdot\mathbf{y}}\left[\bar{\psi}^{(+)}(\mathbf{y},\mathbf{k},\hat{i},s)\overline{\lambda^{L'}}\psi^{(-)}(\mathbf{y},\mathbf{k}',\hat{i}',s')\right]. \end{aligned} \quad (2.49)$$

As can be seen from Eqs (2.44) and (2.48) the polarized double differential cross section, for both the general case and specifically for the nuclear matter approximation, can be written as the contraction of two tensors The first is the projectile (hadronic) tensor $H^{LL'}$ which contains all the information about the projectile and ejectile (including distortions). The other is the target (polarization) tensor $\Pi_{LL'}$, a fundamental many-body quantity that contains all the information about the target nucleus.

If we write the cross section of Eq. (2.48) as a sum of diagonal ($L = L'$) and off-diagonal ($L \neq L'$) terms we obtain

$$\begin{aligned} \frac{d\sigma}{dE'\,d\Omega'} = -\frac{1}{\pi}\mathcal{K}\,\mathrm{Im}\Bigg\{&\sum_{L=S}^{T} F_L(\mathbf{k},\mathbf{K},\mathbf{k}')F^*_{L}(\mathbf{k},\mathbf{K},\mathbf{k}')\int\frac{d^3q}{(2\pi)^3}\,H^{LL}(\mathbf{q})\,\Pi_{LL}(\mathbf{q},\omega) \\ &+\sum_{L\neq L'} F_L(\mathbf{k},\mathbf{K},\mathbf{k}')F^*_{L'}(\mathbf{k},\mathbf{K},\mathbf{k}')\int\frac{d^3q}{(2\pi)^3}\,H^{LL'}(\mathbf{q})\,\Pi_{LL'}(\mathbf{q},\omega)\Bigg\}. \end{aligned} \quad (2.50)$$

For diagonal combinations the following hold:

$$\begin{aligned} \mathrm{Im}\left\{F_L(\mathbf{k},\mathbf{K},\mathbf{k}')F^*_L(\mathbf{k},\mathbf{K},\mathbf{k}')\right\} &= \mathrm{Im}\left\{\left|F_L(\mathbf{k},\mathbf{K},\mathbf{k}')\right|^2\right\} \\ &= 0, \end{aligned} \quad (2.51)$$

$$\begin{aligned} \mathrm{Im}\left\{H^{LL'}(\mathbf{q})\right\} &= \mathrm{Im}\left\{H^L(\mathbf{q})\left[H^L(\mathbf{q})\right]^*\right\} \\ &= 0 \end{aligned} \quad (2.52)$$

and Eq. (2.50) reduces to

$$\begin{aligned} \frac{d\sigma}{dE'\,d\Omega'} = &-\frac{1}{\pi}\mathcal{K}\sum_{L=S}^{T}\left|F_L(\mathbf{k},\mathbf{K},\mathbf{k}')\right|^2\int\frac{d^3q}{(2\pi)^3}\,H^{LL}(\mathbf{q})\,\mathrm{Im}\left\{\Pi_{LL}(\mathbf{q},\omega)\right\} \\ &-\frac{1}{\pi}\mathcal{K}\,\mathrm{Im}\left\{\sum_{L\neq L'} F_L(\mathbf{k},\mathbf{K},\mathbf{k}')F^*_{L'}(\mathbf{k},\mathbf{K},\mathbf{k}')\int\frac{d^3q}{(2\pi)^3}\,H^{LL'}(\mathbf{q})\,\Pi_{LL'}(\mathbf{q},\omega)\right\}. \end{aligned} \quad (2.53)$$

This expression can be used to determine the contributions from the different LL' combinations in a systematic fashion.

The simplicity in form of Eq. (2.48) to a large extent masks the extreme complexity of its numerical implementation. There are a number of factors which add to the numerical burden:

- the use of distorted waves for the projectile and ejectile wave functions,
- the calculation of the polarization tensor,
- the calculation of the multi-dimensional integrals in the hadronic tensor (the d^3x and d^3y integrals) as well as in the final evaluation of the cross section (the d^3q integral),
- convergence issues of the integrals and
- the large number of Lorentz indices which must be contracted - 25 combinations in total since $L, L' \in \{S, P, V, A, T\}$.

All these factors have greatly hampered progress in this model. The availability of computer packages such as Matlab (with its powerful fitting and interpolation functions) as well as cluster computing techniques have, however, finally made it possible to calculate the cross section in a finite and reasonable amount of time. The form of Eq. (2.48) allows the calculation to proceed in a modular fashion with every component easily identified and separately calculated. We can therefore easily and honestly express any assumptions that went into the calculation and profiling the calculation is greatly facilitated. The numerical aspects of the calculation is further elaborated upon in Chapter 3.

2.4 Amplitudes

The representation of the NN scattering matrix we employ, is the well known SPVAT form (IA1), first formulated as the McNeil-Ray-Wallace parametrization [10, 11]:

$$\hat{F} = F_S(I_4 \otimes I_4) + F_P(\gamma^5 \otimes \gamma^5) + F_V(\gamma^\mu \otimes \gamma_\mu) + F_A(\gamma^5\gamma^\mu \otimes \gamma^5\gamma_\mu) + F_T(\sigma^{\mu\nu} \otimes \sigma_{\mu\nu}), \quad (2.54)$$

where the amplitudes F_L, ($L = S,\ P,\ V,\ A,\ T$), are obtained by fitting to free NN scattering data [4] which is consistent with the basic assumption of quasielastic scattering.

Note that the parametrization of the scattering matrix as shown in Eq. (2.54) is, however, incomplete [65]. Nuclear scattering involves the possible creation of nucleon-antinucleon pairs and NN data constrain only the on-shell positive energy portion of the NN amplitudes. Negative energy matrix elements are ambiguous since it is possible to alter them without changing the positive energy elements by adding new covariants of which the positive energy contributions vanish [12]. Theoretical models are therefore needed to provide off-shell and negative energy matrix elements of $\hat{F}$ [18, 66] and provide possible extentions to the SPVAT form. In addition, there exists a pseudoscalar versus pseudovector ambiguity of the pion-nucleon coupling and the model does not properly address the exhange behaviour of NN amplitudes in the nuclear medium [55, 66].

These issues were addressed in Ref. [17] with the Horowitz-Love-Franey meson-exhange model which gives the amplitudes as parametrizations in terms of Yukawa-type meson exchanges. This model extends the positive energy scattering data to the full Dirac space of two particles thereby

prescribing the negative energy matrix elements [15]. The HLF parameters like meson masses, form factors and couplings are determined by fitting to experimental data of free NN scattering which are available only at a few values of $T_{\rm lab}$ [17].

Tjon and Wallace [12–16] address the pion ambiguity and conclude that it is related to the negative energy baryon contributions to the potential. Their solution is to solve the NN integral equations based on meson theory to obtain the complete scattering matrix. In their model the coupling constants and form factors of the meson theory are again fixed by fitting to NN data.

For the current calculations, however, we make use of the SPVAT IA1 form so as to focus on the effects of distortions and nuclear correlations. In Ref. [29] it was found that for elastic proton-nucleus scattering, at least, the difference between the pseudoscalar and pseudovector amplitudes is not important at $T_{\rm lab} = 400$ MeV. Ref. [33] reports that the pseudovector and pseudoscalar forms of pion-nucleon coupling yield similar results for the spin-observables of quasielastic proton-nucleus scattaring at these higher energies.

The IA1 amplitudes employed in this work were obtained from the IA2 representation of the scattering matrix as described in Ref. [16]. By construction the amplitudes in subclass 11 of this representation are identical to the SPVAT parametrization.

2.5 Hadronic tensor

2.5.1 Plane waves

In the plane wave limit we set

$$\psi^{(+)}(\mathbf{x}, \mathbf{k}, \hat{i}, s) = e^{i\mathbf{k}\cdot\mathbf{x}} U(\mathbf{k}, \hat{i}, s), \tag{2.55}$$

$$\psi^{(-)}(\mathbf{x}', \mathbf{k}', \hat{i}', s') = e^{i\mathbf{k}'\cdot\mathbf{x}'} U(\mathbf{k}', \hat{i}', s'), \tag{2.56}$$

where $U(\mathbf{k}, \hat{i}, s)$ is a four-component positive energy Dirac spinor. Using these expressions in Eq. (2.49) results in

$$\begin{aligned} H^{LL'}(\mathbf{q}) &= \int d^3x\, d^3y\, e^{-i\mathbf{q}\cdot(\mathbf{x}-\mathbf{y})} e^{-i\mathbf{k}'\cdot\mathbf{x}} e^{i\mathbf{k}\cdot\mathbf{x}} e^{-i\mathbf{k}\cdot\mathbf{y}} e^{i\mathbf{k}'\cdot\mathbf{y}} \\ &\quad \times \left[\bar{U}(\mathbf{k}', \hat{i}', s')\lambda^L U(\mathbf{k}, \hat{i}, s)\right] \left[\bar{U}(\mathbf{k}, \hat{i}, s)\overline{\lambda^{L'}} U(\mathbf{k}', \hat{i}', s')\right] \\ &= D(|\Delta\mathbf{k} - \mathbf{q}|)\, M^{LL'}(\mathbf{k}, \mathbf{k}'), \end{aligned} \tag{2.57}$$

where

$$D(|\Delta\mathbf{k} - \mathbf{q}|) = \left[\int_0^R d^3r\, e^{i(\mathbf{k}-\mathbf{k}'-\mathbf{q})\cdot\mathbf{r}}\right]^2, \tag{2.58}$$

$$M^{LL'}(\mathbf{k}, \mathbf{k}') = \left[\bar{U}(\mathbf{k}', \hat{i}', s')\lambda^L U(\mathbf{k}, \hat{i}, s)\right] \left[\bar{U}(\mathbf{k}, \hat{i}, s)\overline{\lambda^{L'}} U(\mathbf{k}', \hat{i}', s')\right]. \tag{2.59}$$

Using properties of the Dirac spinors [60]

$$U_a(\mathbf{k},s)\bar{U}_b(\mathbf{k},s) = \left[\frac{\not{p}+M}{2M}\cdot\frac{1+\gamma_5\not{s}}{2}\right]_{ab}$$
$$= \left[\Lambda_+(\mathbf{k},M)\Sigma(\hat{i},s)\right]_{ab}, \tag{2.60}$$

where Λ_+ is the positive energy projection operator and Σ the spin projection operator, the matrix element can be written as

$$M^{LL'}(\mathbf{k},\mathbf{k}') = \left[\bar{U}_a(\mathbf{k}',\hat{i}',s')\lambda^L_{ab}U_b(\mathbf{k},\hat{i},s)\right]\left[\bar{U}_m(\mathbf{k},\hat{i},s)\overline{\lambda^{L'}_{mn}}U_n(\mathbf{k}',\hat{i}',s')\right]$$
$$= \left[U_n(\mathbf{k}',\hat{i}',s')\bar{U}_a(\mathbf{k}',\hat{i}',s')\lambda^L_{ab}U_b(\mathbf{k},\hat{i},s)\bar{U}_m(\mathbf{k},\hat{i},s)\overline{\lambda^{L'}_{mn}}\right]$$
$$= \left[\lambda^L_{ab}\left(\Lambda_+(\mathbf{k},M)\Sigma(\hat{i},s)\right)_{bm}\overline{\lambda^{L'}_{mn}}\left(\Lambda_+(\mathbf{k}',M)\Sigma(\hat{i}',s')\right)_{na}\right]$$
$$= \mathrm{Tr}\left[\lambda^L\Lambda_+(\mathbf{k},M)\Sigma(\hat{i},s)\overline{\lambda^{L'}}\Lambda_+(\mathbf{k}',M)\Sigma(\hat{i}',s')\right]. \tag{2.61}$$

Thus, in the plane wave limit, $H^{LL'}$ reduces to a trace over gamma matrices which can be easily evaluated using trace techniques and identities of the gamma matrices. Alternatively the free nucleon Dirac spinor

$$U(\mathbf{k},s) = \sqrt{\frac{E+M}{2M}}\begin{bmatrix} 1 \\ \frac{\boldsymbol{\sigma}\cdot\mathbf{k}}{E+M}\end{bmatrix}\chi_s \tag{2.62}$$

can be used to evaluate Eq. (2.59) directly. Here χ_s is a Pauli spinor for projection $s = \pm 1/2$ along an arbitrary quantization axis $(\hat{i})$ in the rest frame of the nucleon [67]

$$\chi_s = \sum_{s_z}\chi_{s_z}\mathcal{D}^{1/2}_{s_z s}(\alpha,\beta,\gamma), \tag{2.63}$$

where $\mathcal{D}^{1/2}_{s_z s}(\alpha,\beta,\gamma)$ is the well-known Wigner D-function in terms of the rotation angles of the quantization axis with respect to the $\hat{z}$-axis and χ_{s_z} the spin basis functions for the quantization axis along the $\hat{z}$-axis. This results in

$$U(\mathbf{k},s) = \sqrt{\frac{E+M}{2M}}\begin{bmatrix} D^{1/2}_{1/2,s}(\alpha,\beta,\gamma) \\ D^{1/2}_{-1/2,s}(\alpha,\beta,\gamma) \\ \frac{1}{E+M}\left(k^3 D^{1/2}_{1/2,s}(\alpha,\beta,\gamma) + \left(k^1 - ik^2\right)D^{1/2}_{-1/2,s}(\alpha,\beta,\gamma)\right) \\ \frac{1}{E+M}\left(\left(k^1 + ik^2\right)D^{1/2}_{1/2,s}(\alpha,\beta,\gamma) - k^3 D^{1/2}_{-1/2,s}(\alpha,\beta,\gamma)\right)\end{bmatrix}. \tag{2.64}$$

Note that for the most simplistic description of the projectile, M is the free mass of the nucleon whereas the improved model of Horowitz and Murdock uses an effective mass M^* (see Section 1.2)

and therefore also $E \equiv E^* = \sqrt{\mathbf{k}^2 + M^{*2}}$.

2.5.2 Distorted waves

The inclusion of distortion-effects greatly complicates matters and the wave functions are written in terms of partial wave expansions. The distorted waves are solutions to the Dirac equation with scalar, time-like vector and Coulomb potentials. Since the interaction potentials are only radially dependent, a separation of the wave function into radial and angular parts is the most natural way of obtaining the solution. The distorted wave with outgoing boundary conditions is given by [3, 62, 63, 68]

$$\psi^{(+)}(\mathbf{x},\mathbf{k},\hat{i},s) = \frac{4\pi}{kx}\left(\frac{E(\mathbf{k})+M}{2M}\right)^{1/2} \sum_{ljm_l s_z} i^l e^{i\delta_{lj}} \langle l\tfrac{1}{2} m s_z | j, m+s_z\rangle \, \mathcal{D}^{(1/2)}_{s_z s}(\hat{i})\, Y^*_{lm}(\hat{k}) \times \begin{bmatrix} g_{lj}(kx)\mathcal{Y}_{lj,m+s_z}(\hat{x}) \\ if_{2j-l,j}(kx)\mathcal{Y}_{2j-l,j,m+s_z}(\hat{x}) \end{bmatrix}, \tag{2.65}$$

where

- $x = |\mathbf{x}|$ and $k = |\mathbf{k}|$,
- $\langle l\frac{1}{2} m_l m_s | j m_j\rangle$ is a Clebsch-Gordon coefficient,
- $Y_{lm}(\hat{k})$ is a spherical harmonic function,
- $g_{lj}(z)$ and $f_{lj}(z)$ are radial wave function solutions of Schrodinger-like radial differential equations that contain the central, spin-orbit and Darwin potentials [3, 68],
- $\mathcal{Y}_{lj\mu}(\hat{x})$ is a spin-spherical harmonic function given by

$$\mathcal{Y}_{lj\mu}(\hat{x}) = \sum_{t'_z} \langle l\frac{1}{2}, \mu - t'_z, t'_z | j\mu\rangle Y_{l,\mu-t'_z}(\hat{x})\chi_{t'_z}, \tag{2.66}$$

- the relativistic Coulomb phase shift δ_{lj} is an implicit function of the projectile and target masses, the projectile and target atomic numbers and the momentum $\mathbf{k}$.

If we set $\hat{k} \equiv \hat{z}$ we can eliminate the sum over m_l by using

$$Y^*_{lm}(\hat{z}) = \left(\frac{2l+1}{4\pi}\right)^{1/2} \delta_{m0} \tag{2.67}$$

to write the Dirac distorted wave with outgoing boundary conditions as

$$\psi^{(+)}(\mathbf{x}) = \sum_{ljs_z} A_{ljs_z} \begin{bmatrix} \frac{g_{lj}(kx)}{x}\mathcal{Y}_{ljs_z}(\hat{x}) \\ \frac{if_{2j-l,j}(kx)}{x}\mathcal{Y}_{2j-l,js_z}(\hat{x}) \end{bmatrix}, \tag{2.68}$$

where

$$A_{ljs_z} = \frac{4\pi}{k}\left(\frac{E(\mathbf{k})+M}{2M}\right)^{1/2} i^l e^{i\delta_{lj}} \langle l\frac{1}{2}0s_z|js_z\rangle\, \mathcal{D}^{(1/2)}_{s_z s}(\hat{i}) \left(\frac{2l+1}{4\pi}\right)^{1/2}. \tag{2.69}$$

Let us specialize to $\hat{i} = \hat{l}$ (see Fig. 2.2). This means that $\mathcal{D}^{1/2}_{s_z s}(\hat{i}) = \delta_{s_z,s}$ and Eq. (2.68) simplifies to

$$\psi^{(+)}(\mathbf{x},\mathbf{k},\hat{i},s) = \sum_{lj} A_{ljs} \begin{bmatrix} \frac{g_{lj}(kx)}{x}\mathcal{Y}_{ljs}(\hat{x}) \\ \frac{if_{2j-l,j}(kx)}{x}\mathcal{Y}_{2j-l,js}(\hat{x}) \end{bmatrix}. \tag{2.70}$$

Similarly, the distorted wave function of the ejectile is given by (see Appendix A.1)

$$\psi^{(-)}(\mathbf{x},\mathbf{k}',\hat{i}',s') = \sum_{l'j'm's'_z} B_{l'j'm's'_z} \begin{bmatrix} \eta_{l'j'm's'_z}\frac{g^*_{l'j'}(k'x)}{x}\mathcal{Y}_{l'j',-(m'+s'_z)}(\hat{x}) \\ -i\epsilon_{l'j'm's'_z}\frac{f^*_{2j'-l',j'}(k'x)}{x}\mathcal{Y}_{2j'-l',j',-(m'+s'_z)}(\hat{x}) \end{bmatrix}, \tag{2.71}$$

where

$$B_{l'j'm's'_z} = (-i)(-1)^{s'-1/2}\frac{4\pi}{k'}\left(\frac{E(\mathbf{k}')+M}{2M}\right)^{1/2}(-1)^{s'_z+s'} i^{l'} e^{-i\delta_{lj}}$$
$$\times \langle l'\frac{1}{2}m's'_z|j',m'+s'_z\rangle\, \mathcal{D}^{(1/2)}_{-s'_z s'}(\hat{i}')\, Y_{l'm'}(\hat{k}'), \tag{2.72}$$

$$\eta_{l'j'm's'_z} = i(-1)^{m'+s'_z-j'+l'+1}, \tag{2.73}$$

$$\epsilon_{l'j'm's'_z} = i(-1)^{m'+s'_z+j'-l'+1}. \tag{2.74}$$

2.5.2.1 Calculation of $H^{LL'}(\mathbf{q})$

Consider

$$H^L(\mathbf{q}) = \int d^3x\, e^{-i\mathbf{q}\cdot\mathbf{x}}\bar{\psi}^{(-)}(\mathbf{x})\lambda^L\psi^{(+)}(\mathbf{x}), \tag{2.75}$$

where the goal is to calculate

$$H^{LL'}(\mathbf{q}) = H^L(\mathbf{q})\left[H^{L'}(\mathbf{q})\right]^*. \tag{2.76}$$

The interaction matrix is written in two-component form as

$$\lambda^L = \begin{bmatrix} \lambda^L_{11} & \lambda^L_{12} \\ \lambda^L_{21} & \lambda^L_{22} \end{bmatrix}, \tag{2.77}$$

which leaves the matrix product in Eq. (2.75) in the form

$$\bar{\psi}^{(-)}\lambda^L\psi^{(+)} = \sum_{lj}\sum_{l'j'm's'_z} A_{ljs}B^*_{l'j'm's'_z}\left\{M_{11}+M_{12}+M_{21}+M_{22}\right\}, \tag{2.78}$$

$$M_{11} = \eta^*_{l'j'm's'_z}\frac{g_{lj}(kx)g_{l'j'}(k'x)}{x^2}\mathcal{Y}^\dagger_{l'j',-(m'+s'_z)}(\hat{x})\lambda^L_{11}\mathcal{Y}_{ljs}(\hat{x}), \tag{2.79}$$

$$M_{12} = i\eta^*_{l'j'm's'_z}\frac{f_{2j-l,j}(kx)g_{l'j'}(k'x)}{x^2}\mathcal{Y}^\dagger_{l'j',-(m'+s'_z)}(\hat{x})\lambda^L_{12}\mathcal{Y}_{2j-l,js}(\hat{x}), \tag{2.80}$$

$$M_{21} = -i\epsilon^*_{l'j'm's'_z}\frac{g_{lj}(kx)f_{2j'-l',j'}(k'x)}{x^2}\mathcal{Y}^\dagger_{2j'-l',j',-(m'+s'_z)}(\hat{x})\lambda^L_{21}\mathcal{Y}_{ljs}(\hat{x}), \tag{2.81}$$

$$M_{22} = \epsilon^*_{l'j'm's'_z}\frac{f_{2j-l,j}(kx)f_{2j'-l',j'}(k'x)}{x^2}\mathcal{Y}^\dagger_{2j'-l',j',-(m'+s'_z)}(\hat{x})\lambda^L_{22}\mathcal{Y}_{2j-l,js}(\hat{x}). \tag{2.82}$$

By writing the exponential factor in Eq. (2.75) as a sum of partial waves

$$e^{-i\mathbf{q}\cdot\mathbf{x}} = 4\pi\sum_{LM}\left(i^L\right)^* j_L(qx)Y_{LM}(\hat{q})Y^*_{LM}(\hat{x}) \tag{2.83}$$

and rewriting the spin-spherical harmonics in Eqs (2.79) to (2.82) in terms of spherical harmonics and two-component Pauli spinors

$$\mathcal{Y}_{ljs} = \sum_{t_z}\langle l\frac{1}{2}, s-t_z, t_z|js\rangle Y_{l,s-t_z}\chi_{t_z}, \tag{2.84}$$

Eq. (2.75) can be written as four integrals

$$H^L(\mathbf{q}) = I_{11}+I_{12}+I_{21}+I_{22,} \tag{2.85}$$

where (in spherical coordinates)

$$\begin{aligned} I_{11} = &\sum_{lj}\sum_{l'j'm's'_z} 4\pi A_{ljs}B^*_{l'j'm's'_z}\eta^*_{l'j'm's'_z} \\ &\times\sum_{LM}\left(i^L\right)^* Y_{LM}(\mathbf{q})\left\{\int dr\, j_L(qr)\, g_{lj}(kr)\, g_{l'j'}(k'r)\right\} \\ &\times\sum_{t_z t'_z}\langle l\frac{1}{2}, s-t_z, t_z|js\rangle\langle l'\frac{1}{2}, -m'-s'_z-t'_z, t'_z|j', -m'-s'_z\rangle\left[\chi^\dagger_{t'_z}\,\lambda^L_{11}\,\chi_{t_z}\right] \\ &\times G(l, s-t_z|l', -m'-s'_z-t'_z|LM), \end{aligned} \tag{2.86}$$

$$I_{12} = \sum_{lj} \sum_{l'j'm's'_z} 4\pi A_{ljs} B^*_{l'j'm's'_z} \left(i\eta^*_{l'j'm's'_z} \right)$$
$$\times \sum_{LM} \left(i^L\right)^* Y_{LM}(\mathbf{q}) \left\{ \int dr\, j_L(qr)\, f_{2j-l,j}(kr)\, g_{l'j'}(k'r) \right\}$$
$$\times \sum_{t_z t'_z} \langle 2j-l, \frac{1}{2}, s-t_z, t_z | js \rangle \langle l' \frac{1}{2}, -m'-s'_z-t'_z, t'_z | j', -m'-s'_z \rangle \left[\chi^\dagger_{t'_z}\, \lambda^L_{12}\, \chi_{t_z} \right]$$
$$\times G(2j-l, s-t_z | l', -m'-s'_z-t'_z | LM), \tag{2.87}$$

$$I_{21} = \sum_{lj} \sum_{l'j'm's'_z} 4\pi A_{ljs} B^*_{l'j'm's'_z} \left(-i\epsilon^*_{l'j'm's'_z} \right)$$
$$\times \sum_{LM} \left(i^L\right)^* Y_{LM}(\mathbf{q}) \left\{ \int dr\, j_L(qr)\, g_{lj}(kr)\, f_{2j'-l',j'}(k'r) \right\}$$
$$\times \sum_{t_z t'_z} \langle l, \frac{1}{2}, s-t_z, t_z | js \rangle \langle 2j'-l' \frac{1}{2}, -m'-s'_z-t'_z, t'_z | j', -m'-s'_z \rangle \left[\chi^\dagger_{t'_z}\, \lambda^L_{21}\, \chi_{t_z} \right]$$
$$\times G(l, s-t_z | 2j'-l', -m'-s'_z-t'_z | LM), \tag{2.88}$$

$$I_{22} = \sum_{lj} \sum_{l'j'm's'_z} 4\pi A_{ljs} B^*_{l'j'm's'_z} \epsilon^*_{l'j'm's'_z}$$
$$\times \sum_{LM} \left(i^L\right)^* Y_{LM}(\mathbf{q}) \left\{ \int dr\, j_L(qr)\, f_{2j-l,j}(kr)\, f_{2j'-l',j'}(k'r) \right\}$$
$$\times \sum_{t_z t'_z} \langle 2j-l, \frac{1}{2}, s-t_z, t_z | js \rangle \langle 2j'-l' \frac{1}{2}, -m'-s'_z-t'_z, t'_z | j', -m'-s'_z \rangle \left[\chi^\dagger_{t'_z}\, \lambda^L_{22}\, \chi_{t_z} \right]$$
$$\times G(2j-l, s-t_z | 2j'-l', -m'-s'_z-t'_z | LM). \tag{2.89}$$

The radial integrals in the above equations are treated numerically. The angular parts have been written in terms of the Gaunt coefficients (see Appendix A.2) e.g.

$$G(l, s-t_z | l', -m'-s'_z-t'_z | LM) = \int d\Omega\, Y_{l,s-t_z}(\hat{x})\, Y^*_{l',-m'-s'_z-t'_z}(\hat{x})\, Y^*_{LM}(\hat{x}). \tag{2.90}$$

Since s and t_z are both $\pm 1/2$ we can immediately identify three sets of Gaunt coefficients needed for this calculation:

$$G(l, 0 | l', -m'-s'_z-t'_z | LM), \tag{2.91}$$

$$G(l, -1 | l', -m'-s'_z-t'_z | LM), \tag{2.92}$$

$$G(l, 1 | l', -m'-s'_z-t'_z | LM). \tag{2.93}$$

Additional properties (see Appendix A.2) imply that:

1. $|l - l'| \leq L \leq (l + l')$,
2. $M = s + s'_z + m' - t_z + t'_z$, (eliminates the sum over M).

Under these conditions, the summations present in Eqs (2.86) to (2.89) exhibit the following behaviours:

$$\sum_{lj} \to \sum_{l=0}^{l_{\max}} \sum_{j=|l-1/2|}^{l+1/2}, \tag{2.94}$$

$$\sum_{l'j'm'} \to \sum_{l'=0}^{l'_{\max}} \sum_{j'=|l'-1/2|}^{l'+1/2} \sum_{m'=-l'}^{l'}, \tag{2.95}$$

$$\sum_{s'_z} \to \sum_{s'_z=\pm 1/2}, \tag{2.96}$$

$$\sum_{L} \to \sum_{L=|\tilde{l}-\tilde{l}'|}^{\tilde{l}+\tilde{l}'}, \tag{2.97}$$

$$\sum_{t_z t'_z} \to \sum_{t_z=\pm 1/2} \sum_{t'_z=\pm 1/2}, \tag{2.98}$$

where

$$\tilde{l} = \begin{cases} l & \text{for } I_{11} \text{ or } I_{21}, \\ 2j - l & \text{for } I_{12} \text{ or } I_{22}, \end{cases} \tag{2.99}$$

$$\tilde{l}' = \begin{cases} l' & \text{for } I_{11} \text{ or } I_{12}, \\ 2j' - l' & \text{for } I_{21} \text{ or } I_{22}. \end{cases} \tag{2.100}$$

2.6 Polarization tensor

2.6.1 General derivation in position-space

Using the identity

$$\int_{-\infty}^{\infty} dx_0 \, e^{i(\omega \mp E)x_0} \, \theta(\pm x_0) = \pm \frac{i}{w \mp E \pm i\epsilon} \tag{2.101}$$

and the definition of the nuclear current operator

$$\hat{J}^L(\mathbf{x}) = \hat{\bar{\phi}}(\mathbf{x}) \lambda^L \hat{\phi}(\mathbf{x}), \tag{2.102}$$

$$\hat{J}^{L'}(\mathbf{y}) = \hat{\bar{\phi}}(\mathbf{y}) \overline{\lambda^{L'}} \hat{\phi}(\mathbf{y}), \tag{2.103}$$

we write the contravariant polarization (see Eq. (2.46)) as

$$\Pi^{LL'}(\mathbf{x},\mathbf{y},\omega) = -i\sum_n \langle n|\hat{J}^L(\mathbf{x})|0\rangle\langle 0|\hat{J}^{L'}(\mathbf{y})|n\rangle \int_{-\infty}^{\infty} d(y_0-x_0)e^{i[\omega-(E_n-E_0)](y_0-x_0)}\theta(y_0-x_0)$$
$$+ i\sum_n \langle n|\hat{J}^{L'}(\mathbf{y})|0\rangle\langle 0|\hat{J}^{L}(\mathbf{x})|n\rangle \int_{-\infty}^{\infty} d(y_0-x_0)e^{i[\omega+(E_n-E_0)](y_0-x_0)}\theta(x_0-y_0). \tag{2.104}$$

Since $\hat{H}|0\rangle = E_0|0\rangle$ and $\hat{H}|n\rangle = E_n|n\rangle$, the matrix elements can be written as

$$\begin{aligned} e^{i[\omega-(E_n-E_0)](y_0-x_0)}\langle n|\hat{J}^L(\mathbf{x})|0\rangle\langle 0|\hat{J}^{L'}(\mathbf{y})|n\rangle &= e^{i\omega(y_0-x_0)}\langle n|e^{i\hat{H}x_0}\hat{J}^L(\mathbf{x})e^{-i\hat{H}x_0}|0\rangle \\ &\quad\times\langle 0|e^{i\hat{H}y_0}\hat{J}^{L'}(\mathbf{y})e^{-i\hat{H}y_0}|n\rangle \\ &= e^{i\omega(y_0-x_0)}\langle n|\hat{J}^L(x)|0\rangle\langle 0|\hat{J}^{L'}(y)|n\rangle \end{aligned} \tag{2.105}$$

and

$$\begin{aligned} e^{i[\omega+(E_n-E_0)](y_0-x_0)}\langle n|\hat{J}^L(\mathbf{x})|0\rangle\langle 0|\hat{J}^{L'}(\mathbf{y})|n\rangle &= e^{i\omega(y_0-x_0)}\langle n|e^{i\hat{H}y_0}\hat{J}^{L'}(\mathbf{y})e^{-i\hat{H}y_0}|0\rangle \\ &\quad\times\langle 0|e^{i\hat{H}x_0}\hat{J}^{L}(\mathbf{x})e^{-i\hat{H}x_0}|n\rangle \\ &= e^{i\omega(y_0-x_0)}\langle n|\hat{J}^{L'}(y)|0\rangle\langle 0|\hat{J}^{L}(x)|n\rangle \end{aligned} \tag{2.106}$$

since the time-dependence of the Heisenberg field operators is given by [3, 49]

$$\hat{J}(x) = e^{i\hat{H}x_0}\hat{J}(\mathbf{x})e^{-i\hat{H}x_0}. \tag{2.107}$$

Using Eqs (2.105) and (2.106) in Eq. (2.104) results in

$$\begin{aligned} \Pi^{LL'}(\mathbf{x},\mathbf{y},\omega) &= -i\sum_n \int_{-\infty}^{\infty} d(y_0-x_0)e^{i\omega(y_0-x_0)}\langle n|\hat{J}^L(x)|0\rangle\langle 0|\hat{J}^{L'}(y)|n\rangle\theta(y_0-x_0) \\ &\quad + i\sum_n \int_{-\infty}^{\infty} d(y_0-x_0)e^{i\omega(y_0-x_0)}\langle n|\hat{J}^{L'}(y)|0\rangle\langle 0|\hat{J}^{L}(x)|n\rangle\theta(x_0-y_0) \\ &= -i\int_{-\infty}^{\infty} d(y_0-x_0)e^{i\omega(y_0-x_0)}\langle 0|\hat{J}^{L'}(y)\hat{J}^{L}(x)|0\rangle\theta(y_0-x_0) \\ &\quad + i\int_{-\infty}^{\infty} d(y_0-x_0)_n e^{i\omega(y_0-x_0)}\langle 0|\hat{J}^{L}(x)\hat{J}^{L'}(y)|0\rangle\theta(x_0-y_0). \end{aligned} \tag{2.108}$$

From the definition of the time-ordered product [49]

$$T[\hat{A}(y)\hat{B}(x)] = \hat{A}(y)\hat{B}(x)\theta(y_0 - x_0) - \hat{B}(x)\hat{A}(y)\theta(x_0 - y_0) \tag{2.109}$$

it follows that Eq. (2.108) can be written as

$$i\Pi^{LL'}(\mathbf{x}, \mathbf{y}, \omega) = \int_{-\infty}^{\infty} d(y_0 - x_0) e^{i\omega(y_0 - x_0)} \langle 0|T[\hat{J}^{L'}(y)\hat{J}^{L}(x)]|0\rangle. \tag{2.110}$$

Using Wick's theorem [3, 49] and Eqs (2.102) and (2.103) we write the matrix element as

$$\begin{aligned}
\langle 0|T[\hat{J}^{L'}(y)\hat{J}^{L}(x)]|0\rangle &= \langle 0|T[\hat{\bar{\phi}}(y)\overline{\lambda^{L'}}\hat{\phi}(y)\hat{\bar{\phi}}(x)\lambda^{L}\hat{\phi}(x)]|0\rangle \\
&= \sum_{ijmn} \langle 0|T[\hat{\bar{\phi}}_i(y)\overline{\lambda^{L'}_{ij}}\hat{\phi}_j(y)\hat{\bar{\phi}}_m(x)\lambda^{L}_{mn}\hat{\phi}_n(x)]|0\rangle \\
&= \sum_{ijmn} \overbrace{\hat{\bar{\phi}}_i(y)\overline{\lambda^{L'}_{ij}}\hat{\phi}_j(y)\hat{\bar{\phi}}_m(x)\lambda^{L}_{mn}\hat{\phi}_n(x)}.
\end{aligned} \tag{2.111}$$

From the definition of the fermion propagator [31, 49] (see Appendix B.2)

$$\begin{aligned}
iG_{\alpha\beta}(x, y) &= \langle 0|T[\hat{\phi}_\alpha(x)\hat{\bar{\phi}}_\beta(y)]|0\rangle, \\
&= \overbrace{\hat{\phi}_\alpha(x)\hat{\bar{\phi}}_\beta(y)}
\end{aligned} \tag{2.112}$$

it follows that

$$\begin{aligned}
i\Pi^{LL'}(\mathbf{x}, \mathbf{y}, \omega) &= \int_{-\infty}^{\infty} d(y_0 - x_0) e^{i\omega(y_0 - x_0)} \sum_{ijnm} \lambda^{L}_{mn} \left[-iG_{ni}(x, y)\right] \overline{\lambda^{L'}_{ij}} \left[iG_{jm}(y, x)\right] \\
&= \int_{-\infty}^{\infty} d(y_0 - x_0) e^{i\omega(y_0 - x_0)} \mathrm{Tr}\left[\lambda^{L} G(x, y) \overline{\lambda^{L'}} G(y, x)\right].
\end{aligned} \tag{2.113}$$

2.6.2 Nuclear matter approximation and momentum-space polarization

If we make the nuclear matter approximation (where we have translational invariance [39]) we can write the nucleon propagator (see Appendix B.2) as

$$G(x, y) \equiv G(x - y) = \int \frac{d^4k}{(2\pi)^4} e^{-ik\cdot(x-y)} G(k). \tag{2.114}$$

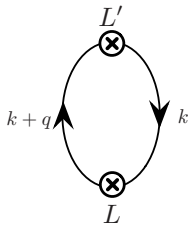

Figure 2.3: Lowest-order (Hartree) polarization where $L, L' \in \{S, P, V, A, T\}$ [2].

Substitution into Eq. (2.113) leads to

$$\begin{aligned} i\Pi^{LL'}(\mathbf{x},\mathbf{y},\omega) &= \int_{-\infty}^{\infty} d(y_0 - x_0) \frac{d^4k}{(2\pi)^4} \frac{d^4k'}{(2\pi)^4} e^{i\omega(y_0-x_0)} e^{-ik'\cdot(y-x)} e^{-ik\cdot(x-y)} \\ &\quad \times \mathrm{Tr}\left[\lambda^L G(k) \overline{\lambda^{L'}} G(k')\right] \\ &= \int_{-\infty}^{\infty} d(y_0 - x_0) \frac{d^4k}{(2\pi)^4} \frac{d^3k'}{(2\pi)^3} \frac{dk'_0}{2\pi} e^{i(\omega+k_0-k'_0)(y_0-x_0)} \\ &\quad \times e^{i\mathbf{k}'\cdot(\mathbf{y}-\mathbf{x})} e^{-i\mathbf{k}\cdot(\mathbf{y}-\mathbf{x})} \mathrm{Tr}\left[\lambda^L G(k) \overline{\lambda^{L'}} G(k'_0, \mathbf{k}')\right] \\ &= \int \frac{d^4k}{(2\pi)^4} \frac{d^3k'}{(2\pi)^3} \frac{dk'_0}{2\pi} \delta(\omega + k_0 - k'_0) \\ &\quad \times e^{i\mathbf{k}'\cdot(\mathbf{y}-\mathbf{x})} e^{-i\mathbf{k}\cdot(\mathbf{y}-\mathbf{x})} \mathrm{Tr}\left[\lambda^L G(k) \overline{\lambda^{L'}} G(k'_0, \mathbf{k}')\right] \\ &= \int \frac{d^4k}{(2\pi)^4} \frac{d^3k'}{(2\pi)^3} e^{i(\mathbf{k}'-\mathbf{k})\cdot(\mathbf{y}-\mathbf{x})} \mathrm{Tr}\left[\lambda^L G(k) \overline{\lambda^{L'}} G(k_0+\omega, \mathbf{k}')\right]. \end{aligned} \tag{2.115}$$

If we let $\mathbf{q} = \mathbf{k}' - \mathbf{k}$ where $q = (\omega, \mathbf{q})$, we can write this as

$$\begin{aligned} \Pi^{LL'}(\mathbf{x},\mathbf{y},\omega) &= \int \frac{d^3q}{(2\pi)^3} e^{-i\mathbf{q}\cdot(\mathbf{x}-\mathbf{y})} \left\{ -i \int \frac{d^4k}{(2\pi)^4} \mathrm{Tr}\left[\lambda^L G(k) \overline{\lambda^{L'}} G(k+q)\right] \right\} \\ &= \int \frac{d^3q}{(2\pi)^3} e^{-i\mathbf{q}\cdot(\mathbf{x}-\mathbf{y})} \Pi^{LL'}(q). \end{aligned} \tag{2.116}$$

2.6.3 Hartree polarization

In the Hartree approximation the ground state is the self-consistent RHA or MFT ground state (see Appendix B.2.3) and the polarization (see Fig. 2.3) can be written as

$$\Pi^{LL'}(q) = -i \int \frac{d^4k}{(2\pi)^4} \mathrm{Tr}\left[\lambda^L G^H(k) \overline{\lambda^{L'}} G^H(k+q)\right]. \tag{2.117}$$

Here the nucleon propagator can be written in terms of Feynman (F) and density-dependent (D) pieces

$$G^H(k) = G_F(k) + G_D(k), \tag{2.118}$$

$$G_F(k) = \left(\bar{\not{k}} + M^*\right)\left[\frac{1}{\bar{k}^2 - M^{*2} + i\epsilon}\right], \tag{2.119}$$

$$G_D(k) = \left(\bar{\not{k}} + M^*\right)\left[\frac{i\pi}{E_k^*}\delta\left(\bar{k}^0 - E_k^*\right)\theta\left(k_F - |\mathbf{k}|\right)\theta\left(\bar{k}^0\right)\right], \tag{2.120}$$

$$\bar{k}^\mu = \left(k^0 - g_V V^0, \mathbf{k}\right), \tag{2.121}$$

$$E_k^* = \sqrt{\mathbf{k}^2 + M^{*2}}, \tag{2.122}$$

where M^* is given by Eq. (B.48) in the MFT approximation and Eq. (B.51) in the RHA.

This allows the polarization of Eq. (2.117) to be written as

$$\Pi^{LL'}(q) = \Pi_{FF}^{LL'}(q) + \Pi_D^{LL'}(q),$$

$$\Pi_{FF}^{LL'}(q) = \int \frac{d^4k}{(2\pi)^4}\frac{-i\mathcal{T}^{LL'}(k, k+q)}{\left[\bar{k}^2 - M^{*2} + i\epsilon\right]\left[\left(\bar{k}+q\right)^2 - M^{*2} + i\epsilon\right]}, \tag{2.123}$$

$$\begin{aligned}\Pi_D^{LL'}(q) = &\int \frac{d^4k}{(2\pi)^4}\frac{\pi\theta\left(k_F - |\mathbf{k}|\right)\theta\left(\bar{k}^0\right)}{E_k^*}\delta\left(\bar{k}^0 - E_k^*\right) \\ &\times\left\{\frac{\mathcal{T}^{LL'}(k, k+q)}{\left(\bar{k}+q\right)^2 - M^{*2} + i\epsilon} + \frac{\mathcal{T}^{LL'}(k-q, k)}{\left(\bar{k}-q\right)^2 - M^{*2} + i\epsilon}\right\} \\ &+ i\int \frac{d^4k}{(2\pi)^4}\frac{\pi^2\theta\left(k_F - |\mathbf{k}|\right)\theta\left(k_F - |\mathbf{k}+\mathbf{q}|\right)\theta\left(\bar{k}^0\right)\theta\left(\bar{k}^0 + q^0\right)}{E_k^* E_{k+q}^*} \\ &\times\delta\left(\bar{k}^0 - E_k^*\right)\delta\left(\bar{k}^0 + q^0 - E_{k+q}^*\right)\mathcal{T}^{LL'}(k, k+q),\end{aligned} \tag{2.124}$$

where

$$\mathcal{T}^{LL'}(k, k+q) = \mathrm{Tr}\left[\lambda^L G^H(k)\overline{\lambda^{L'}}G^H(k+q)\right], \tag{2.125}$$

$$\mathcal{T}^{LL'}(k-q, k) = \mathrm{Tr}\left[\lambda^L G^H(k-q)\overline{\lambda^{L'}}G^H(k)\right]. \tag{2.126}$$

Expressions for the traces are shown in Appendix C.1.

Here Π_D consists of three pieces: Π_{FD}, Π_{DF} and Π_{DD}. These terms originate from the polarization of the Fermi sea. The first two contain only one density-dependent contribution and describe particle-hole excitations and the Pauli blocking of nucleon-antinucleon excitations. Π^{DD} cancels Pauli-forbidden particle-hole excitations contained in these terms [39].

Π_{FF} (also know as the vacuum polarization) originates from the polarization of the Dirac sea. It is explicitly density-independent although implicitly it does depend on the density due to the presence of M^*. It describes $\mathrm{N\bar{N}}$ excitations, is divergent and has to be regularized and renormalized [31, 39]. The imaginary part of this piece vanishes for spacelike momentum transfers

and where $q_\mu^2 < 4M^{*2}$ (the threshold for nucleon-antinucleon production). The real part of Π_{FF} describes the virtual excitation of nucleon-antinucleon pairs. In a calculation based on the MFT ground state, where the vacuum contributions to the self-energies are ignored, it is consistent to ommit the vacuum polarization completely [39, 69]. Inclusion thereof leads to the so-called RHA polarization and renormalized RPA. The difference between the lowest-order MFT and RHA Hartree polarizations therefore originate from the different self-consistent masses of the nucleons (see Appendix B). The differences in RPA based on MFT and RHA is further enhanced by the inclusion of Π_{FF} for RHA and the different meson couplings and masses.

Note that the Pauli-blocking of nucleon-antinucleon pairs present in Π_D is retained in the MFT approximation, amongst other, to satisfy current conservation [40, 44, 69].

2.6.3.1 Density-dependent polarization

Since both the real and imaginary parts of Π^D contribute to the polarization we now turn to the calculation of these quantities. In Eq. (2.124) the integral over k^0 can be performed by making a shift of variables from k^0 to $\bar{k}^0$. Note that this eliminates the constant vector potential of the mean-field leaving the only traces of the relativistic ground state dynamics in the effective mass [2].

To proceed with the integrals over the traces (see Tables C.1 to C.5) we construct $q'^\eta = \left(q^0, 0, 0, |\mathbf{q}|\right)$ by applying a rotation operator to $q^\mu = (q^0, \mathbf{q})$ (where $\mathbf{q}$ is the integration variable of the three dimensional integral in Eq. (2.48)). By identifying the Euler angles as the angles specified by the $\mathbf{q}$ i.e.

$$\beta = \theta_q, \quad \alpha = \phi_q,$$

we can define a rotation operator

$$\begin{aligned} R(\alpha,\beta) = R_z(\alpha)R_y(\beta) &= \begin{bmatrix} 1 & 0 & 0 & 0 \\ 0 & \cos\alpha & -\sin\alpha & 0 \\ 0 & \sin\alpha & \cos\alpha & 0 \\ 0 & 0 & 0 & 1 \end{bmatrix} \begin{bmatrix} 1 & 0 & 0 & 0 \\ 0 & \cos\beta & 0 & \sin\beta \\ 0 & 0 & 1 & 0 \\ 0 & -\sin\beta & 0 & \cos\beta \end{bmatrix} \\ &= \begin{bmatrix} 1 & 0 & 0 & 0 \\ 0 & \cos\alpha\cos\beta & -\sin\alpha & \cos\alpha\sin\beta \\ 0 & \sin\alpha\cos\beta & \cos\alpha & \sin\alpha\sin\beta \\ 0 & -\sin\beta & 0 & \cos\beta \end{bmatrix}. \end{aligned} \tag{2.127}$$

If we make the association $\Lambda \equiv R(\alpha,\beta)$ the application of this rotation to $q'^\eta = \left(q^0, 0, 0, |\mathbf{q}|\right)$ can

be written as

$$q^\mu = \Lambda^\mu_\eta q'^\eta$$

$$q = \left(q^0, |\mathbf{q}|\cos\alpha\sin\beta, |\mathbf{q}|\sin\alpha\sin\beta, |\mathbf{q}|\cos\beta\right), \tag{2.128}$$

and similarly for k

$$k^\mu = \Lambda^\mu_\eta k'^\eta, \tag{2.129}$$

which implies, for example, for cases where the choice of LL' leads to 2 Lorentz indices

$$\begin{aligned}\Pi^{\mu\nu}(q) &= \int d^4k\, T^{\mu\nu}(k,q) \\ &= \int d^4k\, T^{\mu\nu}\left(k(k'), q(q')\right) \\ &= \Lambda^\mu_\eta \Lambda^\nu_\delta \int d^4k'\, T'^{\eta\delta}(k', q') \\ &= \Lambda^\mu_\eta \Lambda^\nu_\delta \Pi'^{\eta\delta}(q').\end{aligned} \tag{2.130}$$

Since we are integrating over all k' we can make the replacement $k' \to k$. The expressions for the integrands $T^{LL'}$ are invariant under spatial rotation (see Eq. (2.124) as well as Appendix C.1), implying that $T'^{LL'} = T^{LL'}$ and we can therefore conclude that

$$\Pi^{\mu\nu}(q) = \Lambda^\mu_\eta \Lambda^\nu_\delta \Pi^{\eta\delta}(q'). \tag{2.131}$$

Clearly this can be extended to the other polarizations. Thus, we can calculate the polarization tensors in a rotated coordinate system ($\mathbf{q}'$-space) where $\mathbf{q}'$ lies along the $\hat{z}$-axis of $\mathbf{k}$-integration. Rotation can then be used to obtain the polarizations in the original $\mathbf{q}$-space. Further discussion relates to the calculation in $\mathbf{q}'$-space. Note that, what we denote as q in the following, is therefore in actual fact q'.

2.6.3.1.1 Real part of the polarization The real part of $\Pi_D^{LL'}$ is obtained by applying the Cauchy Principal Value theorem

$$\frac{1}{\omega \pm i\epsilon} = \mathcal{P}(\omega) \mp i\pi\delta(\omega) \tag{2.132}$$

and can be written as

$$\begin{aligned}\mathrm{Re}\left\{\Pi_D^{LL'}\right\} &= \frac{1}{16\pi^3}\mathcal{P}\int_0^\infty d^3k \frac{\theta\left(k_F - |\mathbf{k}|\right)}{E_k^*}\left\{\frac{\mathcal{T}^{LL'}(k, k+q)}{q_\mu^2 + 2k\cdot q} + \frac{\mathcal{T}^{LL'}(k-q, k)}{q_\mu^2 - 2k\cdot q}\right\}_{k^0 = E_k^*} \\ &= \frac{1}{16\pi^3}\mathcal{P}\int_0^{k_F} d|\mathbf{k}| \int_0^\pi d\theta \int_0^{2\pi} d\phi\, \sin\theta \frac{\mathbf{k}^2}{E_k^*}\left\{\frac{\mathcal{T}^{LL'}(k, k+q)}{q_\mu^2 + 2k\cdot q} + \frac{\mathcal{T}^{LL'}(k-q, k)}{q_\mu^2 - 2k\cdot q}\right\}_{k^0 = E_k^*} \\ &= \frac{1}{16\pi^3}\mathcal{P}\int_0^{k_F} d|\mathbf{k}|\, \frac{\mathbf{k}^2}{E_k^*} I_\Omega^{LL'}(k,q).\end{aligned} \tag{2.133}$$

The angular part, $I_{\Omega}^{LL'}(k,q)$, can be calculated analytically using the following properties:

- integration over the angle ϕ results in zero contributions from terms containing linear combinations of k^1 and k^2,
- $\left(k^1\right)^2$ or $\left(k^2\right)^2$ can be rewritten as $\frac{1}{2}\mathbf{k}^2\left(1-\cos^2\theta\right)$ since integration over ϕ of these factors yield the same result,
- $k\cdot q = E_k^* q^0 - |\mathbf{k}||\mathbf{q}|\cos\theta$,
- any terms containing q^1 or q^2 are trivially 0 because of our choice for q^μ.

The remaining terms in the integral are all independent of ϕ and we can therefore write

$$I_{\Omega}^{LL'} = 2\pi I_{\theta}^{LL'}. \tag{2.134}$$

Results for $I_{\theta}^{LL'}$ are shown in Appendix C.4. The radial integral is performed numerically.

2.6.3.1.2 Imaginary part of the polarization Application of Eq. (2.132) to obtain the imaginary part of $\Pi_D^{LL'}$ results in

$$\mathrm{Im}\left\{\Pi_D^{LL'}\right\} = Im_1 + Im_2, \tag{2.135}$$

with

$$\begin{aligned} Im_1 = &-\frac{1}{4}\int \frac{d^4k}{(2\pi)^2}\frac{\theta\left(k_F-|\mathbf{k}|\right)\theta\left(\bar{k}^0\right)}{E_k^*}\delta\left(\bar{k}^0-E_k^*\right) \\ &\times\left\{\delta\left[\left(\bar{k}+q\right)^2-M^{*2}\right]\mathcal{T}^{LL'}(k,k+q)+\delta\left[\left(\bar{k}-q\right)^2-M^{*2}\right]\mathcal{T}^{LL'}(k-q,k)\right\}, \end{aligned} \tag{2.136}$$

$$\begin{aligned} Im_2 = &\int \frac{d^4k}{(2\pi)^2}\frac{\theta\left(k_F-|\mathbf{k}|\right)\theta\left(k_F-|\mathbf{k}+\mathbf{q}|\right)\theta\left(\bar{k}^0\right)\theta\left(\bar{k}^0+q^0\right)}{4E_k^*E_{k+q}^*} \\ &\times\delta\left(\bar{k}^0-E_k^*\right)\delta\left(\bar{k}^0+q^0-E_{k+q}^*\right)\mathcal{T}^{LL'}(k,k+q). \end{aligned} \tag{2.137}$$

Next we use the identity

$$\delta\left[\left(\bar{k}\pm q\right)^2-M^{*2}\right] = \frac{\delta\left(\bar{k}^0\pm q^0-E_{k\pm q}^*\right)+\delta\left(\bar{k}^0\pm q^0+E_{k\pm q}^*\right)}{2E_{k\pm q}^*}, \tag{2.138}$$

where we have used the fact that

$$E_{k+q}^{*2} = (\mathbf{k}+\mathbf{q})^2 + M^{*2} \tag{2.139}$$

to rewrite Eq. (2.136) as

$$Im_1 = -\frac{1}{8}\int \frac{d^4k}{(2\pi)^2}\frac{\theta\left(k_F-|\mathbf{k}|\right)\theta\left(\bar{k}^0\right)}{E_k^*}\delta\left(\bar{k}^0-E_k^*\right)$$
$$\times\left\{\frac{\delta\left(\bar{k}^0+q^0-E_{k+q}^*\right)}{E_{k+q}^*}\mathcal{T}^{LL'}\left(k,k+q\right)+\frac{\delta\left(\bar{k}^0-q^0-E_{k-q}^*\right)}{E_{k-q}^*}\mathcal{T}^{LL'}\left(k-q,k\right)\right\}. \quad (2.140)$$

Here the second term originating from Eq. (2.138) can be disregarded since the step function allows $\bar{k}^0$ values larger than zero only. Next we write Eq. (2.137) in a similar form by dividing it into two equal parts and replacing k by $k-q$ in the second part

$$Im_2 = \frac{1}{8}\int \frac{d^4k}{(2\pi)^2}\frac{\theta\left(k_F-|\mathbf{k}|\right)\theta\left(\bar{k}^0\right)}{E_k^*}\delta\left(\bar{k}^0-E_k^*\right)$$
$$\times\left\{\frac{\delta\left(\bar{k}^0+q^0-E_{k+q}^*\right)}{E_{k+q}^*}\theta\left(k_F-|\mathbf{k}+\mathbf{q}|\right)\theta\left(\bar{k}^0+q^0\right)\mathcal{T}^{LL'}\left(k,k+q\right)\right.$$
$$\left.+\frac{\delta\left(\bar{k}^0-q^0-E_{k-q}^*\right)}{E_{k-q}^*}\theta\left(k_F-|\mathbf{k}-\mathbf{q}|\right)\theta\left(\bar{k}^0-q^0\right)\mathcal{T}^{LL'}\left(k-q,k\right)\right\}. \quad (2.141)$$

Adding Eq. (2.140) to Eq. (2.141) and integrating over $\bar{k}_0$ gives

$$Im\left\{\Pi_D^{LL'}\right\} = Im_A + Im_B,$$

$$Im_A = -\frac{1}{8}\int \frac{d^3k}{(2\pi)^2}\frac{\theta\left(k_F-|\mathbf{k}|\right)\theta\left(E_{k+q}^*-q^0\right)\theta\left(|\mathbf{k}+\mathbf{q}|-k_F\right)}{E_k^*E_{k+q}^*}$$
$$\times\delta\left(E_{k+q}^*-q^0-E_k^*\right)\mathcal{T}^{LL'}\left(k,k+q\right)_{\bar{k}^0=E_{k+q}^*-q^0}, \quad (2.142)$$

$$Im_B = -\frac{1}{8}\int \frac{d^3k}{(2\pi)^2}\frac{\theta\left(k_F-|\mathbf{k}|\right)\theta\left(E_{k-q}^*\right)\theta\left(|\mathbf{k}-\mathbf{q}|-k_F\right)}{E_k^*E_{k-q}^*}$$
$$\times\delta\left(E_{k-q}^*+q^0-E_k^*\right)\mathcal{T}^{LL'}\left(k-q,k\right)_{\bar{k}^0=E_{k-q}^*+q^0}, \quad (2.143)$$

where use was made of the fact that the energy of the scattered nucleon is always positive. These integrals can be simplified by using

$$E_k^{*2} = \mathbf{k}^2 + M^{*2} \quad (2.144)$$

and therefore from Eq. (2.139) that

$$E^{*2}_{k\pm q} = (\mathbf{k} \pm \mathbf{q})^2 + M^{*2}$$
$$= E^{*2}_k \pm 2|\mathbf{k}||\mathbf{q}| \cos\theta_\pm + \mathbf{q}^2, \tag{2.145}$$
$$\cos\theta_\pm = \frac{\pm E^{*2}_{k\pm q} \mp E^{*2}_k - \mathbf{q}^2}{2|\mathbf{k}||\mathbf{q}|}. \tag{2.146}$$

By making the following subtitutions:

$$|\mathbf{k}| \to E^*_k, \tag{2.147}$$
$$\cos\theta_\pm \to E^*_{k\pm q}, \tag{2.148}$$

Eq. (2.142) is rewritten in spherical coordinates using

$$\int d^3k = \int_0^{k_F} \mathbf{k}^2 dk \int_{-1}^{1} d|cos\theta_+| \int_0^{2\pi} d\phi$$
$$= \frac{2\pi}{|\mathbf{q}|} \int dE^*_k dE^*_{k+q} \theta \left[4\left(E^2_k - M^{*2}\right)|\mathbf{q}|^2 - \left(E^{*2}_{k+q} - E^{*2}_k - \mathbf{q}^2\right)^2\right]$$
$$\times \theta\left(E^*_k - M^*\right) \theta(E_F - E^*_k) E^*_k E^*_{k+q} \tag{2.149}$$

and similarly for Eq. (2.143) using

$$\int d^3k = \int_0^{k_F} \mathbf{k}^2 dk \int_{-1}^{1} d|cos\theta_-| \int_0^{2\pi} d\phi$$
$$= \frac{-2\pi}{|\mathbf{q}|} \int dE^*_k dE^*_{k-q} \theta \left[4\left(E^2_k - M^{*2}\right)|\mathbf{q}|^2 - \left(E^{*2}_k - E^{*2}_{k-q} + \mathbf{q}^2\right)^2\right]$$
$$\times \theta\left(E^*_k - M^*\right) \theta(E_F - E^*_k) E^*_k E^*_{k-q}. \tag{2.150}$$

Here the step-function

$$\theta\left[4\left(E^2_k - M^{*2}\right)\mathbf{q}^2 - \left(E^{*2}_{k+q} - E^{*2}_k - \mathbf{q}^2\right)^2\right] \tag{2.151}$$

ensures that $|\cos\theta| \leq 1$ and we have defined

$$E_F = \sqrt{k_F^2 + M^{*2}}. \tag{2.152}$$

This transformation leads to the following changes in the step functions of Eqs (2.142) and (2.143):

$$\theta\left(k_F - |\mathbf{k}|\right) \theta\left(E^*_{k+q} - q^0\right) \theta\left(|\mathbf{k} + \mathbf{q}| - k_F\right) = \theta\left(E_F - E^*_k\right) \theta\left(E^*_{k+q} - q^0\right) \theta\left(E^*_{k+q} - E_F\right), \tag{2.153}$$

$$\theta\left(k_F - |\mathbf{k}|\right) \theta\left(E^*_{k-q}\right) \theta\left(|\mathbf{k} - \mathbf{q}| - k_F\right) = \theta\left(E_F - E^*_k\right) \theta\left(E^*_{k-q}\right) \theta\left(E^*_{k-q} - E_F\right). \tag{2.154}$$

Performing the integrals over $E^*_{k\pm q}$ yields

$$Im_A = -\frac{1}{16\pi|\mathbf{q}|}\int dE^*_k\,\theta\left(E_F - E^*_k\right)\theta\left(E^*_k\right)\theta\left(E^*_k - M^*\right)\theta\left(-E_F + E^*_k + q^0\right)$$
$$\times\,\theta\left(-E^{*2}_k q^2_\mu - M^{*2}\mathbf{q}^2 - E^*_k q^0 q^2_\mu - \frac{q^4_\mu}{4}\right)\mathcal{T}^{LL'}\left(k, k+q\right)_{\bar{k}^0 = E^*_k}, \tag{2.155}$$

$$Im_B = -\frac{1}{16\pi|\mathbf{q}|}\int dE^*_k\,\theta\left(E_F - E^*_k\right)\theta\left(E^*_k - q^0\right)\theta\left(E^*_k - M^*\right)\theta\left(-E_F + E^*_k - q^0\right)$$
$$\times\,\theta\left(-E^{*2}_k q^2_\mu - M^{*2}\mathbf{q}^2 + E^*_k q^0 q^2_\mu - \frac{q^4_\mu}{4}\right)\mathcal{T}^{LL'}\left(k-q, k\right)_{\bar{k}^0 = E^*_k}. \tag{2.156}$$

The step-functions in Eq. (2.156) require that E_k be both below and above the Fermi surface. The contribution of this integral is therefore zero and we can conclude that

$$\mathrm{Im}\left\{\Pi^{LL'}_D\right\} = -\frac{1}{16\pi|\mathbf{q}|}\int dE^*_k\,\theta\left(E_F - E^*_k\right)\theta\left(E^*_k - M^*\right)\theta\left(-E_F + E^*_k + q^0\right)$$
$$\times\,\theta\left(-E^{*2}_k q^2_\mu - M^{*2}\mathbf{q}^2 - E^*_k q^0 q^2_\mu - \frac{q^4_\mu}{4}\right)\mathcal{T}^{LL'}\left(k, k+q\right)_{\bar{k}^0 = E^*_k}. \tag{2.157}$$

This integral can be solved analytically if use is made of the following properties:

- The θ-functions impose limits on the integral as follows [3, 70, 71]:

$$E_{\mathrm{upper}} = E_F, \tag{2.158}$$

$$E_{\mathrm{max}} = \max\left[M^*, E_{\mathrm{upper}} - q^0, \frac{1}{2}\left(-q^0 + |\mathbf{q}|\sqrt{1 - \frac{4M^{*2}}{q^2_\mu}}\right)\right], \tag{2.159}$$

$$E_{\mathrm{lower}} = \min\left[E_{\mathrm{max}}, E_{\mathrm{upper}}\right]. \tag{2.160}$$

- $\mathbf{k}\cdot\mathbf{q} = E^*_k q^0 - k\cdot q = E^*_k q^0 + \frac{1}{2}q^2_\mu$, which follows from Eq. (2.146) and the subsequent integral over E_{k+q}.

Note that in this formalism, the Lorentz indices have the same position (contravariant) as the L and L' indices.

As an example we now examine the $LL' = SS$ polarization ($\overline{\lambda^{L'}} = \lambda^L = I_4$). The trace of Eq. (2.125) is given by $4\left(M^{*2} + k^2 + k\cdot q\right)$. Following the steps outlined above it is rewritten as follows:

$$\mathcal{T}^{SS}\left(k, k+q\right) = 8M^{*2} + 4\left(\bar{k}^0 q^0 - \mathbf{k}\cdot\mathbf{q}\right)$$
$$= 8M^{*2} + 4\left(E^*_k q^0 - E^*_k q^0 - \frac{1}{2}q^2_\mu\right)$$
$$= 8M^{*2} - 2q^2_\mu. \tag{2.161}$$

Eq. (2.157) therefore becomes

$$\mathrm{Im}\left\{\Pi_D^{SS}\right\} = -\frac{1}{16\pi|\mathbf{q}|}\int dE_k^*\,\theta\left(E_F - E_k^*\right)\theta\left(E_k^*\right)\theta\left(-E_F + E_k^* + q^0\right)$$
$$\times\,\theta\left(-E_k^{*2}q_\mu^2 - M^{*2}\mathbf{q}^2 - E_k^* q^0 q_\mu^2 - \frac{q_\mu^4}{4}\right)\left(8M^{*2} - 2q_\mu^2\right). \tag{2.162}$$

Performing the integral over E_k^* leads to the final expression

$$\mathrm{Im}\left\{\Pi_D^{SS}\right\} = -\frac{1}{8\pi|\mathbf{q}|}\left(4M^{*2} - q_\mu^2\right)\left(E_{\mathrm{upper}} - E_{\mathrm{lower}}\right) \tag{2.163}$$

as also shown in [3, 39, 43].

Imaginary parts of the polarizations are shown in Appendix C.3.

2.6.3.2 Vacuum polarization

The renormalized nucleon-antinucleon contribution to the polarization tensor in nuclear matter is calculated in Ref. [72]:

$$\Pi_{FF}^{SS} = \frac{3}{2\pi^2}\left\{M^2 + 3M^{*2} - 4M^*M - \frac{1}{6}q_\mu^2\right.$$
$$\left. - \int_0^1 d\alpha\ \left[M^{*2} - q_\mu^2\alpha(1-\alpha)\ln\left[\left(M^{*2} - q_\mu^2\alpha(1-\alpha)\right)/M^2\right]\right]\right\}, \tag{2.164}$$

$$\Pi_{FF}^{VV} = \left(-g^{\mu\nu} + \frac{q^\mu q^\nu}{q_\mu^2}\right)\frac{q_\mu^2}{\pi^2}\int_0^1 d\alpha\,\alpha(1-\alpha)\ln\left[\left(M^{*2} - q_\mu^2\alpha(1-\alpha)\right)/M^2\right], \tag{2.165}$$

where a renormalization point of $q_\mu^2 \approx 0$ is assumed since in RHA the parameters are fitted to describe mean meson fields in nuclear matter and not to meson-nucleon scattering. Note that the mixed scalar-vector vacuum polarization vanishes in nuclear matter [41].

2.6.4 Random-phase approximation polarization

In the Hartree approximation the residual interaction of the particle-hole pair created in the nucleus by the external probe is neglected [41]. The RPA takes this interaction into account by summing the uncorrelated Hartree responses (ring diagrams) to all orders [53]. The particle-hole or nucleon-antinucleon pair that is excited in the nucleus travels through the many-body medium and interacts with the self-consistent mean-field. Since the fitting of bulk nuclear properties constrains only isoscalar particle-hole interactions significantly [40] and to demonstrate the effect of RPA, we restrict our calculation to isoscalar excitations. Note that although direct transitions to particle-antiparticle states are forbidden in the Hartree approximation for space-like momentum transfers, these states can affect quantities such as transition strength through virtual polarization [73] if one examines the RHA response.

The present calculation requires only the polarization calculated by summing the lowest order (uncorrelated) isoscalar polarizations to infinite order:

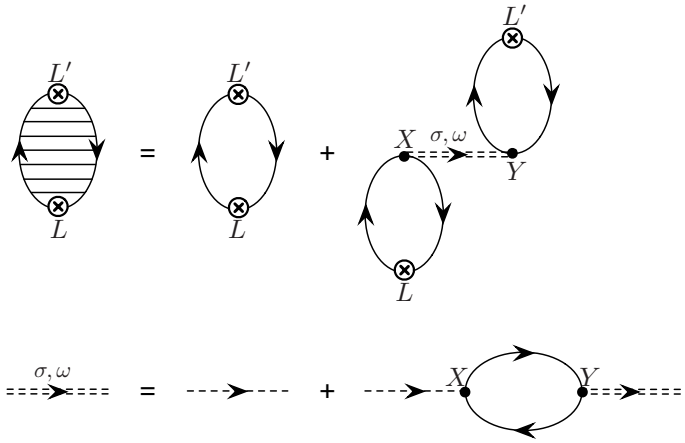

Figure 2.4: Diagrammatic representation of the RPA summation [2] and the Dyson's equation for the isoscalar interaction.

$$\tilde{\Pi}^{LL'} = \Pi^{LL'} + \Pi^{LS} D^{(\sigma)}_{SS} \Pi^{SL'} + \Pi^{LV} D^{(\omega)}_{VV} \Pi^{VL'} + \Pi^{LS} D^{(\sigma)}_{SS} \Pi^{SX} D_{XX} \Pi^{XL'} + \Pi^{LV} D^{(\omega)}_{VV} \Pi^{VY} D_{YY} \Pi^{YL'} ..., \tag{2.166}$$

where the meson-nucleon couplings are fully specified in the QHD-I interaction Lagrangian: I_4 (for the scalar σ meson) and γ^μ (for the vector ω meson). The X and Y vertices in Eq. (2.166) can therefore only refer to S and V. Here the residual particle-hole interactions are written in terms of $\sigma + \omega$ contributions:

$$D^{(\sigma)}_{SS}(\mathbf{q}, \omega) = D^{(\sigma)}(q) = g_s^2 \Delta^0(q) = \frac{g_s^2}{q_\mu^2 - m_s^2}, \tag{2.167}$$

$$D^{(\omega)}_{VV}(\mathbf{q}, \omega) = D^{(\omega)}_{\alpha\beta}(q) = \left(-g_{\alpha\beta} + \frac{q_\alpha q_\beta}{m_v^2} \right) \frac{g_v^2}{q_\mu^2 - m_v^2}. \tag{2.168}$$

Note that in nuclear matter the ω meson always couples to a conserved baryon current (i.e. $q_\mu \Pi^{\mu\nu} = 0$) and the $q_\alpha q_\beta$ term will therefore not contribute to the RPA reponse [43, 69].

Eq. (2.166) can be written as

$$\tilde{\Pi}^{LL'}(q) = \Pi^{LL'}(q) + \Pi^{Li}(q)\, \tilde{D}_{ij}(q)\, \Pi^{jL'}(q), \tag{2.169}$$

where $\tilde{D}$ is known as the medium-modified interaction [2] and can be viewed as the modification of the meson propagators due to coupling to nuclear excitations [69] (see Appendix B.2.3). Here latin indices i and j denote the elementary coupling of a nucleon to a meson (i.e. σ ($i = -1$) and ω ($i = 0,\ 1,\ 2,\ 3$)). $\tilde{D}$ contains all the RPA dynamics and satisfies the following Dyson's equation (see Fig. 2.4):

$$\tilde{D}_{ij}(q) = D^0_{ij}(q) + D^0_{ik}(q)\, \Pi^{kl}_0(q)\, \tilde{D}_{lj}(q) \tag{2.170}$$

or as the solution of a 5×5 matrix equation

$$\tilde{D} = (1 - D^0\Pi_0)^{-1} D^0, \tag{2.171}$$

where the free-space interaction matrix D^0 is given by

$$D^0_{ij} = \begin{bmatrix} D^{(\sigma)} & 0 \\ 0 & D^{(\omega)}_{\alpha\beta} \end{bmatrix}. \tag{2.172}$$

Since the elementary coupling of the nucleon to the σ and ω mesons have been chosen as the bare scalar and vector couplings and mixing of scalar and vector polarizations can occur in the medium, the mixed polarization matrix Π_0 used in the evaluation of the medium-modified interaction of Eq. (2.171) is given by

$$\Pi^{ij}_0 = \begin{bmatrix} \Pi^{SS} & \Pi^{SV} \\ \Pi^{VS} & \Pi^{VV} \end{bmatrix}, \tag{2.173}$$

where the individual Hartree components are calculated according to the procedure outlined in Section 2.6.3. We can therefore identify

$$i = -1 \Leftrightarrow S, \tag{2.174}$$

$$i = 0,\ 1,\ 2,\ 3 \Leftrightarrow V. \tag{2.175}$$

The expressions for these polarizations are exactly the polarization insertions shown in Eqs (B.18), (B.20) and (B.21) (without the couplings). Note that for a MFT calculation these Hartree polarizations would only consist of Π^D whereas a RHA calculation would include Π^{FF} to account for in-medium virtual excitation of nucleon-antinucleon pairs. Current conservation is however satisfied in both cases [39].

As an example we consider the next-to-lowest order polarization given symbolically by the matrix equation

$$\begin{aligned} \Pi^{LX}\tilde{D}^0_{XY}\Pi^{YL'} &= \begin{bmatrix} \Pi^{LS} & \Pi^{LV} \end{bmatrix} \begin{bmatrix} D^{(\sigma)}_{SS} & 0 \\ 0 & D^{(\omega)}_{VV} \end{bmatrix} \begin{bmatrix} \Pi^{SL'} \\ \Pi^{VL'} \end{bmatrix} \\ &= \Pi^{LS} D^{(\sigma)}_{SS} \Pi^{SL'} + \Pi^{LV} D^{(\omega)}_{VV} \Pi^{VL'}, \end{aligned} \tag{2.176}$$

which clearly reproduces the lowest-order correction terms in Eq. (2.166).

Chapter 3

Analysis and results

3.1 Polarizations

3.1.1 Details of implementation

According to Eq. (2.53) only the imaginary parts of the polarizations are needed for the diagonal terms. They are calculated using the polarization expressions shown in Appendix C.3. The expressions for $LL' = SS$, PP, VV and AA agree with those derived in Refs [39] and [43]. The expression for $LL' = TT$ has, to our knowledge, never been published for $\lambda^T = \sigma^{\mu\nu}$ due to the form-factor parametrization ($\lambda^T = {}^{i\sigma^{\mu\nu}q_\mu}/_{2M}$) employed by most authors (see Refs [43] and [47]).

In addition to the imaginary parts discussed above, the expressions for $LL' = SV$, VS, PA and AP agree with those derived in Refs [39] and [43]. Expressions for the imaginary parts for $LL' = VT$, TV, AT and TA have not been published in the form needed here and those for $LL' = ST$, TS, PT and TP have, to our knowledge, not been published. Note, however, that if we multiply or contract the explicit formulae given in Appendix C.3 for these combinations directly with the relevant expressions as used in the pseudovector and form-factor parametrization

$$q^\mu \quad \text{for} \quad L = P, \tag{3.1}$$

$$-q^\mu \quad \text{for} \quad L' = P, \tag{3.2}$$

$$\frac{iq_\mu}{2M} \quad \text{for} \quad L = T, \tag{3.3}$$

$$-\frac{iq_\mu}{2M} \quad \text{for} \quad L' = T, \tag{3.4}$$

where $q^\mu = \left(q^0, 0, 0, |\mathbf{q}|, \right)$, we obtain the following:

- PA

$$\begin{aligned} \mathrm{Im}\left(\Pi'^{PA}\right) &= q^\mu \mathrm{Im}\left(\Pi^{PA}\right) = q^\mu \mathrm{Im}\left(\Pi^\nu\right) \\ &= q^\mu q^\nu \left[-\frac{M^*}{4\pi|\mathbf{q}|}E_1\right], \end{aligned} \tag{3.5}$$

- *AP*

$$\mathrm{Im}\left(\Pi'^{AP}\right) = \mathrm{Im}\left(\Pi^{AP}\right)(-q^{\nu}) = \mathrm{Im}\left(\Pi^{\mu}\right)(-q^{\nu}) = -\mathrm{Im}\left(\Pi'^{PA}\right). \tag{3.6}$$

- *VT*

$$\mathrm{Im}\left(\Pi'^{VT}\right) = \mathrm{Im}\left(\Pi^{VT}\right)\left(-\frac{iq_{\alpha}}{2M}\right) = \mathrm{Im}\left(\Pi^{\mu\nu\alpha}\right)\left(-\frac{iq_{\alpha}}{2M}\right) \tag{3.7}$$

$$\mathrm{Im}(\Pi'^{00}) = \frac{M^{*}|\mathbf{q}|}{8\pi M}E_1, \tag{3.8}$$

$$\mathrm{Im}(\Pi'^{03}) = \frac{q^0}{|\mathbf{q}|}\mathrm{Im}(\Pi'^{00}), \tag{3.9}$$

$$\mathrm{Im}(\Pi'^{30}) = \mathrm{Im}(\Pi'^{03}), \tag{3.10}$$

$$\mathrm{Im}(\Pi'^{33}) = \left[\frac{q^0}{|\mathbf{q}|}\right]^2 \mathrm{Im}(\Pi'^{00}), \tag{3.11}$$

$$\mathrm{Im}(\Pi'^{11}) = \frac{q_{\mu}^2}{|\mathbf{q}|^2}\mathrm{Im}(\Pi'^{00}), \tag{3.12}$$

$$\mathrm{Im}(\Pi'^{22}) = \mathrm{Im}(\Pi'^{11}). \tag{3.13}$$

- *TV*

$$\mathrm{Im}\left(\Pi'^{TV}\right) = \left(\frac{iq_{\alpha}}{2M}\right)\mathrm{Im}\left(\Pi^{TV}\right) = \left(\frac{iq_{\alpha}}{2M}\right)\mathrm{Im}\left(\Pi^{\mu\alpha\nu}\right) = \mathrm{Im}\left(\Pi'^{VT}\right). \tag{3.14}$$

- *TT*

$$\mathrm{Im}\left(\Pi'^{TT}\right) = \left(\frac{iq_{\alpha}}{2M}\right)\mathrm{Im}\left(\Pi^{TT}\right)\left(-\frac{iq_{\beta}}{2M}\right) = \left(\frac{iq_{\alpha}}{2M}\right)\mathrm{Im}\left(\Pi^{\mu\alpha\nu\beta}\right)\left(-\frac{iq_{\beta}}{2M}\right) \tag{3.15}$$

$$\mathrm{Im}(\Pi'^{00}) = \frac{q_{\mu}^2}{8\pi M^2|\mathbf{q}|}\left[E_3 + q^0E_2 + \left(\frac{q_0^2}{4} + \frac{M^{*2}|\mathbf{q}|^2}{q_{\mu}^2}\right)E_1\right], \tag{3.16}$$

$$\mathrm{Im}(\Pi'^{03}) = \frac{q^0}{|\mathbf{q}|}\mathrm{Im}(\Pi'^{00}), \tag{3.17}$$

$$\mathrm{Im}(\Pi'^{30}) = \mathrm{Im}(\Pi'^{03}), \tag{3.18}$$

$$\mathrm{Im}(\Pi'^{33}) = \left[\frac{q^0}{|\mathbf{q}|}\right]^2 \mathrm{Im}(\Pi'^{00}), \tag{3.19}$$

$$\mathrm{Im}(\Pi'^{11}) = -\frac{q_{\mu}^2}{16\pi M^2|\mathbf{q}|^3}\left[q_{\mu}^2E_3 + q^0q_{\mu}^2E_2 + \left(\frac{q_{\mu}^2}{4} - M^{*2}|\mathbf{q}|^2\right)E_1\right], \tag{3.20}$$

$$\mathrm{Im}(\Pi'^{22}) = \mathrm{Im}(\Pi'^{11}). \tag{3.21}$$

These expressions for the imaginary parts correspond exactly to those published in Ref. [43].

Since the cross sections of off-diagonal terms involve the multiplication of three complex quantities, the real parts of the polarizations also play a role. They are calculated numerically according to Eq. (2.133) using the expressions in Appendix C.4. The real parts of the diagonal terms SS and VV also play a role in the RPA where the medium-modified interaction is constructed as a product of three complex matrices. Numerical results for the real parts of SS, SV and VV are in exact agreement with the results obtained when using the analytical expressions published in Ref. [39]. Expressions for the real parts of other terms have, to our knowledge, not been published.

RPA polarizations are calculated according to the procedure outlined in Section 2.6.4. The medium-modified interaction is constructed as a symbolic matrix product in Mathematica and inverted analytically resulting in a 5×5 matrix with non-zero components $\tilde{D}_{ij}$ $(i, j = -1, 0, 1, 2, 3)$ given by

$$\tilde{D}_{-1-1} = \frac{D^{(\sigma)} \left(\Pi^{00} \left(D_{00}^{(\omega)} - f^2 D_{00}^{(\omega)} \right) - 1 \right)}{A}, \tag{3.22}$$

$$\tilde{D}_{-10} = \tilde{D}_{0-1} = -\frac{\Pi^{S0} D^{(\sigma)} D_{00}^{(\omega)}}{A}, \tag{3.23}$$

$$\tilde{D}_{-13} = \tilde{D}_{3-1} = \frac{f \Pi^{S0} D^{(\sigma)} D_{00}^{(\omega)}}{A}, \tag{3.24}$$

$$\tilde{D}_{00} = \frac{D_{00}^{(\omega)} \left(- \left(D^{(\sigma)} \left(\Pi^{S0} \right)^2 + \Pi^{00} - \Pi^{00} \Pi^{SS} D^{(\sigma)} \right) D_{00}^{(\omega)} f^2 + \Pi^{SS} D^{(\sigma)} - 1 \right)}{A}, \tag{3.25}$$

$$\tilde{D}_{03} = \tilde{D}_{30} = \frac{f \left(D^{(\sigma)} \left(\Pi^{S0} \right)^2 + \Pi^{00} - \Pi^{00} \Pi^{SS} D^{(\sigma)} \right) \left(D_{00}^{(\omega)} \right)^2}{A}, \tag{3.26}$$

$$\tilde{D}_{11} = \tilde{D}_{22} = -\frac{D_{00}^{(\omega)}}{\Pi^{22} D_{00}^{(\omega)} + 1}, \tag{3.27}$$

$$\tilde{D}_{33} = \frac{D_{00}^{(\omega)} \left(- \left(D^{(\sigma)} \left(\Pi^{S0} \right)^2 + \Pi^{00} \right) D_{00}^{(\omega)} + \Pi^{SS} D^{(\sigma)} (\Pi^{00} D_{00}^{(\omega)} - 1) + 1 \right)}{A}, \tag{3.28}$$

where

$$A = \Pi^{SS} D^{(\sigma)} - \left(f^2 - 1 \right) \left(D^{(\sigma)} \left(\Pi^{S0} \right)^2 + \Pi^{00} - \Pi^{00} \Pi^{SS} D^{(\sigma)} \right) D_{00}^{(\omega)} - 1, \tag{3.29}$$

$$f = \frac{q^0}{|\mathbf{q}|}. \tag{3.30}$$

Note the following: due to the fact that the PS and PV traces are zero (see Appendix C.1), LL' combinations where one or both vertices are P will have no RPA correction, e.g. $\tilde{\Pi}^{LP} = \Pi^{LP}$.

RPA corrections to the RHA polarization neccesitates the inclusion of the vacuum polarizations in the polarization matrix used to calculate the medium-modified interaction. These are determined using Eqs (2.164) and (2.165). Note that the structure given above for the medium-modified

Table 3.1: Mean-field parameter sets and effective nucleon masses in a nuclear matter approximation to the Walecka model (QHD-I) [31].

Model	g_s^2	g_v^2	m_s (MeV)	m_v (MeV)	M^*/M ($k_F = 1.42$ fm^{-1})
MFT	91.64	136.2	550	783	0.556
RHA	62.89	79.78	550	783	0.718

interaction is still valid since (compare Eqs (C.16) to (C.21) and (C.57) to (C.62))

$$\Pi_{FF}^{03} = \Pi_{FF}^{30} = f\,\Pi_{FF}^{00}, \tag{3.31}$$

$$\Pi_{FF}^{33} = f^2\Pi_{FF}^{00}, \tag{3.32}$$

$$\Pi_{FF}^{22} = \Pi_{FF}^{11}. \tag{3.33}$$

3.1.2 Results

Real and imaginary parts of the independent components of the MFT and RHA polarizations at nuclear saturation density with and without RPA corrections are shown in Fig. 3.1. Note that we avoid the linear and transverse response function formalism [30, 39, 41, 43], since it is not directly applicable to our model. Parameter sets are shown in Table 3.1 and values for M^* were obtained by solving Eqs (B.45) and (B.51) where $M = 939$ MeV.

Since the goal of this project was not explicitly to investigate the role of the different mesons on the Hartree and RPA reponses, we only show a few plots for the polarizations where the general difference between free mass, MFT and RHA calculations can be seen. When comparing the results for the Hartree polarizations it becomes evident that with decreasing mass ($M_{\text{free}} > M^*_{\text{RHA}} > M^*_{\text{MFT}}$) the peaks are shifted to larger energy transfer and become wider. It is also clear that the general trend of the RPA is to reduce the magnitude of the polarizations.

3.2 Cross sections

3.2.1 Calculational checks

Since some of the traces involved in the calculation of the polarizations are zero (see Appendix C.1), not all terms in Eq. (2.53) contribute to the cross section. In addition, the terms that do contribute can be divided in three groups according to the symmetries of the hadronic tensors (see Eq. (2.45))

$$\left(H^{LL'}\right)^* = H^{L'L} \tag{3.34}$$

and polarizations tensors (see Appendix C.1) . If we define $Z^{LL'} = F_L(\mathbf{k},\mathbf{K},\mathbf{k}')F^*_{L'}(\mathbf{k},\mathbf{K},\mathbf{k}')H^{LL'}(\mathbf{q})$, these categories are:

- Type 1:

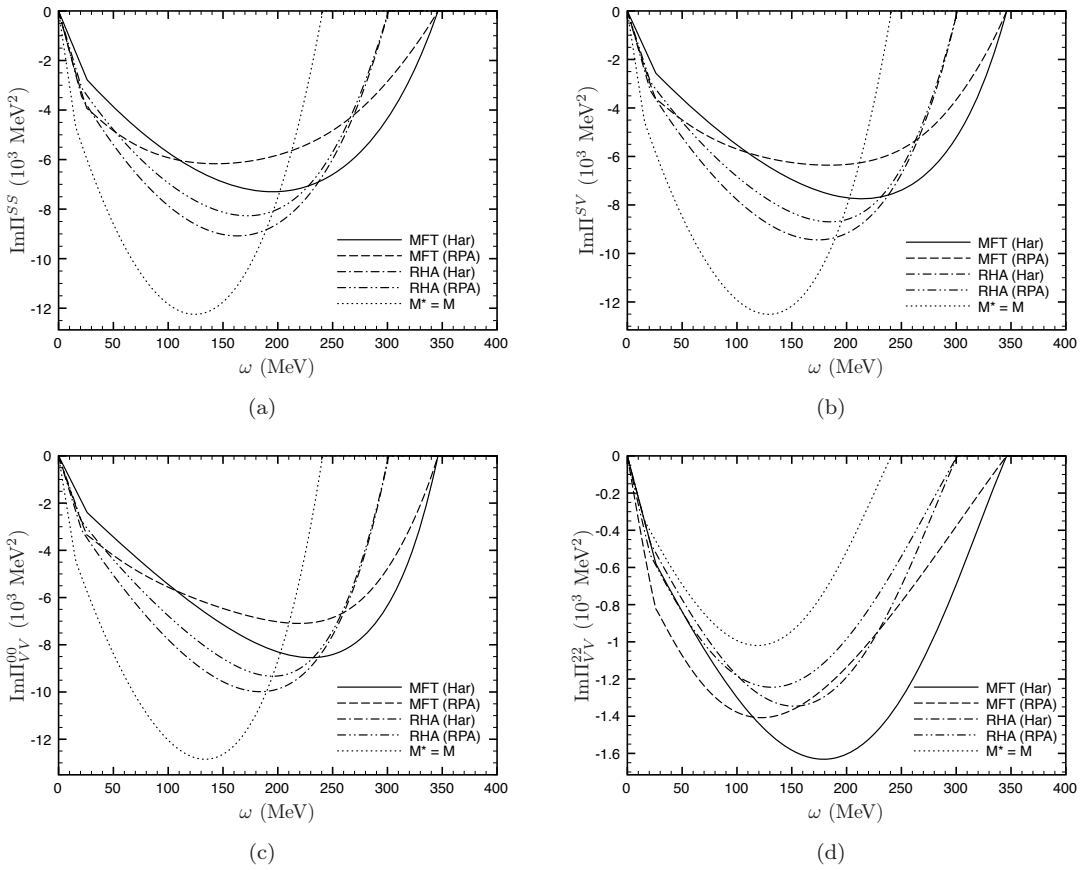

Figure 3.1: Examples of imaginary parts of nuclear matter polarizations at saturation density calculated for the parameters shown in Table 3.1 for $|\mathbf{q}| = 500$ MeV.

$$\begin{aligned} \mathrm{Im}\left\{Z^{LL'}\Pi_{LL'} + Z^{L'L}\Pi_{L'L}\right\} &= \mathrm{Im}\left\{Z^{LL'}\Pi_{LL'} - \left(Z^{LL'}\right)^{*}\Pi_{LL'}\right\} \\ &= 2\mathrm{Im}\left\{Z^{LL'}\right\}\mathrm{Re}\left\{\Pi_{LL'}\right\}, \end{aligned} \tag{3.35}$$

$$LL' = ST,\, VA,\, VT. \tag{3.36}$$

- Type 2:

$$\begin{aligned} \mathrm{Im}\left\{Z^{LL'}\Pi_{LL'} + Z^{L'L}\Pi_{L'L}\right\} &= \mathrm{Im}\left\{Z^{LL'}\Pi_{LL'} + \left(Z^{LL'}\right)^{*}\Pi_{LL'}\right\} \\ &= 2\mathrm{Re}\left\{Z^{LL'}\right\}\mathrm{Im}\left\{\Pi_{LL'}\right\}, \end{aligned} \tag{3.37}$$

$$LL' = SV,\, PT,\, AT,\, AP. \tag{3.38}$$

- Diagonals:

$$\mathrm{Im}\left\{Z^{LL'}\Pi_{LL'} + Z^{L'L}\Pi_{L'L}\right\} = \mathrm{Im}\left\{Z^{LL}\Pi_{LL} + \left(Z^{LL}\right)^{*}\Pi_{LL}\right\}$$

$$= 2\mathrm{Re}\left\{Z^{LL}\right\}\mathrm{Im}\left\{\Pi_{LL}\right\}, \tag{3.39}$$

$$LL' = SS,\ PP,\ VV,\ AA,\ TT. \tag{3.40}$$

The cross section can then be written as

$$\frac{d\sigma}{dE'\,d\Omega'} = -\frac{1}{\pi}\mathcal{K}\int\frac{d^3q}{(2\pi)^3}\sum_{L,L'}\left[\text{Diagonals} + \text{Type 1} + \text{Type 2}\right]. \tag{3.41}$$

This form was used to verify the cross section calculated according to Eq. (2.48).

The implementation of the polarization rotation procedure as outlined in Section 2.6.3.1 was validated by a comparison of plane wave cross sections to results obtained when applying a rotation of the form [74]

$$S(R_\theta) = \cos\frac{\theta}{2} - i\gamma^5\hat{\theta}\cdot\boldsymbol{\alpha}\sin\frac{\theta}{2}, \tag{3.42}$$

(with $\hat{\theta} = \hat{y}$ in our case (see Fig. 2.2)) to the Dirac spinors to obtain the hadronic tensors in a coordinate system where $q^\mu = \left(q^0, 0, 0, |\mathbf{q}|\right)$ which was then contracted with the unrotated polarizations. The results were in complete agreement.

In the case of $(\vec{p}, \vec{p}\,')$ scattering, the amplitudes are half isoscalar and half isovector. This implies that the cross section of Eq. (2.48) can be written as

$$\frac{d\sigma}{dE'\,d\Omega'} = -\frac{1}{\pi}\mathcal{K}\,\mathrm{Im}\left\{\sum_{L,L'=S}^{T}\left(\frac{1}{2}F_L^{\mathrm{isos}} + \frac{1}{2}F_L^{\mathrm{isov}}\right)\right.$$

$$\times\left(\frac{1}{2}F_{L'}^{\mathrm{isos}\,*} + \frac{1}{2}F_{L'}^{\mathrm{isov}\,*}\right)$$

$$\left.\times\int\frac{d^3q}{(2\pi)^3}\,H^{LL'}(\mathbf{q})\,\Pi_{LL'}(\mathbf{q},\omega)\right\}. \tag{3.43}$$

In the Walecka model (QHD-I) nucleons interact through the exchange of isoscalar mesons only and the nucleon propagators do not have isovector components [41]. The cross section can therefore be written in terms of decoupled isoscalar and isovector channels as

$$\frac{d\sigma}{dE'\,d\Omega'} = -\frac{1}{\pi}\mathcal{K}\,\mathrm{Im}\left\{\sum_{L,L'=S}^{T}\left[\frac{1}{4}F_L^{\mathrm{isos}}F_{L'}^{\mathrm{isos}\,*}\int\frac{d^3q}{(2\pi)^3}\,H^{LL'}(\mathbf{q})\,\Pi_{LL'}(\mathbf{q},\omega)\right.\right.$$

$$\left.\left. + \frac{1}{4}F_L^{\mathrm{isov}}F_{L'}^{\mathrm{isov}\,*}\int\frac{d^3q}{(2\pi)^3}\,H^{LL'}(\mathbf{q})\,\Pi_{LL'}(\mathbf{q},\omega)\right]\right\}. \tag{3.44}$$

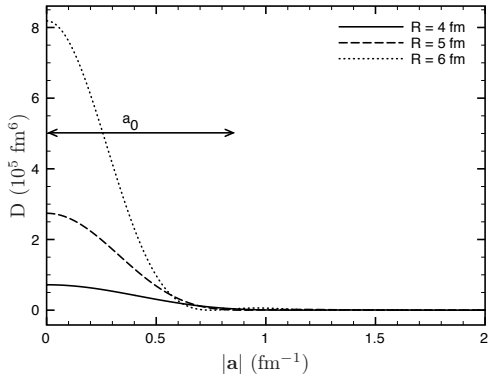

Figure 3.2: $D(|\mathbf{a}|)$ for different values of R.

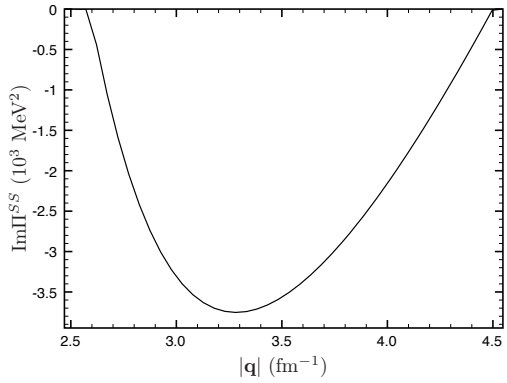

Figure 3.3: $\mathrm{Im}\Pi^{SS}(\mathbf{q},\omega)$ as a function of $|\mathbf{q}|$ in MFT at $\omega = 250$ MeV and $k_F = 0.955$ fm^{-1} (for ^{40}Ca at $T_{\mathrm{lab}} = 500$ MeV).

Since our model at present only takes isoscalar correlations into account, only the isoscalar channel is affected and the cross section with isoscalar RPA corrections is calculated as

$$\left(\frac{d\sigma}{dE'\,d\Omega'}\right)_{\mathrm{RPA}} = -\frac{1}{\pi}\mathcal{K}\,\mathrm{Im}\left\{\sum_{L,L'=S}^{T}\left[\frac{1}{4}F_L^{\mathrm{isos}}F_{L'}^{\mathrm{isos}\,*}\int\frac{d^3q}{(2\pi)^3}\,H^{LL'}(\mathbf{q})\,\tilde{\Pi}_{LL'}(\mathbf{q},\omega)\right.\right.$$
$$\left.\left.+\;\frac{1}{4}F_L^{\mathrm{isov}}F_{L'}^{\mathrm{isov}\,*}\int\frac{d^3q}{(2\pi)^3}\,H^{LL'}(\mathbf{q})\,\Pi_{LL'}(\mathbf{q},\omega)\right]\right\}. \qquad (3.45)$$

3.2.2 Plane wave cross section

3.2.2.1 Details of implementation

If the projectile and ejectile are modelled as plane waves (see Section 2.5.1) the cross section shown in Eq. (2.48) reduces to

$$\frac{d\sigma}{dE'\,d\Omega'} = -\frac{1}{\pi}\mathcal{K}\,\mathrm{Im}\left\{\sum_{L,L'=S}^{T}F_L(\mathbf{k},\mathbf{K},\mathbf{k}')F_{L'}^{*}(\mathbf{k},\mathbf{K},\mathbf{k}')\right.$$
$$\left.\times M^{LL'}(\mathbf{k},\mathbf{k}')\int\frac{d^3q}{(2\pi)^3}\,\Pi_{LL'}(\mathbf{q},\omega)\,D(|\Delta\mathbf{k}-\mathbf{q}|)\right\}. \qquad (3.46)$$

To compute the cross section, the upper radial limit on the integral in Eq. (2.58) has to be known. Clearly the d^3q integral in Eq. (3.46) is a convolution in which the momentum-space volume of the function $D(|\Delta\mathbf{k}-\mathbf{q}|) = D(|\mathbf{a}|)$ is given by

$$V_D = \int d^3a\,D(|\mathbf{a}|) = (2\pi)^3\,\frac{4\pi}{3}R^3 = (2\pi)^3\,V_N, \qquad (3.47)$$

where V_N is the volume of a sphere of radius R.

Upon inspection of Fig. 3.2 it becomes evident that $D(|\mathbf{a}|)$ approaches a Dirac-delta function

in the limit $R \to \infty$. One is therefore tempted to make the replacement (Method A)

$$D(|\Delta\mathbf{k} - \mathbf{q}|) \approx V_D \delta(\Delta\mathbf{k} - \mathbf{q}), \tag{3.48}$$

which results in a cross section of the form

$$\frac{d\sigma}{dE'\, d\Omega'} = -\frac{1}{\pi} \mathcal{K} V_N \mathrm{Im} \left\{ \sum_{L,L'=S}^{T} F_L(\mathbf{k}, \mathbf{K}, \mathbf{k}') F^*_{L'}(\mathbf{k}, \mathbf{K}, \mathbf{k}')\, M(\mathbf{k}, \mathbf{k}')\, \Pi_{LL'}(\mathbf{k} - \mathbf{k}', \omega) \right\}. \tag{3.49}$$

Here the volume can be determinded from the density of nuclear matter ρ_B [31] and the number of nucleons A

$$V_N = \frac{A}{\rho_B} = \frac{3\pi^2 A}{2k_F^3} \tag{3.50}$$

which implies a radius of

$$R = \left(1.125\pi \frac{A}{k_F^3} \right)^{1/3}. \tag{3.51}$$

Alternatively (Method B) this value of R can be used in Eqs (2.58) to perform the d^3r integral analytically using the partial wave expansion of the exponential function (Eq. (2.83)) resulting in

$$D(|\Delta\mathbf{k} - \mathbf{q}|) = \left[4\pi \frac{\sin(|\Delta\mathbf{k} - \mathbf{q}|R) - |\Delta\mathbf{k} - \mathbf{q}|R\cos(|\Delta\mathbf{k} - \mathbf{q}|R)}{|\Delta\mathbf{k} - \mathbf{q}|^3} \right]^2 \tag{3.52}$$

and subsequently the d^3q integral in Eq. (3.46) can be performed numerically. Note that this operation does not pose a problem since (i) the polarizations are non-negligible only for a finite range of $|\mathbf{q}|$ and (ii) the point where $|\Delta\mathbf{k} - \mathbf{q}| = 0$ is easily avoided in a numerical integration scheme. Even if the latter was not the case, the limit is well-defined and given by

$$\lim_{|\mathbf{a}| \to 0} D(|\mathbf{a}|) = \frac{16\pi^2 R^6}{9}. \tag{3.53}$$

A cross section comparison of these two methods is shown in Fig. 3.4.

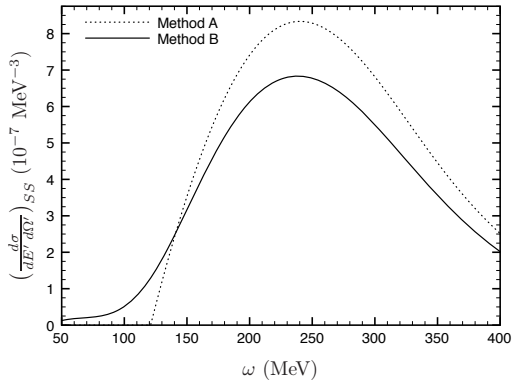

Figure 3.4: Comparison of $LL' = SS$ cross sections calculated using two different methods as discussed in Section 3.2.2.1.

Clearly there is a discrepancy due to an error that is made when approximating $D(|\Delta\mathbf{k} - \mathbf{q}|) \approx V_D \delta(\Delta\mathbf{k} - \mathbf{q})$. This is certainly to be expected since R is far from infinite. Since Eq. (3.46) involves

the convolution of Π and D, this replacement assumes that $\Pi(\mathbf{q},\omega)$ stays relatively constant over the momentum-space radius $a_0 \approx 1$ fm^{-1} as determined by $D(|\mathbf{a}|)$ (see Fig. 3.2). Fig. 3.3 shows, however, that at least for Π^{SS} this is not the case. In the calculation of the plane wave cross section we therefore made use of Method B. Here the limits of the $d|\mathbf{q}|$ integral are fixed by the non-negligible domain of $f(|\mathbf{q}|,\omega)$, where

$$\begin{aligned}\frac{d\sigma}{dE'\,d\Omega'} &= \int_{q_{\min}}^{q_{\max}} d|\mathbf{q}|\; f(|\mathbf{q}|,\omega) \\ &= \int_{q_{\min}}^{q_{\max}} d|\mathbf{q}|\; \left[-\frac{|\mathbf{q}|^2}{8\pi^4}\mathcal{K}\,\mathrm{Im}\left\{ \sum_{L,L'=S}^{T} F_L(\mathbf{k},\mathbf{K},\mathbf{k}')F^*_{L'}(\mathbf{k},\mathbf{K},\mathbf{k}') \right.\right. \\ &\qquad \left.\left. \times \int d\phi_q\, d\theta_q\, \sin\theta_q\, H^{LL'}(|\mathbf{q}|,\theta_q,\phi_q)\,\Pi_{LL'}(|\mathbf{q}|,\theta_q,\phi_q,\omega) \right\} \right]. \end{aligned} \tag{3.54}$$

Fig. 3.5 shows the behaviour of the plane wave $\psi^{(+)}(\mathbf{x},\mathbf{k},\hat{i},s) = e^{i\mathbf{k}\cdot\mathbf{x}}U(\mathbf{k},\hat{i},s)$.

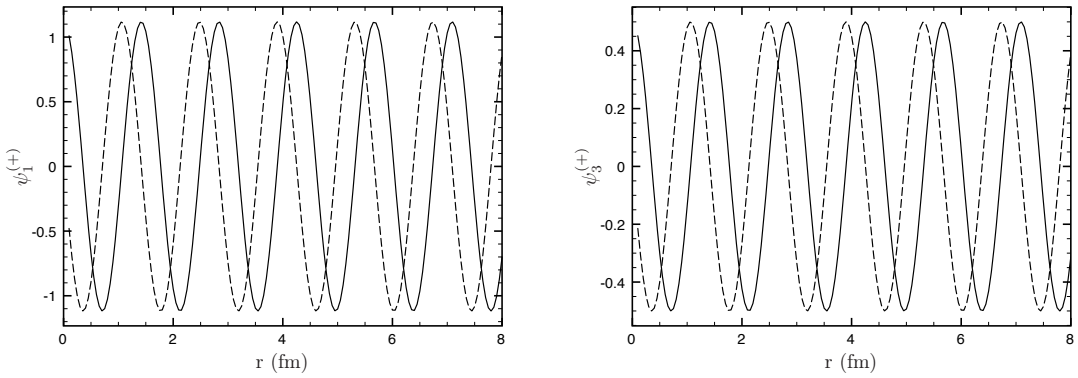

(a) 1st component (b) 3rd component

Figure 3.5: Real (solid) and imaginary (dashed) parts of the first (upper) and third (lower) components of the Dirac plane wave as a function of radius. This wave was generated for $T_{\mathrm{lab}} = 500$ MeV and $(\hat{i},s) = (\hat{l},1/2)$ for ^{40}Ca. θ and ϕ were arbitrarily chosen as $\pi/1.23$ and $2\pi/5.43$ radians respectively. The second and fourth components are zero.

3.2.2.2 Results

LL' contributions to the cross section were calculated using $k_F = 0.955$ fm^{-1} for ^{40}Ca$(\vec{p},\vec{p}\,')$ at a projectile energy $T_{\mathrm{lab}} = 500$ MeV [33] (parameter set shown in Table 3.2). This is lower than the Fermi momentum at saturation density ($k_F = 1.3$ fm^{-1}) since quasielastic proton scattering peaks at the nuclear surface [4, 33] due to a decrease in transmission through the inner nucleus at higher beam energies. For comparison, results were also generated for $k_F = 1.3$ fm^{-1}. All cross section results are plotted in the centre-of-mass frame.

Figs 3.6 to 3.9a and 3.10 to 3.13a show the contributions from the different LL' combinations to the cross section for $k_F = 0.955$ fm^{-1} and $k_F = 1.3$ fm^{-1} respectively. Even though the shape and sign of some of these curves may seem unphysical when (erroneously) interpreted as measurable

Table 3.2: Parameter values and effective masses for different values of k_F [39]. These values are used in the calculation of the cross sections.

Model	g_s^2	g_v^2	m_s (MeV)	m_v (MeV)	M^*/M (1.3 fm^{-1})	M^*/M (0.955 fm^{-1})
MFT	109.626	190.431	520	783	0.541	0.817

cross sections in their own right, it is important to note that these appearances are a result of the parametrization in terms of S, P, V, A and T and that the final measurable cross section (the sum of the LL' contributions) shown in Fig. 3.9b, is in fact consistently positive and exhibits the familiar shape of the quasielastic peak. It is, however, interesting to note that the largest effect on the cross section arises from $LL' = SS, SV, VS, VV, AA$ and TT combinations.

The result for the polarized double differential cross section summed over all LL' (Fig. 3.9b) shows a clear shift to higher energy transfer ($\omega_{\text{peak}} \sim 1/2M^*$), a decrease in the magnitude, and a widening ($\Delta\omega \sim 1/M^*$) of the quasielastic peak associated with a decrease in the mass of the target nucleon when the $M = M^*$ and MFT calculations are compared. This becomes especially evident when comparing the lower density ($k_F = 0.955$ fm^{-1}, $M^* = 0.817M$) and saturation density ($k_F = 1.3$ fm^{-1}, $M^* = 0.541M$) curves. Fig. 3.14 shows how the cross section shifts to higher energy transfer and decreases with increasing scattering angles. These phenomena are consistent with the general features of RIA+RMF models for quasielastic scattering of leptons and hadrons [1, 2, 30, 33, 42, 46].

In addition, the RPA correction further tends to reduce the magnitude of the quasielastic peak in the MFT result due to the attractive particle-hole interaction [46]. This effect increases with target density as is evident from the saturation density results. In addition, Fig. 3.14 shows that the correlations become slightly stronger at lower scattering angles (for similar values of the energy transfer) where momentum transfer is lower. Ref. [39] ascribes this to the damping of meson propagators at large $|\mathbf{q}|$. The impact of isoscalar correlations does not seem to be very large for this specific reaction and kinematics. We comment on this in the conclusion.

3.2.3 Distorted wave cross section

3.2.3.1 Details of implementation

The behaviour of the distorted waves can be seen in Figs 3.15 and 3.16. Here they have been generated according to Eq. (2.68) for zero Coulomb distortions ($\delta_{lj} = 0$) as described in Ref. [3]. Beyond $l_{\max} = 60$ they do not change significantly, however, due to constraints in computational resources, we set $l_{\max} = l'_{\max} = 30$. As can be seen in Fig. 3.16, the first, second and third components of the distorted waves are already in good quantitative agreement with the $l_{\max} = 60$ results. Note that beyond $r = 8$ fm the plane wave behaviour is restored (for ^{40}Ca).

The distorted wave cross section is calculated according to Eq. (2.53) with the hadronic tensor computed according to Eqs (2.76) and (2.85). The numerical complexity of the calculation of the cross section in the distorted wave case cannot be over-emphasized. Strictly speaking the integral is over nine dimensions, namely d^3x, d^3y and d^3q. The primary reason for the numerical complexity is the use of the partial wave expansion of the distorted waves and convergence issues of the multi-dimensional integrals. A brute force approach with Gaussian quadrature and Monte Carlo methods proved cumbersome and did, indeed, lead to poor convergence.

In Eqs (2.86) to (2.89) we showed that the multi-dimensional spatial integrals can be reduced to a one-dimensional radial integral and the two-dimensional angular integrals which reduce to the so-called Gaunt coefficients. These latter quantities exhibit a number of symmetries which aid in the evaluation of the hadronic tensor. Nonetheless, even their calculation is a highly non-trivial matter. The reason for this is that the Gaunt coefficients, in our case, are functions of five input variables. Calculating them by evaluating the surface integral of the spherical harmonics during the cross section calculation is not efficient due in part to the recursion involved in the calculation of the spherical harmonics [75] which need to be calculated for high values of angular momentum, but mostly due to convergence problems in the integration itself (due to highly oscillatory spherical harmonics) which require a high amount of grid points or a high-degree Gaussian quadrature formula [76]. Alternatively the Gaunt coefficients can be calculated beforehand and stored in large arrays. It is easy to show that a straightforward implementation of Eq. (2.90) in, for example, Mathematica, for the three types of coefficients listed in Eqs (2.91) to (2.93) will result in tens of millions of coefficients for $l_{\max} = 30$, many of which are 0 and containing a high degree of duplication due to symmetries that have not been taken into account. Calculating this amount of coefficients is not only extremely time-consuming but also requires a few gigabytes of storage on a physical disk or in memory. We therefore rather made use of the method of Rash and Yu [77, 78] to generate the Gaunt coefficients in Mathematica and implement them in the cross section calculation in Fortran. Here the coefficients are defined as (see also Eq. (A.27))

$$G_{\mathrm{RY}}(l_1m_1|l_2m_2|l_3m_3) = \int d\Omega\, Y_{l_1m_1}(\hat{x})\, Y_{l_2m_2}(\hat{x})\, Y_{l_3m_3}(\hat{x}) = (-1)^{m_2+m_3} G(l_1m_1|l_2m_2|l_3m_3). \tag{3.55}$$

These coefficients are invariant under any permutation of l, m pairs as well as spatial reflection $(m_1, m_2, m_3 \to -m_1, -m_2, -m_3)$. In conjunction with the selection rules similar to those stated in Appendix A.2 this implies that they can be generated for $l_1 \geq l_2 \geq l_3$, $m_3 \geq 0$, $-l_2 \leq m_2 \leq \min(l_1 - m_3, l_2)$ and $m_1 = -m_2 - m_3$. In Fortran they are stored in an array of pointers indexed by l_1, l_2, l_3, m_3 according to

$$\begin{aligned} c &= \sum_{i=0}^{l_1}\sum_{j=0}^{i}\sum_{k=0}^{j} k + \sum_{j}^{l_2}\sum_{k=0}^{j} k + \sum_{k=0}^{l_3} k + m_3 + 1 \\ &= \frac{1}{24} l_1 \left(6 + l_1 \left(11 + l_1 \left(6 + l_1\right)\right)\right) + \frac{1}{6} l_2 \left(2 + l_2 \left(3 + l_2\right)\right) + \frac{1}{2} l_3 \left(l_3 + 1\right) + m_3 + 1 \end{aligned} \tag{3.56}$$

and each of these pointers points to a vector indexed by m_2 according to

$$i = m_2 + l_2 + 1. \tag{3.57}$$

Note that computation time and storage space needed can be greatly reduced if the selection rules are hard-coded. In the end, approximately 400 MB of storage space was required and the once-off calculation of all coefficients was completed in 24 hours on a desktop PC with an Intel Core 2 Duo processor and 4 GB of RAM.

The radial integrals in Eqs (2.86) to (2.89) were evaluated using the standard Gaussian integration subroutine, *gauleg,* fully discussed on page 145 of Ref. [75]. The difficulty here was due to the fact that the distorted upper and lower radial wave functions, g_{lj} and f_{lj} respectively, are not analytical expressions but are stored in large arrays for the different values of l and j and

the kinematical quantity $z = kr$ or $z = k'r$. Convergence for these integrals were obtained for 30 Gaussian grid points for an upper limit of $r = 8$ fm (the range of the nuclear potential for ^{40}Ca).

The method of separating the spatial integrals into radial and angular parts does not work for the momentum integral (d^3q integral) since the polarization tensor does not necessarily exhibit such symmetries. We therefore now face the dilemma of having to calculate a three-dimensional integral where the integrand is a highly complex quantity with a strong oscillatory nature. A number of integration methods [79–82] were explored for this problem but all turned out to be of little practical use. This is where the powerful interpolation and fitting procedures of Matlab became a primary calculational tool. The key point to note is that the three-dimensional integral d^3q can be written as $d^3q = d|\mathbf{q}|\, d\Omega_q$. A straightforward application of the Gaussian integration method would then require N^3 integration points where N is the number of Gaussian integration points needed for one dimension. We can, however, perform the two-dimensional integral over (say) the angular part (N^2 Gaussian grid points) for a certain set of $|\mathbf{q}|$ values, by defining the function $f(|\mathbf{q}|, \omega)$ as shown in Eq. (3.54). Since this function is now defined on a grid of $|\mathbf{q}|$ values we can use an interpolation scheme (be it analytical or a spline method) to calculate $f(|\mathbf{q}|, \omega)$ for any value of $|\mathbf{q}|$. This function is fairly well-behaved and the remaining one-dimensional integral can be performed numerically for a low number of grid points. The whole calculational procedure can be automated with the *cftool* interpolation and fitting package in Matlab. Using this method we have devised a novel calculational procedure to evaluate the distorted wave cross section in a reasonable time. For example, the calculation of the function $f(|\mathbf{q}|, \omega)$ for 40^2 grid points (in the angular space) and one grid point in the $|\mathbf{q}|$ space takes approximately four days on a desktop PC with a 3 GHz Intel Pentium 4 processor and 2 GB of RAM. At this point we employ cluster computing methods, where each cluster PC calculates the cross section for different $|\mathbf{q}|$ and ω values. Distribution of the calculational burden across the cluster PCs enables one to obtain the distorted wave cross section as a function of ω. This emphasizes, once again, the computational difficulty in the evaluation of the distorted wave cross section. By contrast, the complete plane wave cross section requires only 11 hours for evaluation on a single PC. However, the whole procedure is automated and human intervention is only required at the start and at the end to collect the results.

3.2.3.2 Results

The accuracy of the fitting procedure was verified for the plane wave cross section as shown in Figs 3.17 to 3.19 for $T_{\text{lab}} = 500$ MeV, $(\hat{\imath}, s) = (\hat{l}, 1/2)$, $(\hat{\imath}', s') = (\hat{l}', 1/2)$ and $\theta_{\text{cm}} = 40^\circ$ for $^{40}\text{Ca}(\vec{p}, \vec{p}')$. Here we used 40^3 integration points to compute the full three-dimensional integral and $40^2 \times 11$ points for the fitting calculation. All cross section results are plotted in the centre-of-mass frame.

Figs 3.20 to 3.21 show the results of the $40^2 \times 11$ fiting procedure for the RDWIA calculation. From these results it seems that the number of points in $|\mathbf{q}|$ space (11) is sufficient to interpolate the $f(|\mathbf{q}|, \omega)$ reliably due to its relative smoothness. Similarly to the RPWIA calculation shown in Figs 3.17 to 3.19, spline interpolants were used.

From the final result for $LL' = SS$ shown in Fig. 3.22 it is clear that the RDWIA cross section is quenched relative to the RPWIA, even at $l_{\max} = 30$, and that the peak is shifted slightly. The inclusion of RPA correlations lead to further quenching.

The RPWIA cross section results can give guidance when calculating the RDWIA LL' contributions since

- fitting calculations and final results for a specific combination in the RDWIA can be compared immediately to the RPWIA result to check for consistent behaviour,
- RPWIA results show that the LL' combinations can be arranged according to the relative magnitude of their contributions to the cross section. By calculating the LL' contributions with the largest effect on the cross section first, one can obtain a clearer picture of the final RDWIA result fairly early on.

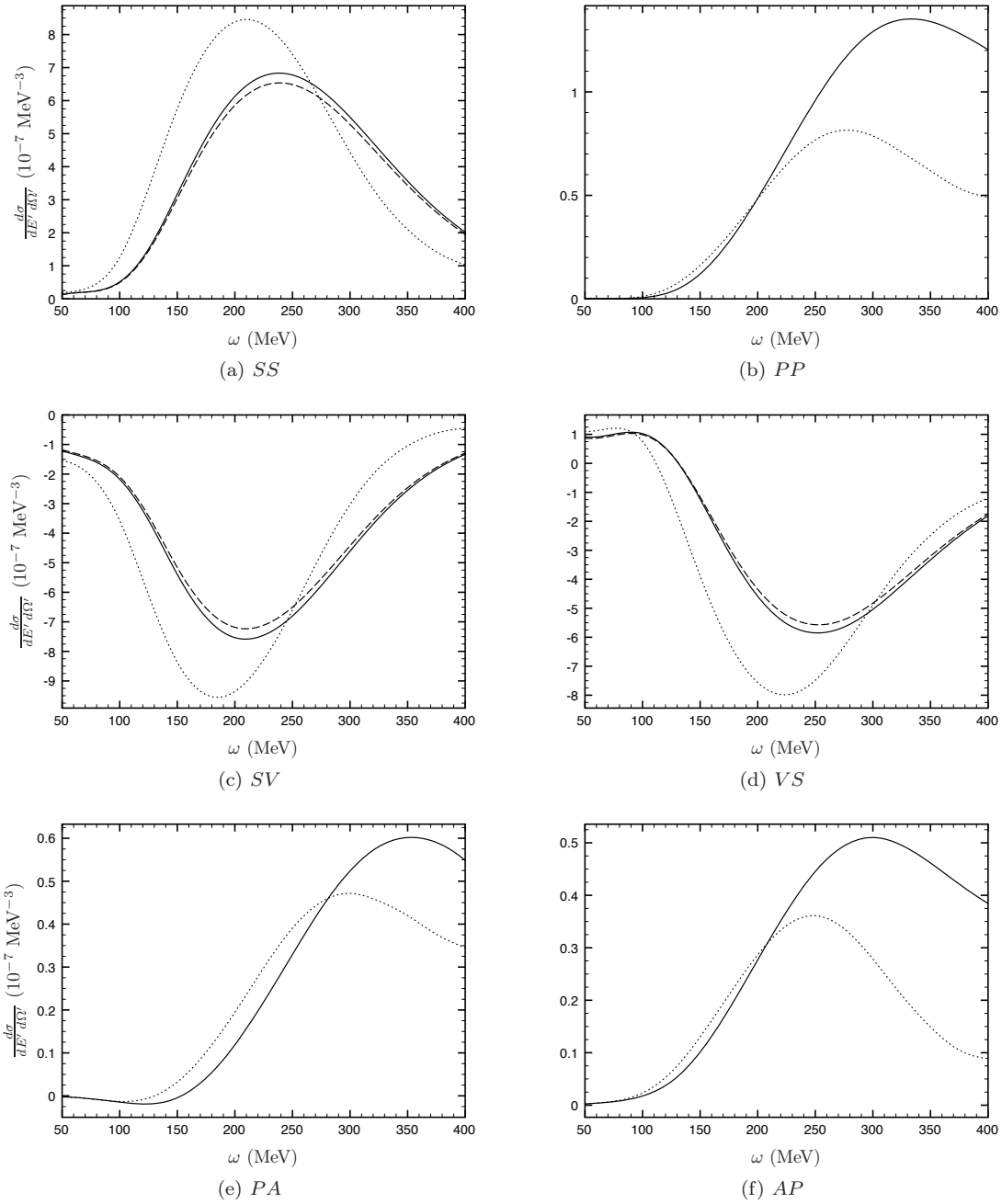

(a) SS (b) PP

(c) SV (d) VS

(e) PA (f) AP

Figure 3.6: Plane wave differential cross sections for LL' combinations as indicated for the reaction ^{40}Ca$(\vec{p},\vec{p}\,')$. In all figures the solid line indicates the MFT (Hartree), the dashed line the MFT (RPA) and the dotted line the $M^* = M$ (Hartree) calculations. Where the RPA result is not shown it coincides with the Hartree result. Here $T_{\rm lab} = 500$ MeV, $k_F = 0.955$ fm^{-1}, $(\hat{i}, s) = (\hat{l}, 1/2)$, $(\hat{i}', s') = (\hat{l}', 1/2)$ and $\theta_{\rm cm} = 40^\circ$.

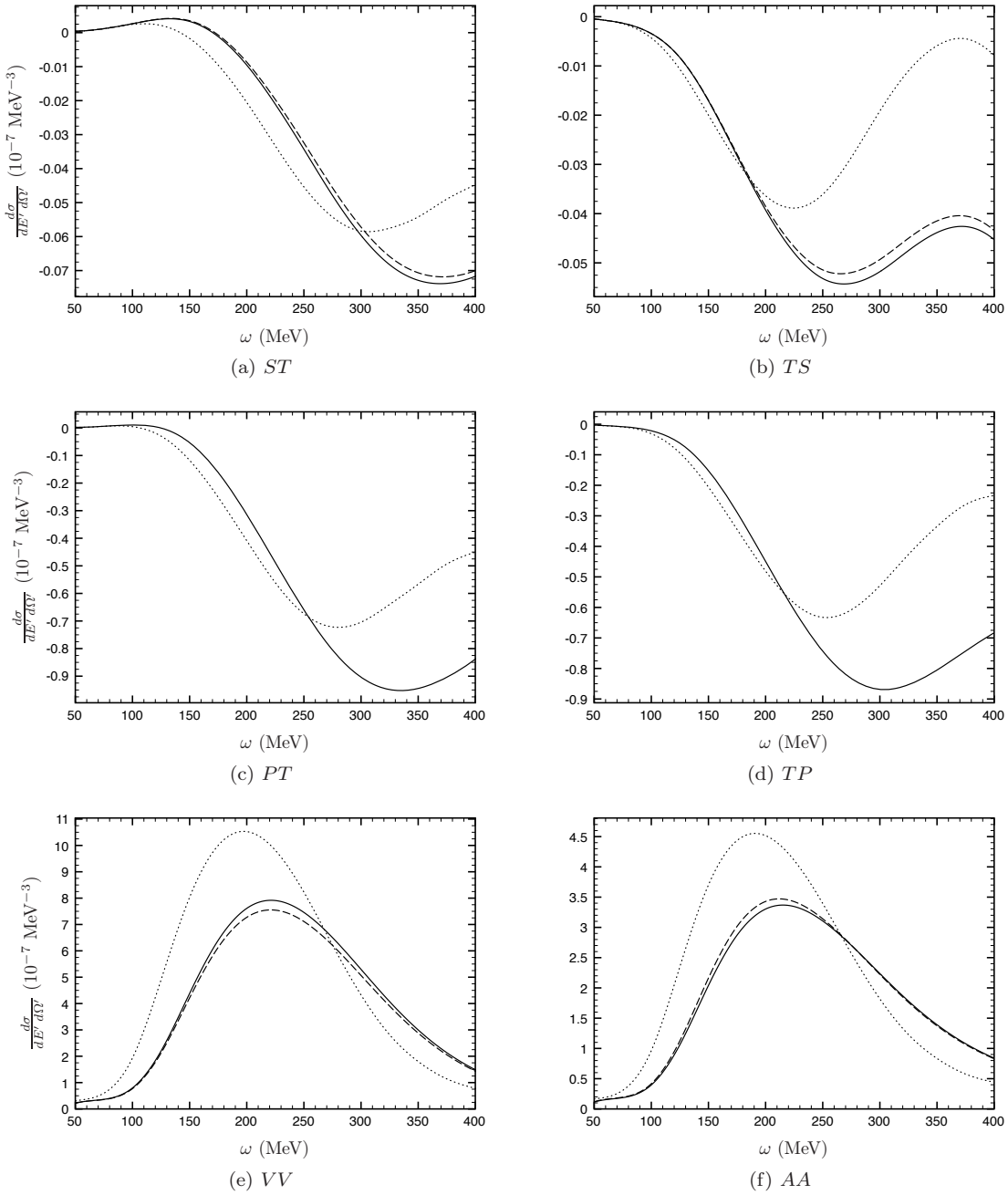

(a) ST (b) TS

(c) PT (d) TP

(e) VV (f) AA

Figure 3.7: Plane wave differential cross sections for LL' combinations as indicated for the reaction $^{40}\mathrm{Ca}(\vec{p},\vec{p}\,')$. In all figures the solid line indicates the MFT (Hartree), the dashed line the MFT (RPA) and the dotted line the $M^* = M$ (Hartree) calculations. Where the RPA result is not shown it coincides with the Hartree result. Here $T_{\mathrm{lab}} = 500$ MeV, $k_F = 0.955$ fm^{-1}, $(\hat{i}, s) = (\hat{l}, 1/2)$, $(\hat{i}', s') = (\hat{l}', 1/2)$ and $\theta_{\mathrm{cm}} = 40^\circ$.

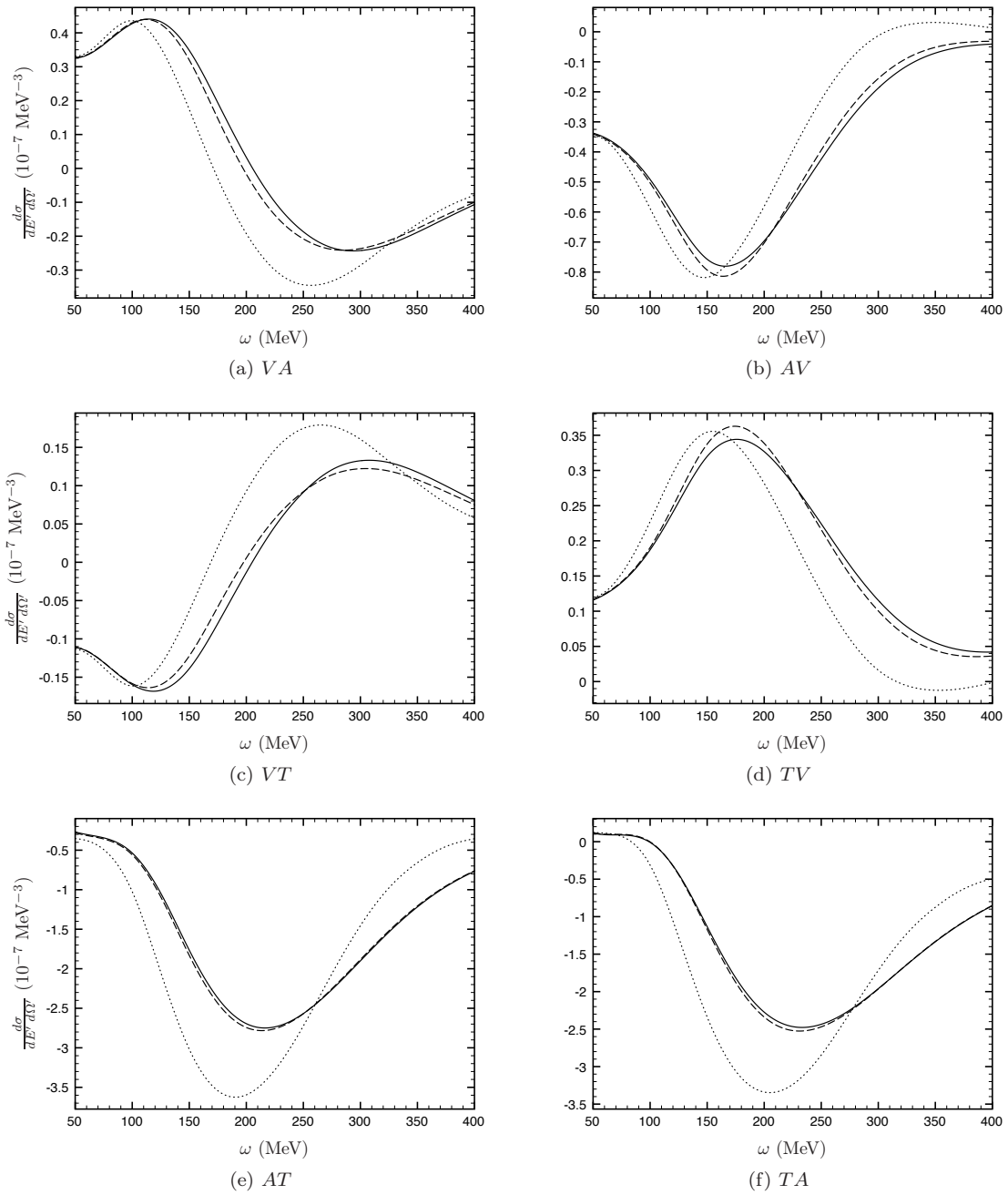

(a) VA (b) AV

(c) VT (d) TV

(e) AT (f) TA

Figure 3.8: Plane wave differential cross sections for LL' combinations as indicated for the reaction $^{40}\mathrm{Ca}(\vec{p},\vec{p}\,')$. In all figures the solid line indicates the MFT (Hartree), the dashed line the MFT (RPA) and the dotted line the $M^* = M$ (Hartree) calculations. Where the RPA result is not shown it coincides with the Hartree result. Here $T_{\mathrm{lab}} = 500$ MeV, $k_F = 0.955$ fm^{-1}, $(\hat{\imath}, s) = (\hat{l}, 1/2)$, $(\hat{\imath}', s') = (\hat{l}', 1/2)$ and $\theta_{\mathrm{cm}} = 40^\circ$.

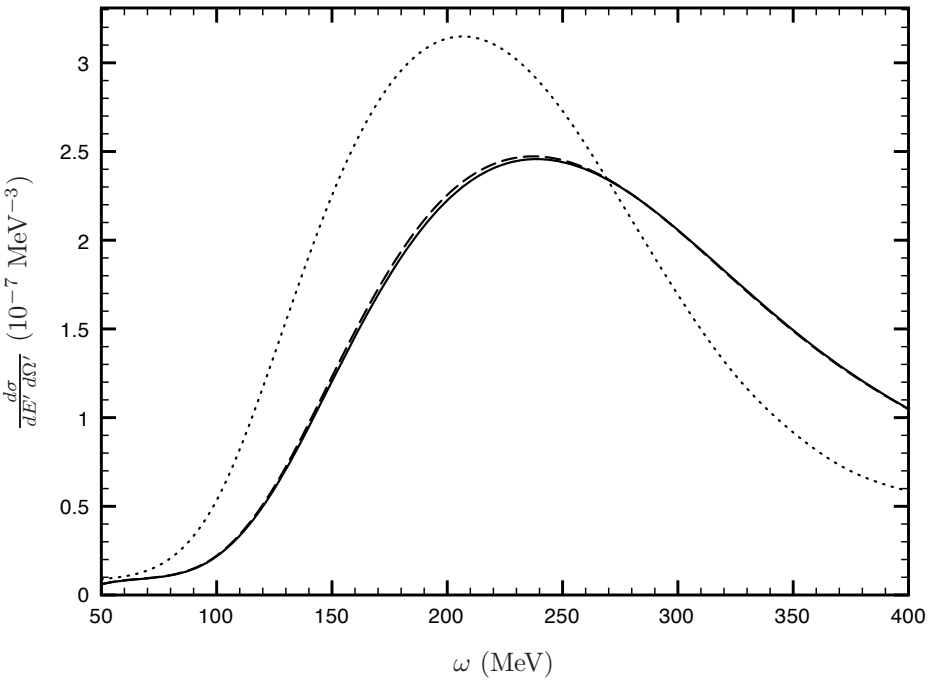

(a) TT

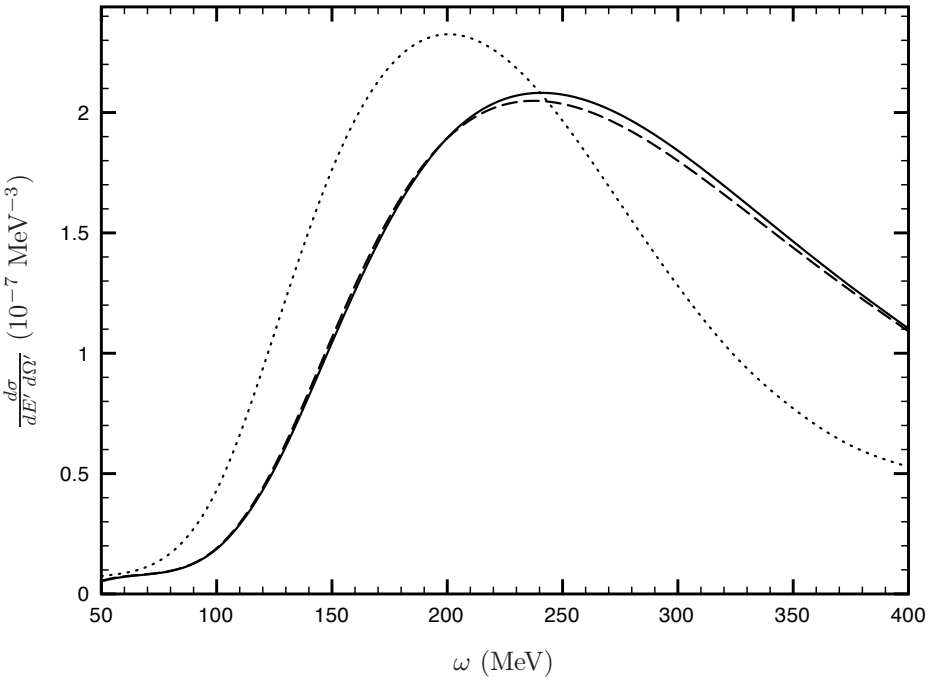

(b) Total

Figure 3.9: Plane wave differential cross sections for LL' combinations as indicated for the reaction $^{40}\mathrm{Ca}(\vec{p},\vec{p}\,')$. In all figures the solid line indicates the MFT (Hartree), the dashed line the MFT (RPA) and the dotted line the $M^* = M$ (Hartree) calculations. Where the RPA result is not shown it coincides with the Hartree result. Here $T_{\mathrm{lab}} = 500$ MeV, $k_F = 0.955$ fm^{-1}, $(\hat{\imath}, s) = (\hat{l}, 1/2)$, $(\hat{\imath}', s') = (\hat{l}', 1/2)$ and $\theta_{\mathrm{cm}} = 40^\circ$.

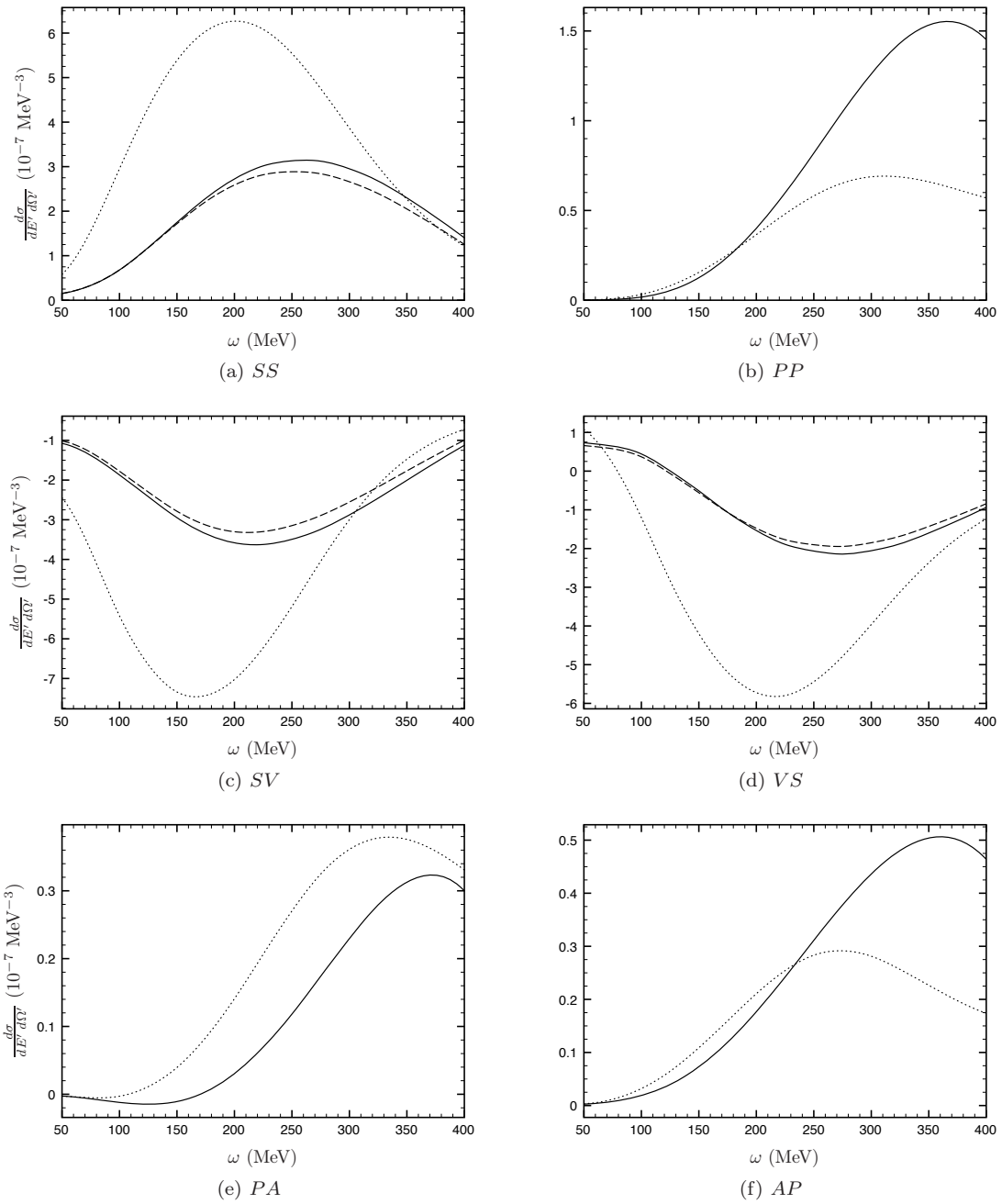

Figure 3.10: Plane wave differential cross sections for LL' combinations as indicated for the reaction ^{40}Ca$(\vec{p},\vec{p}\,')$. In all figures the solid line indicates the MFT (Hartree), the dashed line the MFT (RPA) and the dotted line the $M^* = M$ (Hartree) calculations. Where the RPA result is not shown it coincides with the Hartree result. Here $T_{\rm lab} = 500$ MeV, $k_F = 1.3$ fm^{-1}, $(\hat{i}, s) = (\hat{l}, 1/2)$, $(\hat{i}', s') = (\hat{l}', 1/2)$ and $\theta_{\rm cm} = 40^\circ$.

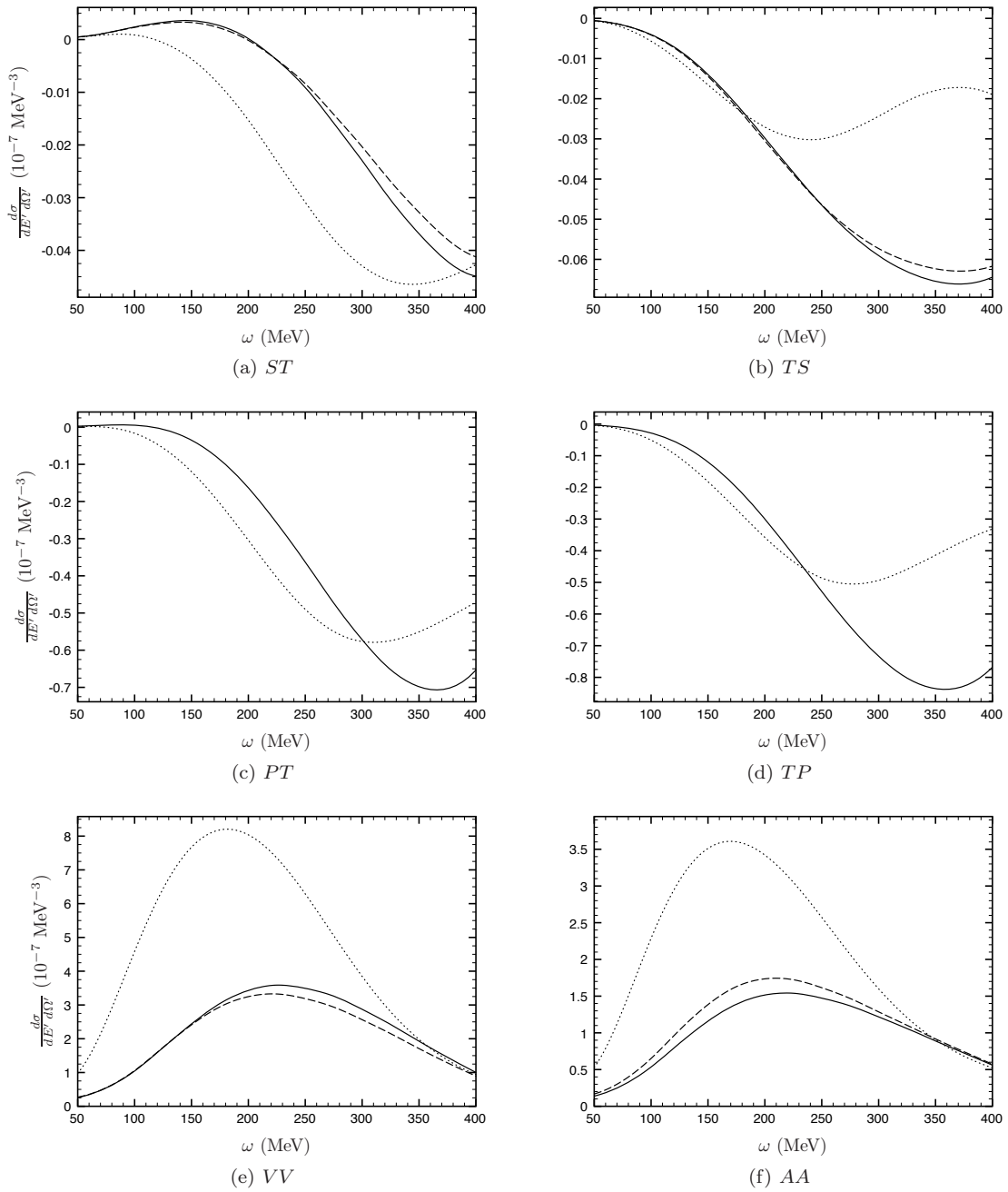

(a) ST (b) TS

(c) PT (d) TP

(e) VV (f) AA

Figure 3.11: Plane wave differential cross sections for LL' combinations as indicated for the reaction $^{40}\mathrm{Ca}(\vec{p},\vec{p}\,')$. In all figures the solid line indicates the MFT (Hartree), the dashed line the MFT (RPA) and the dotted line the $M^* = M$ (Hartree) calculations. Where the RPA result is not shown it coincides with the Hartree result. Here $T_{\mathrm{lab}} = 500$ MeV, $k_F = 1.3$ fm^{-1}, $(\hat{i}, s) = (\hat{l}, 1/2)$, $(\hat{i}', s') = (\hat{l}', 1/2)$ and $\theta_{\mathrm{cm}} = 40^\circ$.

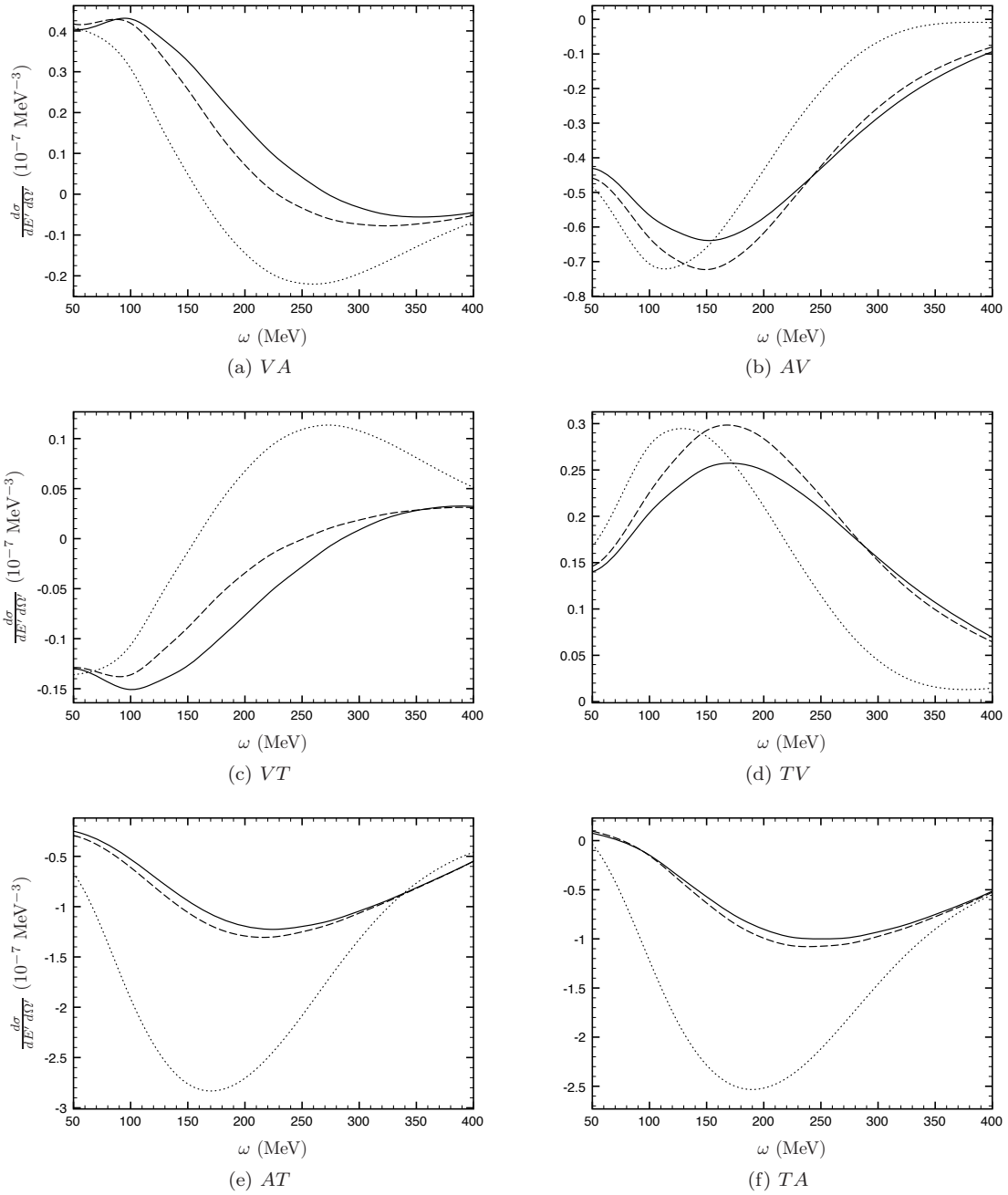

(a) VA (b) AV

(c) VT (d) TV

(e) AT (f) TA

Figure 3.12: Plane wave differential cross sections for LL' combinations as indicated for the reaction $^{40}\mathrm{Ca}(\vec{p},\vec{p}\,')$. In all figures the solid line indicates the MFT (Hartree), the dashed line the MFT (RPA) and the dotted line the $M^* = M$ (Hartree) calculations. Where the RPA result is not shown it coincides with the Hartree result. Here $T_{\mathrm{lab}} = 500$ MeV, $k_F = 1.3$ fm^{-1}, $(\hat{\imath}, s) = (\hat{l}, 1/2)$, $(\hat{\imath}', s') = (\hat{l}', 1/2)$ and $\theta_{\mathrm{cm}} = 40^\circ$.

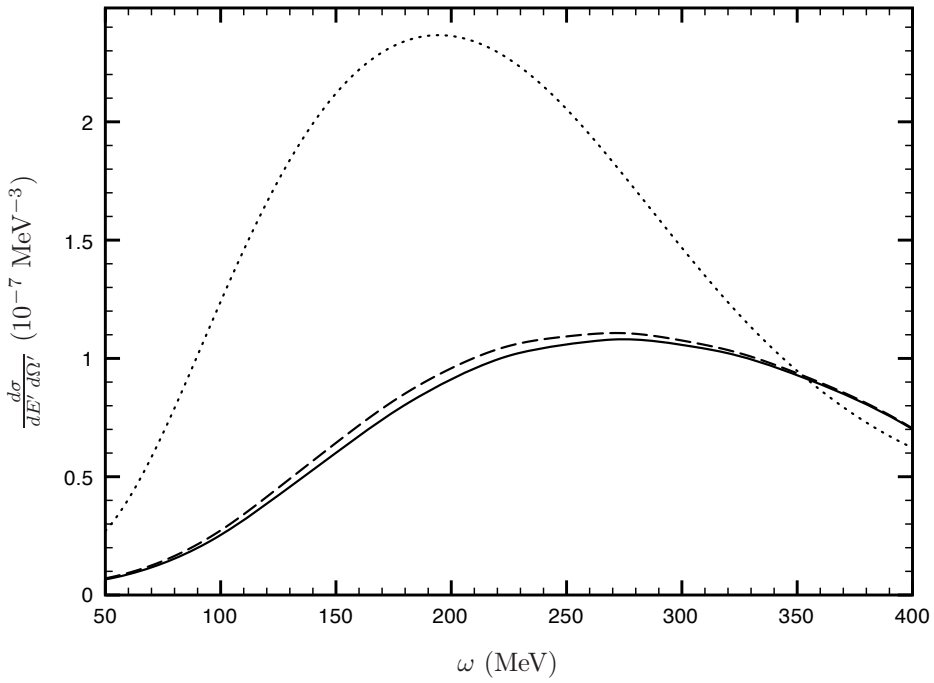

(a) TT

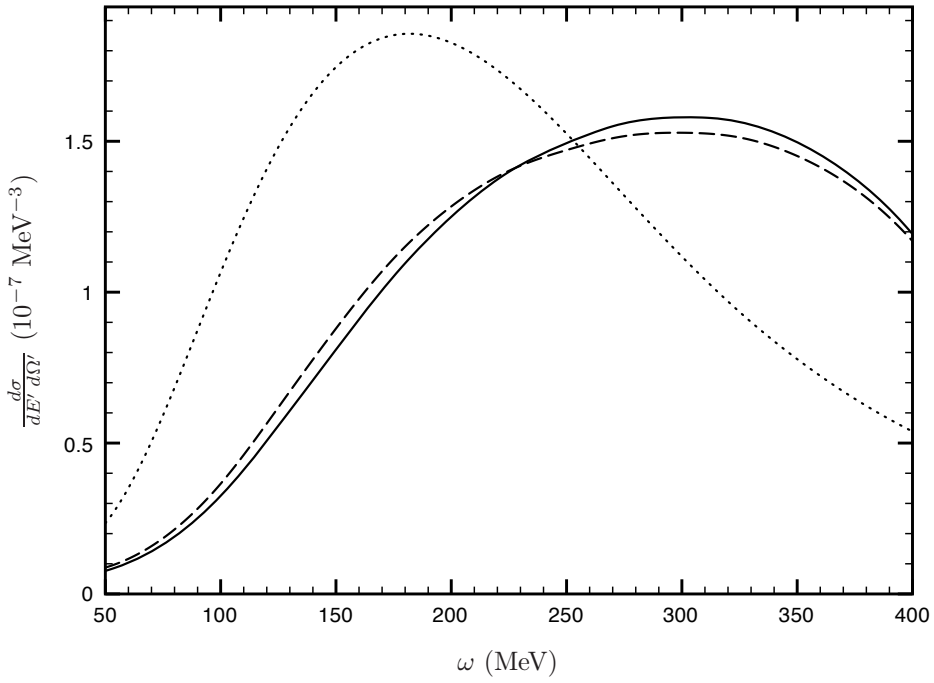

(b) Total

Figure 3.13: Plane wave differential cross sections for LL' combinations as indicated for the reaction ^{40}Ca$(\vec{p},\vec{p}\,')$. In all figures the solid line indicates the MFT (Hartree), the dashed line the MFT (RPA) and the dotted line the $M^* = M$ (Hartree) calculations. Where the RPA result is not shown it coincides with the Hartree result. Here $T_{\rm lab} = 500$ MeV, $k_F = 1.3$ fm^{-1}, $(\hat{i}, s) = (\hat{l}, 1/2)$, $(\hat{i}', s') = (\hat{l}', 1/2)$ and $\theta_{\rm cm} = 40^\circ$.

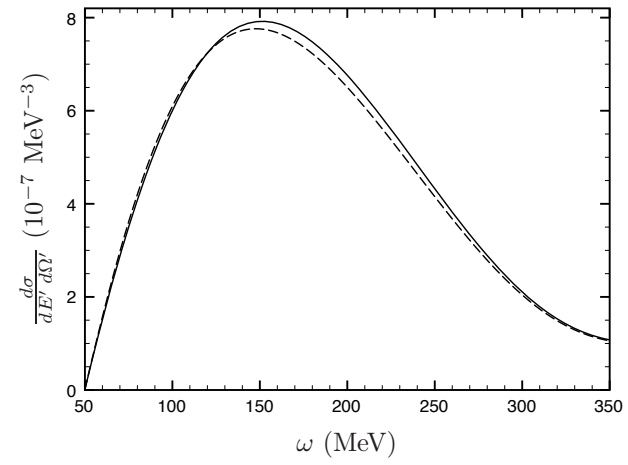

(a) $\theta_{\rm cm} = 30°$

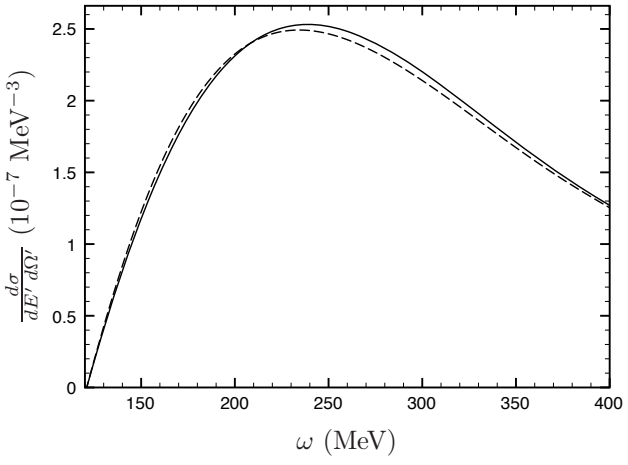

(b) $\theta_{\rm cm} = 40°$

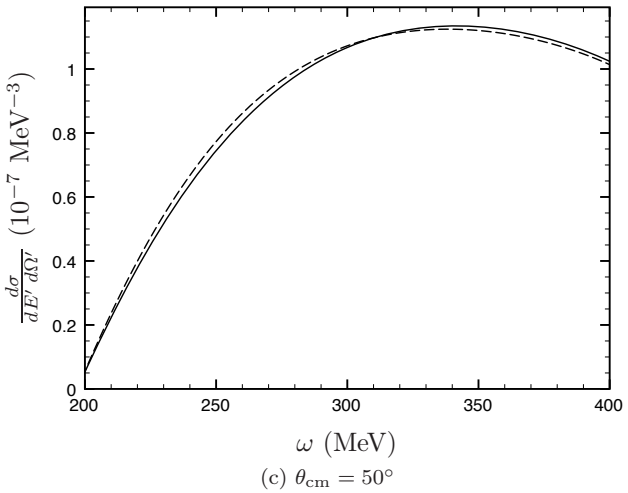

(c) $\theta_{\rm cm} = 50°$

Figure 3.14: Plane wave differential cross sections summed over all LL' combinations for different centre-of-mass angles for the reaction ^{40}Ca$(\vec{p},\vec{p}\,')$. In all figures the solid line indicates the MFT (Hartree) and the dashed line the MFT (RPA) calculations. Here $T_{\rm lab} = 500$ MeV, $k_F = 0.955$ fm^{-1}, $(\hat{i},s) = (\hat{l},1/2)$ and $(\hat{i}',s') = (\hat{l}',1/2)$. These cross sections were calculated using Method A as discussed in Section 3.2.2.1.

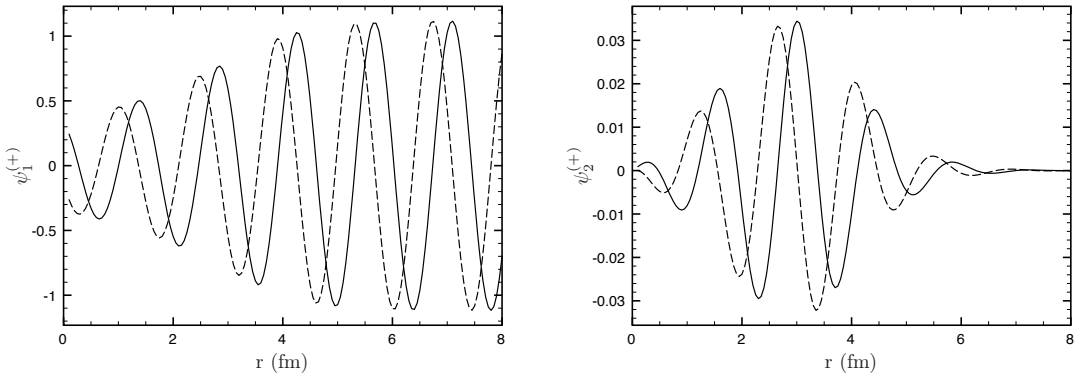

(a) 1st component

(b) 2nd component

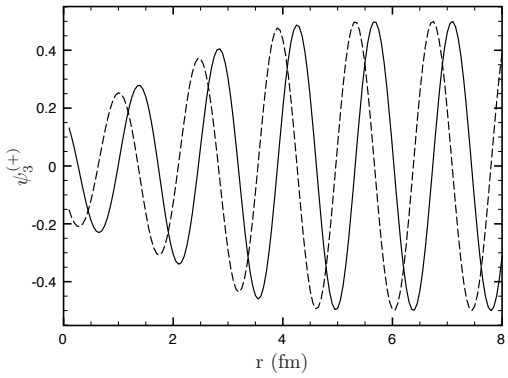

(c) 3rd component

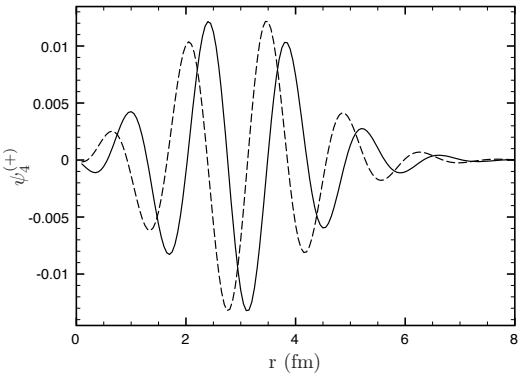

(d) 4th component

Figure 3.15: Real (solid) and imaginary (dashed) parts of the four components of the Dirac distorted wave as a function of radius. This wave was generated for $T_{\text{lab}} = 500$ MeV, $(\hat{l}, s) = (\hat{l}, 1/2)$ and $l_{\max} = 60$ for ^{40}Ca. θ and ϕ were arbitrarily chosen as $\pi/1.23$ and $2\pi/5.43$ respectively. Beyond $r = 8$ fm the plane wave behaviour is restored.

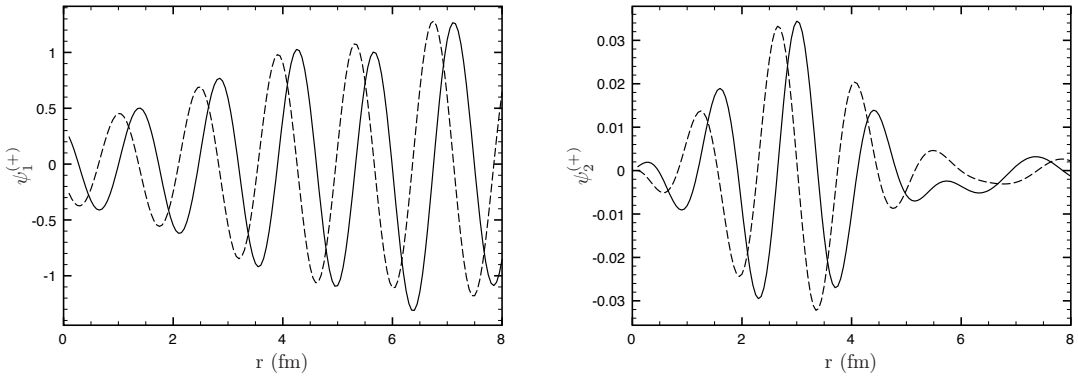

(a) 1st component

(b) 2nd component

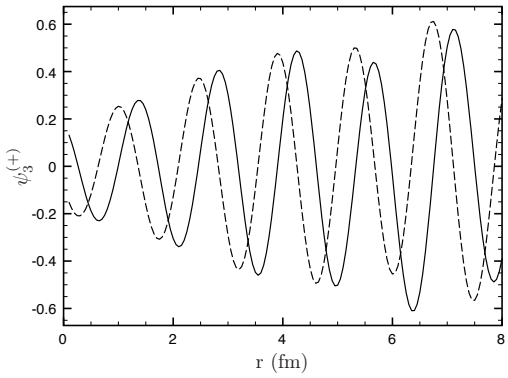

(c) 3rd component

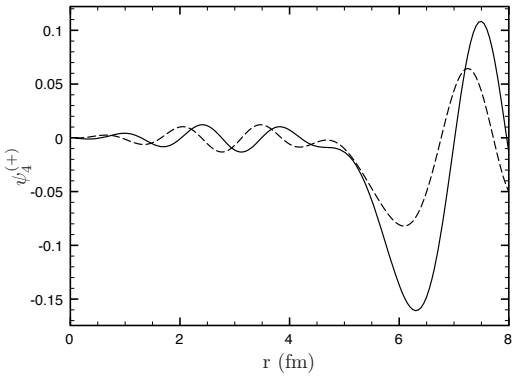

(d) 4th component

Figure 3.16: Real (solid) and imaginary (dashed) parts of the four components of the Dirac distorted wave as a function of radius. This wave was generated for $T_{\rm lab} = 500$ MeV, $(\hat{i}, s) = (\hat{l}, 1/2)$, and $l_{\rm max} = 30$ for ^{40}Ca. θ and ϕ were arbitrarily chosen as $\pi/1.23$ and $2\pi/5.43$ respectively. Beyond $r = 8$ fm the plane wave behaviour is restored.

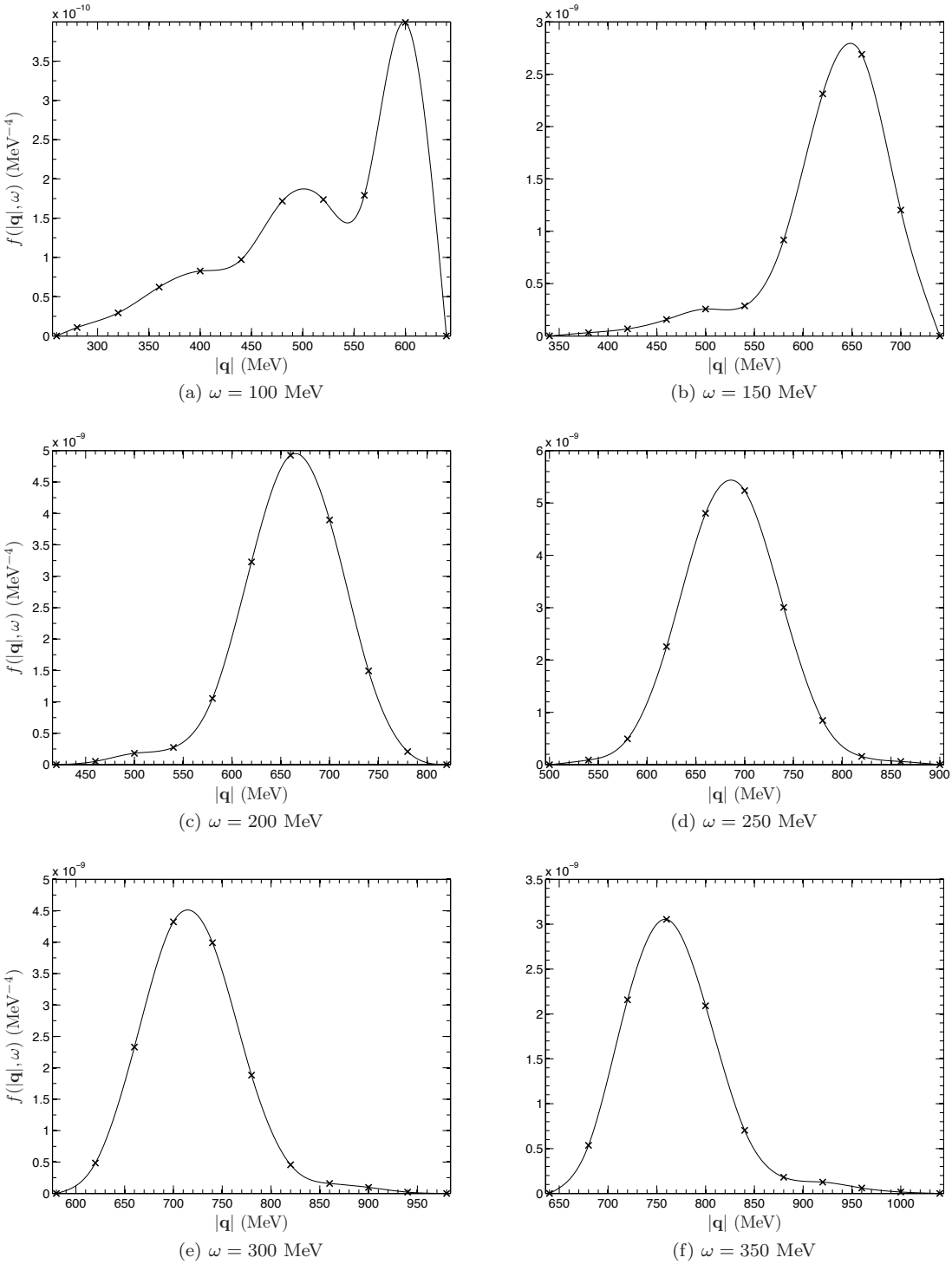

(a) $\omega = 100$ MeV (b) $\omega = 150$ MeV

(c) $\omega = 200$ MeV (d) $\omega = 250$ MeV

(e) $\omega = 300$ MeV (f) $\omega = 350$ MeV

Figure 3.17: $f(|\mathbf{q}|, \omega)$ in the RPWIA for values of ω as indicated. Crosses indicate where $f(|\mathbf{q}|, \omega)$ was calculated exactly (using the lowest-order MFT response of the target) and lines indicate interpolants.

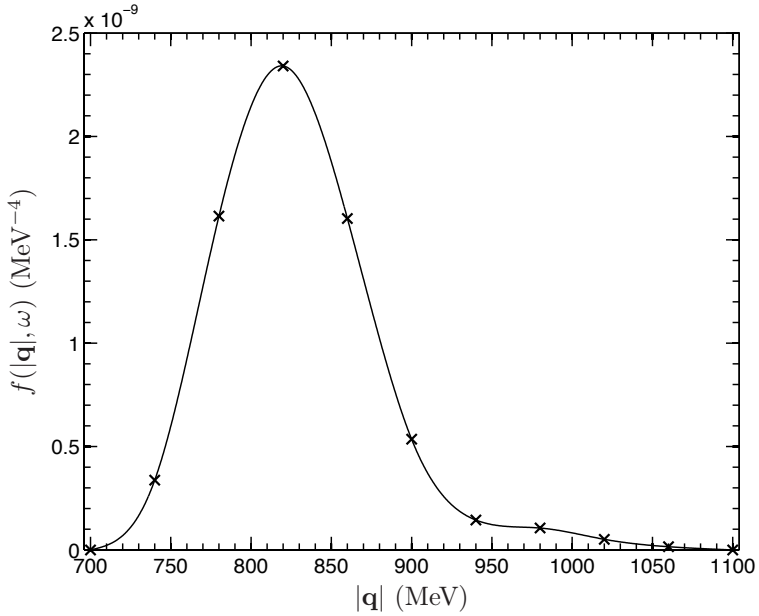

(a) $\omega = 400$ MeV

Figure 3.18: $f(|\mathbf{q}|, \omega)$ in the RPWIA for values of ω as indicated. Crosses indicate where $f(|\mathbf{q}|, \omega)$ was calculated exactly (using the lowest-order MFT response of the target) and lines indicate interpolants.

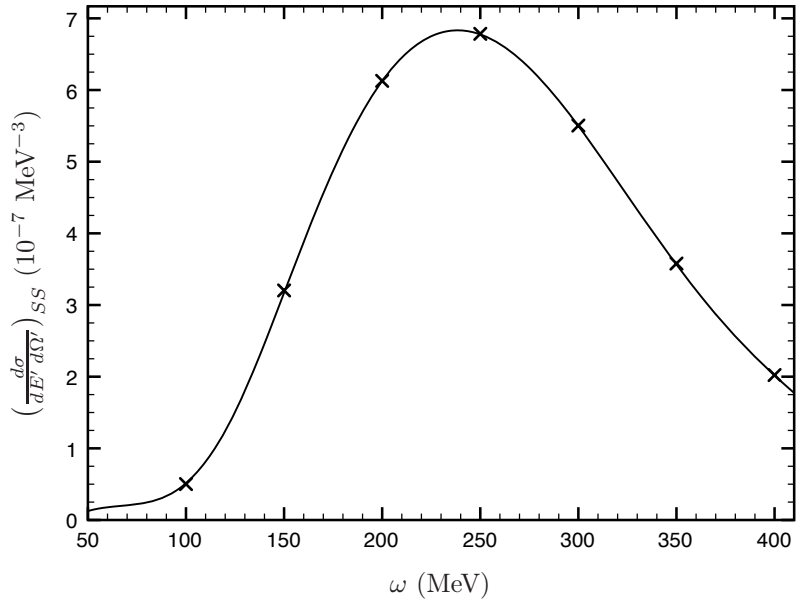

Figure 3.19: Comparison of the fitted values (crosses) with the full numerical integration method (line) (see Eq. (3.46)) of obtaining the plane wave cross section. For every value of ω, 40^3 integration points were used to compute the full three-dimensional integral and $40^2 \times 11$ points for the fitting calculation.

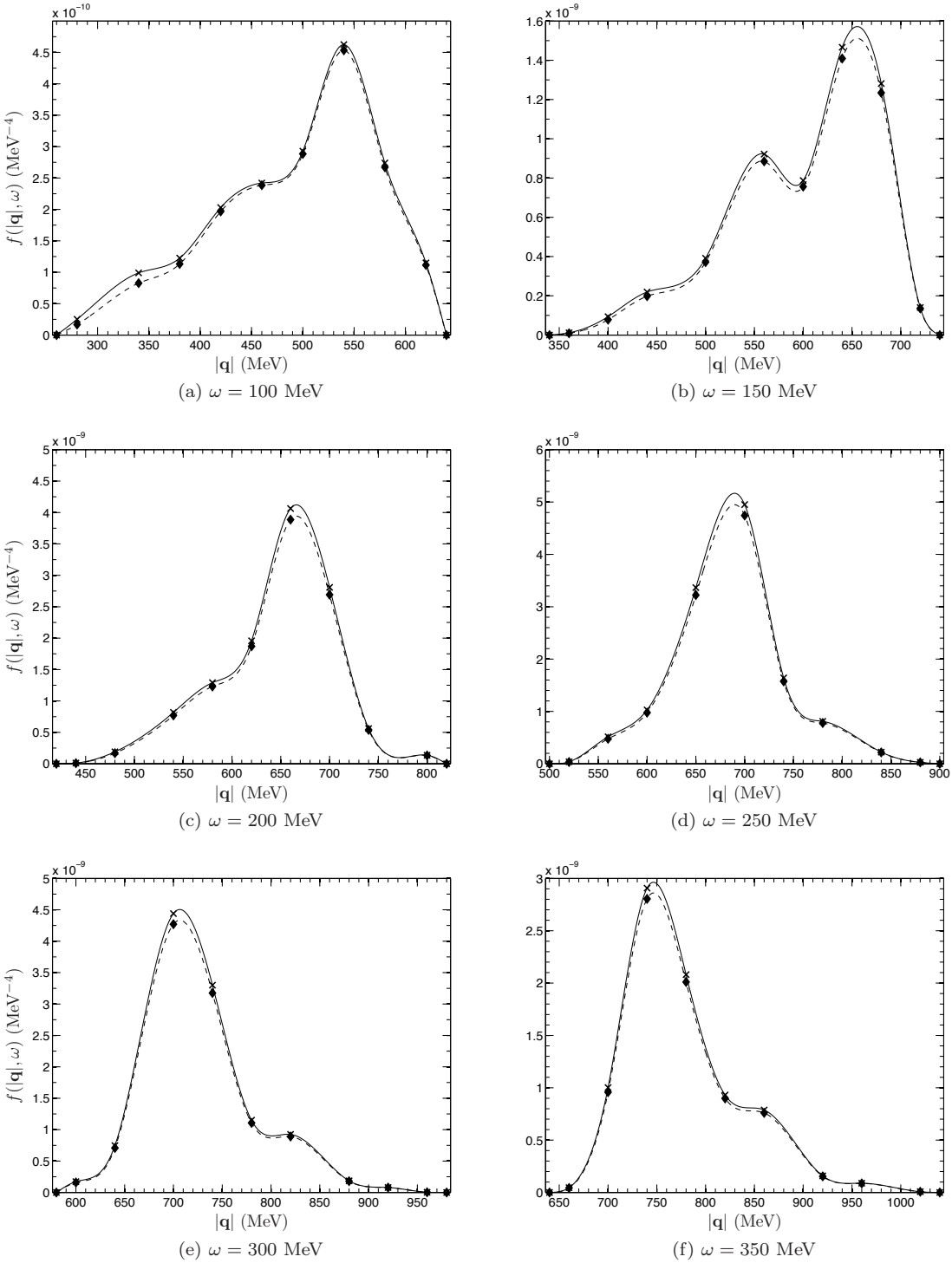

(a) $\omega = 100$ MeV (b) $\omega = 150$ MeV

(c) $\omega = 200$ MeV (d) $\omega = 250$ MeV

(e) $\omega = 300$ MeV (f) $\omega = 350$ MeV

Figure 3.20: $f(|\mathbf{q}|, \omega)$ in the RDWIA for values of ω as indicated. Crosses (diamonds) indicate where $f(|\mathbf{q}|, \omega)$ was calculated exactly using lowest-order MFT (MFT + RPA). Lines indicate interpolants.

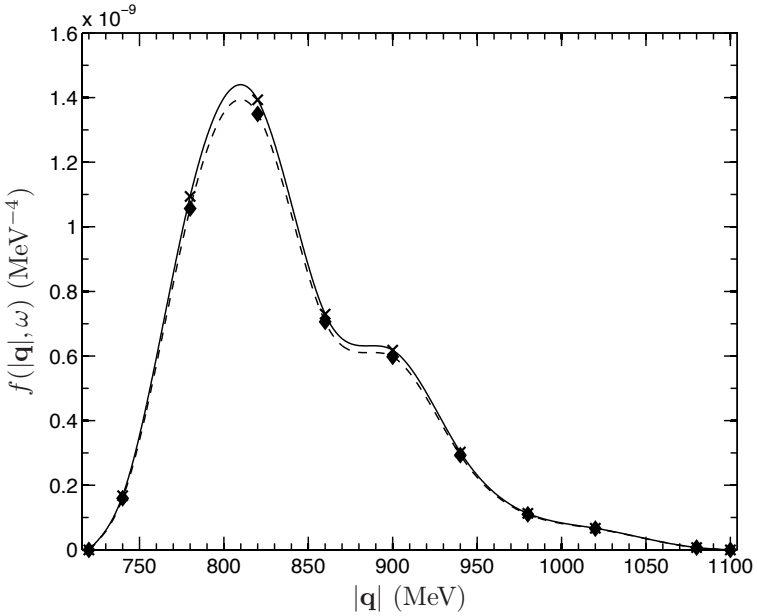

(a) $\omega = 400$ MeV

Figure 3.21: $f(|\mathbf{q}|, \omega)$ in the RDWIA for values of ω as indicated. Crosses (diamonds) indicate where $f(|\mathbf{q}|, \omega)$ was calculated exactly using lowest-order MFT (MFT + RPA). Lines indicate interpolants.

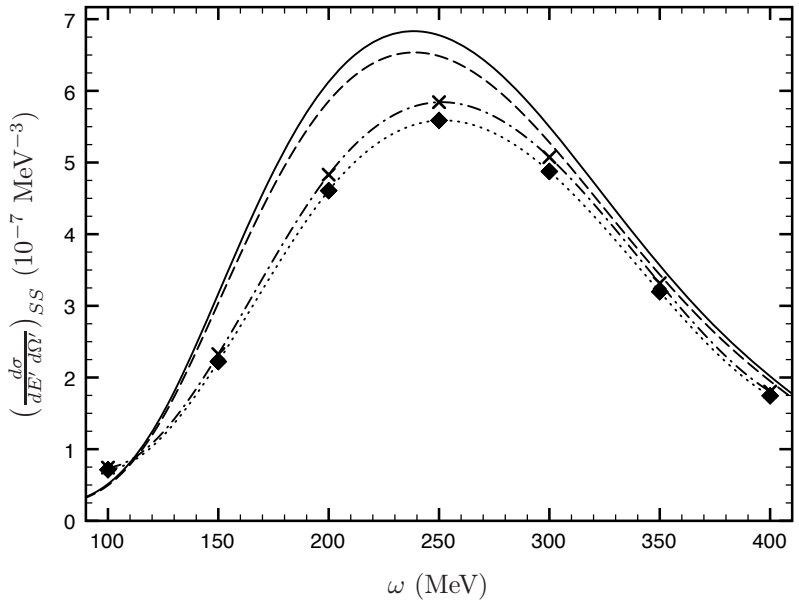

Figure 3.22: Comparison of the RPWIA and RDWIA cross sections for $LL' = SS$ for the reaction $^{40}\mathrm{Ca}(\vec{p}, \vec{p}')$. The solid (dashed) line indicates the RPWIA and lowest-order MFT (MFT + RPA) result. The dashed-dotted (dotted) line indicates the RDWIA and lowest-order MFT (MFT + RPA) result. Crosses and diamonds indicate the result of the $40^2 \times 11$ fitting calculation for every value of ω. Here $T_{\mathrm{lab}} = 500$ MeV, $k_F = 0.955$ fm^{-1}, $(\hat{l}, s) = (\hat{l}, 1/2)$, $(\hat{l}', s') = (\hat{l}', 1/2)$, $\theta_{\mathrm{cm}} = 40^\circ$ and $l_{\max} = 30$.

3.3 Conclusion and outlook

We have shown how a standard RIA treatment of scattering and the assumption of a two-body SPVAT form for the nuclear current operator can be used to formulate a fully relativistic model for inclusive quasielastic nucleon-nucleus scattering. For the current calculations we have adopted a nuclear matter desciption of the target although a finite nucleus calculation can also be performed with this model. An important feature of our model is the separation of projectile and target responses into separate and independent tensors. This allows for the combination of different models for the projectile and target. We performed a baseline calculation by modelling the projectile and ejectile as relativistic plane waves (RPWIA) and using a relativistic nuclear matter description for the target (MFT). It was shown how the target description could be extended to include particle-hole correlations (RPA). In addition we presented the formalism for incorporating the distortion effect of the nuclear potential on the projectile and ejectile (RDWIA) and investigated techniques for optimizing this highly non-trivial calculation.

Preliminary results for the polarized double differential cross section look promising:

- The differential cross section displays the familiar quasielastic peak. The peak widens and moves to higher energy transfer with a decrease in the effective mass of nucleons in the target. In addition, it moves to higher energy transfer and decreases with an increase in the scattering angle.

- RPA correlations tend to soften and reduce the nuclear response and therefore the magnitude of the quasielastic peak due to the attractive particle-hole interaction. This effect increases with increasing target density. It is also expected to increase with a lowering in beam energy due to an increase in the apparent density of the target. At lower scattering angles this effect is slightly enhanced.

- The modulation of the projectile and ejectile wave functions by the nuclear potential (RDWIA) decreases the cross section when compared to the RPWIA result (at least in the $LL' = SS$ channel already).

However, some work remains to be done to obtain a more complete picture of the effects of the RPA and RDWIA.

The decrease of the cross section is expected to be more significant if isovector (ρ and π) RPA correlations are also included. In fact, if the model is to be applied to quasielastic $(\vec{p},\vec{n})$ reactions, the isovector correlations become very important since these reactions probe only the isovector response of the nucleus. Our attempt here was simply to demonstrate the application of the RPA to our model of proton-nucleus scattering. The form of Eq. (3.45), however, allows for a straightforward inclusion of isovector RPA correlations similar to that of Ref. [2]. This would entail the construction of an additional medium-modified interaction for the isovector channel by specifying the free-space interaction matrix of the π and ρ mesons as well as the mixed polarization matrix as determined by the coupling of the isovector mesons to the nucleon.

Judging by Figs 3.15 and 3.16 the amount of partial waves currently used is not yet satisfactory. Furthermore, all LL' contributions to the distorted wave cross section need to be calculated. Unfortunately the extreme numerical effort makes both these undertakings very time-consuming. Nonetheless, we are making progress with these additions, guided by the plane wave results in

determining the relative importance of different LL' contributions, and we hope to incorporate them in the near future.

Appendix A

Hadronic tensor

A.1 Derivation of the ejectile distorted wave function

The Dirac wave function with incoming boundary conditions which we use for the ejectile is defined in terms of the time-reversal operator given by [60, 83]

$$\mathcal{T} = TK, \tag{A.1}$$

where K is the complex conjugation operator and

$$T = i\gamma^1\gamma^3 = \begin{bmatrix} -\sigma_2 & 0 \\ 0 & -\sigma_2 \end{bmatrix}. \tag{A.2}$$

An energy projection operator $\Lambda_\rho(\mathbf{k}, M)$ (where $\rho = \pm$), is given by

$$\Lambda_\rho(\mathbf{k}, M) = \sum_s U^{(\rho)}(\mathbf{p}, s)\, \bar{U}^{(\rho)}(\mathbf{p}, s) = \left(\frac{\rho \not{k} + M}{2M}\right), \tag{A.3}$$

where $U^{(+)}(\mathbf{p}, s) = U(\mathbf{p}, s)$ and $U^{(-)}(\mathbf{p}, s) = V(\mathbf{p}, s)$ refer to positive and negative energy solutions of the free Dirac equation. Using the identities

$$U(\mathbf{k}, \hat{i}', s') = \left(\frac{2M}{E(k) + M}\right)^{1/2} \Lambda_+(\mathbf{k}, M)\, U(\mathbf{0}, \hat{i}', s'), \tag{A.4}$$

$$\mathcal{T}\, \Lambda_+(\mathbf{k}, M)\, \mathcal{T}^{-1} = \Lambda_+(-\mathbf{k}, M), \tag{A.5}$$

and

$$\mathcal{T}\, U(\mathbf{0}, \hat{i}', s') = i(-1)^{1/2+s'} U(\mathbf{0}, \hat{i}', -s'), \tag{A.6}$$

it follows that

$$\mathcal{T}\left[\psi^{(+)}(\mathbf{x}, \mathbf{k}, \hat{i}, s)\right] = i(-1)^{1/2+s} \psi^{(+)}(\mathbf{x}, -\mathbf{k}, \hat{i}, -s). \tag{A.7}$$

To obtain the wave with incoming boundary conditions with the correct sign for the momentum and spin we therefore define it as

$$\psi^{(-)}(\mathbf{x},\mathbf{k},\hat{i},s) = -i(-1)^{s-1/2}\mathcal{T}\left[\psi^{(+)}(\mathbf{x},-\mathbf{k},\hat{i},-s)\right]. \tag{A.8}$$

In the plane wave limit (i.e. when there is no scattering potential) the wave function with outgoing boundary conditions is given by

$$\psi^{(+)}(\mathbf{x},\mathbf{k},\hat{i},s) = Ne^{-i\mathbf{k}\cdot\mathbf{x}}U(\mathbf{k},\hat{i},s), \tag{A.9}$$

where N is a normalization factor. Substitution of this expression into Eq. (A.8) yields

$$\begin{aligned}\psi^{(-)}(\mathbf{x},\mathbf{k},\hat{i},s) &= -i(-1)^{s-1/2}\left[i(-1)^{1/2-s}\psi^{(+)}(\mathbf{x},\mathbf{k},\hat{i},s)\right]\\ &= \psi^{(+)}(\mathbf{x},\mathbf{k},\hat{i},s),\end{aligned} \tag{A.10}$$

which is exactly what one would expect according to the Lippmann-Schwinger equation with zero potential [67].

Since we cannot fix the direction of the ejectile momentum as we did for the projectile, Eq. (2.65) must be used when evaluating Eq. (A.8) for the distorted wave with outgoing boundary conditions:

$$\begin{aligned}\psi^{(-)}(\mathbf{x},\mathbf{k},\hat{i},s) &= -i(-1)^{s-1/2}TK\left[\psi^{(+)}(\mathbf{x},-\mathbf{k},\hat{i},-s)\right]\\ &= -i(-1)^{s-1/2}i\gamma^1\gamma^3\left[\psi^{(+)}(\mathbf{x},-\mathbf{k},\hat{i},-s)\right]^*\\ &= -i(-1)^{s-1/2}\begin{bmatrix}-\sigma_2 & 0\\ 0 & -\sigma_2\end{bmatrix}\left[\psi^{(+)}(\mathbf{x},-\mathbf{k},\hat{i},-s)\right]^*,\end{aligned} \tag{A.11}$$

where

$$\begin{aligned}\left[\psi^{(+)}(\mathbf{x},-\mathbf{k},\hat{i},-s)\right]^* = \frac{4\pi}{kx}\left(\frac{E(\mathbf{k})+M}{2M}\right)^{1/2}&\sum_{ljms_z}\left(i^l\right)^* e^{-i\delta_{lj}}\langle l\frac{1}{2}ms_z|j,m+s_z\rangle\\ &\times\left[\mathcal{D}^{(1/2)}_{s_z,-s}(\hat{i})\right]^* Y_{lm}(-\hat{k})\begin{bmatrix}g^*_{lj}(kx)\mathcal{Y}^*_{lj,m+s_z}(\hat{x})\\ -if^*_{2j-l,j}(kx)\mathcal{Y}^*_{2j-l,j,m+s_z}(\hat{x})\end{bmatrix}.\end{aligned} \tag{A.12}$$

Using the identities

$$\left(i^l\right)^* = (-i)^l = (-1)^l i^l, \tag{A.13}$$

$$\begin{aligned}\left[\mathcal{D}^{(1/2)}_{s_z,-s}(\hat{i})\right]^* &= (-1)^{s_z-(-s)}\mathcal{D}^{(1/2)}_{-s_z,s}(\hat{i}) \\ &= (-1)^{s_z+s}\mathcal{D}^{(1/2)}_{-s_z,s}(\hat{i}),\end{aligned} \tag{A.14}$$

$$Y_{lm}(-\hat{k}) = (-1)^l Y_{lm}(\hat{k}), \tag{A.15}$$

we write Eq. (A.12) as

$$\begin{aligned}\left[\psi^{(+)}(\mathbf{x},-\mathbf{k},\hat{i},-s)\right]^* = \frac{4\pi}{kx}\left(\frac{E(\mathbf{k})+M}{2M}\right)^{1/2}\sum_{ljms_z}(-1)^{2l}i^l(-1)^{s_z+s}e^{-i\delta_{lj}}\langle l\frac{1}{2}ms_z|j,m+s_z\rangle \\ \times\,\mathcal{D}^{(1/2)}_{-s_z,s}(\hat{i})\,Y_{lm}(\hat{k})\begin{bmatrix} g^*_{lj}(kx)\mathcal{Y}^*_{lj,m+s_z}(\hat{x}) \\ -if^*_{2j-l,j}(kx)\mathcal{Y}^*_{2j-l,j,m+s_z}(\hat{x})\end{bmatrix}.\end{aligned} \tag{A.16}$$

Use of this expression in Eq. (A.11) as well as the fact that $(-1)^{2l}=1$ (because $l\in\mathcal{Z}$) yields

$$\begin{aligned}\psi^{(-)}(\mathbf{x},\mathbf{k},\hat{i},s) = -i(-1)^{s-1/2}\frac{4\pi}{kx}\left(\frac{E(\mathbf{k})+M}{2M}\right)^{1/2}\sum_{ljms_z}i^l(-1)^{s_z+s}e^{-i\delta_{lj}}\langle l\frac{1}{2}ms_z|j,m+s_z\rangle \\ \times\,\mathcal{D}^{(1/2)}_{-s_z,s}(\hat{i})\,Y_{lm}(\hat{k})\begin{bmatrix} g^*_{lj}(kx)\left(-\sigma_2\mathcal{Y}^*_{lj,m+s_z}(\hat{x})\right) \\ -if^*_{2j-l,j}(kx)\left(-\sigma_2\mathcal{Y}^*_{2j-l,j,m+s_z}(\hat{x})\right)\end{bmatrix}.\end{aligned} \tag{A.17}$$

We now investigate the effect of the Pauli matrix σ_2 on the spin-spherical harmonics $\mathcal{Y}_{ljm}$. From Eq. (2.66) it follows that

$$\mathcal{Y}^*_{lj\mu}(\hat{x}) = \sum_{t'_z}\langle l\frac{1}{2},\mu-t'_z,t'_z|j\mu\rangle Y^*_{l,\mu-t'_z}(\hat{x})\chi_{t'_z}. \tag{A.18}$$

Using the fact that $Y^*_{lm}(\hat{x}) = (-1)^m Y_{l,-m}(\hat{x})$, we can write

$$-\sigma_2\mathcal{Y}^*_{lj\mu}(\hat{x}) = \sum_{s'_z}\langle l\frac{1}{2},\mu-s'_z,s'_z|j\mu\rangle(-1)^{\mu-s'_z}Y_{l,s'_z-\mu}(\hat{x})\left(-\sigma_2\chi_{s'_z}\right). \tag{A.19}$$

The effect of the Pauli matrix on the spinor is

$$-\sigma_2\chi_{s'_z} = i(-1)^{s'_z+1/2}\chi_{-s'_z}, \tag{A.20}$$

which leaves Eq. (A.19) in the form

$$-\sigma_2\mathcal{Y}^*_{lj\mu}(\hat{x}) = i(-1)^{\mu+1/2}\sum_{t'_z}\langle l\frac{1}{2},\mu+t'_z,-t'_z|j\mu\rangle Y_{l,\mu+t'_z}(\hat{x})\chi_{t'_z}, \tag{A.21}$$

where we have relabelled the summation index $-s'_z \to t'_z$. If we rewrite Eq. (2.66) as

$$\mathcal{Y}_{lj,-\mu}(\hat{x}) = \sum_{t'_z} \langle l\frac{1}{2}, -(\mu + t'_z), t'_z | j, -\mu \rangle Y_{l,\mu+t'_z}(\hat{x}) \chi_{t'_z}, \tag{A.22}$$

it bears a striking resemblance to Eq. (A.21). The similarity becomes even more apparent if we make use of the following identity for the Clebsh-Gordon coefficients:

$$\langle j_1 j_2 m_1 m_2 | j m \rangle = (-1)^{j_1+j_2-j} \langle j_1 j_2, -m_1, -m_2 | j, -m \rangle, \tag{A.23}$$

which implies that

$$\langle l\frac{1}{2}, \mu + t'_z, -t'_z | j \mu \rangle = (-1)^{l+1/2-j} \langle l\frac{1}{2}, -(\mu + t'_z), t_z | j, -\mu \rangle. \tag{A.24}$$

Therefore Eq. (A.21) can be written as

$$-\sigma_2 \mathcal{Y}^*_{lj\mu}(\hat{x}) = i(-1)^{l+\mu-j+1} \mathcal{Y}_{lj,-\mu}(\hat{x}). \tag{A.25}$$

Recasting the expression into a form appropriate for Eq. (A.17) yields

$$\psi^{(-)}(\mathbf{x}, \mathbf{k}, \hat{i}, s) = -i(-1)^{s-1/2} \frac{4\pi}{kx} \left(\frac{E(\mathbf{k}) + M}{2M} \right)^{1/2} \sum_{ljms_z} i^l (-1)^{s_z+s} e^{-i\delta_{lj}} \langle l\frac{1}{2} m s_z | j, m + s_z \rangle$$

$$\times \mathcal{D}^{(1/2)}_{-s_z,s}(\hat{i})\, Y_{lm}(\hat{k}) \begin{bmatrix} g^*_{lj}(kx)\, i(-1)^{l+m+s_z-j+1} \mathcal{Y}_{lj,-(m+s_z)}(\hat{x}) \\ -i f^*_{2j-l,j}(kx)\, i(-1)^{m+s_z+j-l+1} \mathcal{Y}_{2j-l,j,-(m+s_z)}(\hat{x}) \end{bmatrix}. \tag{A.26}$$

A.2 Gaunt coefficients

Let

$$G(l_1 m_1 | l_2 m_2 | l_3 m_3) = \int d\Omega\, Y_{l_1,m_1}(\hat{x})\, Y^*_{l_2 m_2}(\hat{x})\, Y^*_{l_3 m_3}(\hat{x}), \tag{A.27}$$

where

$$Y_{lm}(\theta, \phi) = \begin{cases} (-1)^m \left(\frac{(2l+1)}{4\pi} \frac{(l-m)!}{(l+m)!} \right)^{1/2} P_{lm}(\cos\theta)\, e^{im\phi}; & m \geq 0 \\ (-1)^{|m|} Y^*_{l|m|}(\theta, \phi); & m < 0. \end{cases} \tag{A.28}$$

with $P_{lm}(\cos\theta)$ the Legendre polynomial of degree l. As such, the Gaunt coefficients have certain selection rules for them to be non-zero [76]:

- $m_3 = m_1 - m_2$,
- $|l_1 - l_2| \leq l_3 \leq l_1 + l_2$
- $l_1 + l_2 + l_3$ must be even.

Appendix B

Hadronic propagators

B.1 Field equations of QHD-I

The starting point for the derivation of the nucleon propagator is the model for the NN interaction in terms of meson-exchange as presented in Ref. [31]. In its simplest form (Walecka Model or QHD-I), this model contains a neutral scalar meson (σ) which couples to the scalar baryon density and represents in an effective phenomenological way the exchange of two pions [39], as well as a neutral vector meson (ω) which couples to the conserved baryon current and provides repulsion. The Langrangian is written in terms of the usual field operators of relativistic quantum field theory as

$$\mathcal{L} = \bar{\psi}\left[\gamma_\mu\left(i\partial^\mu - g_v V^\mu\right) - \left(M - g_s\phi\right)\right]\psi + \frac{1}{2}\left(\partial_\mu\phi\partial^\mu\phi - m_s^2\phi^2\right)$$
$$- \frac{1}{4}\left(\partial_\mu V_\nu - \partial_\nu V_\mu\right)\left(\partial^\mu V^\nu - \partial^\nu V^\mu\right) + \frac{1}{2}m_v^2 V_\mu V^\mu + \delta L. \tag{B.1}$$

Here ψ, ϕ and V represent the nucleon, scalar meson and vector meson field respectively, M, m_s and m_v represent their masses and g_s and g_v are the meson-nucleon couplings which are determined phenomenologically to reproduce nuclear matter properties at saturation density ($k_F = 1.42$ fm^{-1}, $E_B = -15.75$ MeV) [31, 48, 84]. δL contains terms neccesary for renormalization. This Lagrangian embodies the short-range repulsive and large-distance attractive features of the observed nucleon-nucleon interaction and thus forms a suitable approximate description of baryon-baryon interaction in general and bulk nuclear properties [40, 85] . This model can be extended to include, amongst others, an isovector ρ meson.

The application of the Euler-Lagrange equations to Eq. (B.1) yield the field equations as a set of coupled non-linear differential equations:

$$\left(\partial_\mu\partial^\mu + m_s^2\right)\phi = g_s\bar{\psi}\psi, \tag{B.2}$$

$$\partial_\mu\left(\partial^\mu V^\nu - \partial^\nu V^\mu\right) + m_v^2 V^\nu = g_v\bar{\psi}\gamma^\nu\psi, \tag{B.3}$$

$$\left[\gamma_\mu\left(i\partial^\mu - g_v V^\mu\right) - \left(M - g_s\phi\right)\right]\psi = 0. \tag{B.4}$$

B.2 Green's function formalism

In general the baryon propagators for the nucleon ($G_{\alpha\beta}$) and the scalar (Δ) and vector ($D_{\mu\nu}$) mesons are written as [85]

$$iG_{\alpha\beta}(x-x') = \langle\Psi|T[\psi_\alpha(x)\bar{\psi}_\beta(x')]|\Psi\rangle = i\int \frac{d^4k}{(2\pi)^4} G_{\alpha\beta}(k)e^{ik\cdot(x-x')}, \tag{B.5}$$

$$i\Delta(x-x') = \langle\Psi|T[\phi(x)\phi(x')]|\Psi\rangle = i\int \frac{d^4k}{(2\pi)^4} \Delta(k)e^{ik\cdot(x-x')}, \tag{B.6}$$

$$iD_{\mu\nu}(x-x') = \langle\Psi|T[V_\mu(x)V_\nu(x)]|\Psi\rangle = i\int \frac{d^4k}{(2\pi)^4} D_{\mu\nu}(k)e^{ik\cdot(x-x')}, \tag{B.7}$$

where $T[...]$ is the time-ordered product [86], $d^4k = dk_0\, d^3k$, $x = (x_0, \mathbf{x})$ and $k\cdot x = k_0x_0 - \mathbf{k}\cdot\mathbf{x}$.

B.2.1 Fermi gas model

If the state $|\Psi\rangle$ is the non-interacting zero-temperature ground state $|\Psi_0\rangle$ consisting of filled Fermi and Dirac seas and no free mesons, the well known non-interacting Green's functions ($G^0_{\alpha\beta}$, Δ^0 and $D^0_{\mu\nu}$) are obtained where

$$\begin{aligned} G^0_{\alpha\beta}(k) &= (\gamma_\mu k^\mu + M)_{\alpha\beta}\left[\frac{1}{k^2 - M^2 + i\epsilon} + \frac{i\pi}{E^0(\mathbf{k})}\delta\left(k^0 - E^0(k)\right)\theta\left(k_F - |\mathbf{k}|\right)\right] \\ &= G^0_F(k)_{\alpha\beta} + G^0_D(k)_{\alpha\beta}, \end{aligned} \tag{B.8}$$

$$\Delta^0(k) = \frac{1}{k^2 - m_s^2 + i\epsilon}, \tag{B.9}$$

$$D^0_{\mu\nu}(k) = \left[-g_{\mu\nu} + \frac{k_\mu k_\nu}{m_v^2}\right]\frac{1}{k^2 - m_v^2 + i\epsilon}, \tag{B.10}$$

where $E^0(\mathbf{k}) = \left(\mathbf{k}^2 + M^2\right)^{1/2}$. Note that G^0_F (Feynman propagator) describes the free propagation of baryons and antibaryons whereas G^0_D (Density-dependent propagator) describes the propagation of holes in the Fermi sea and corrects the propagation of positive energy baryons for the Pauli exclusion principle. As expected, Eq. (B.5) reduces to the Feynman propagator for free nucleons when $k_F \to 0$ (i.e. no Fermi sea is present).

B.2.2 Interacting propagator

The full interacting propagator can be obtained by writing the baryon propagator in terms of Heisenberg field operators as

$$iG_{\alpha\beta}(x,x') = \langle\Psi|T[\hat{\psi}_{H\alpha}(x)\hat{\bar{\psi}}_{H\beta}(x')]|\Psi\rangle, \tag{B.11}$$

where $|\Psi\rangle$ is now the interacting ground state. The Feynman rules can be used to write this as an expansion in terms of coupling constants and non-interacting propagators. The constituent parts of the diagrams as given in Ref. [31] are shown in Fig. B.1.

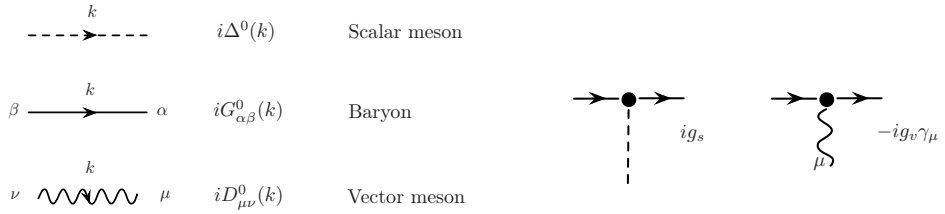

(a) Propagators (b) Vertices

Figure B.1: Components of the Feynman diagrams for QHD-I [31].

The interacting propagator can therefore be written as shown in Figure B.2 or more concisely as a Dyson's equation (Figure B.3)

$$iG = iG^0 + iG^0(-i\Sigma)iG, \tag{B.12}$$

where Σ is known as the self-energy (Figure B.4).

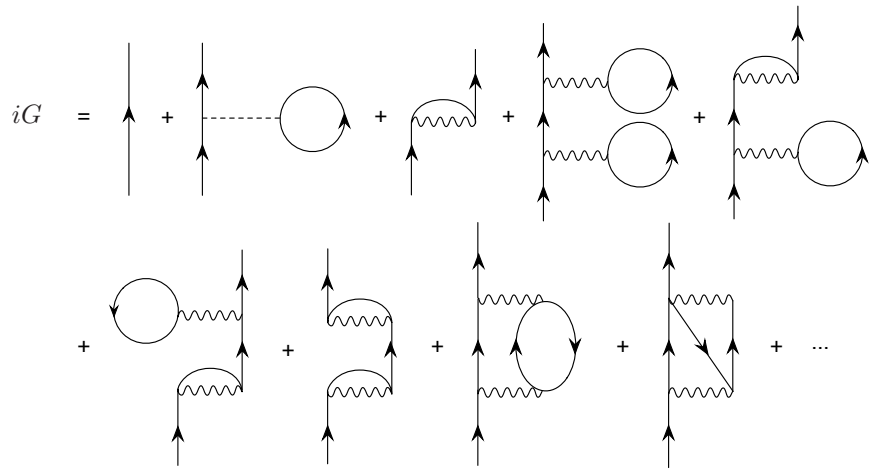

Figure B.2: Diagrammatic expansion of the interacting nucleon propagator [87].

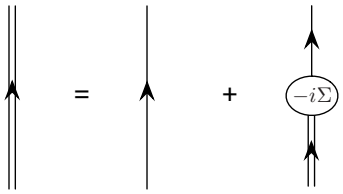

Figure B.3: The interacting nucleon propagator written as a Dyson's equation [87].

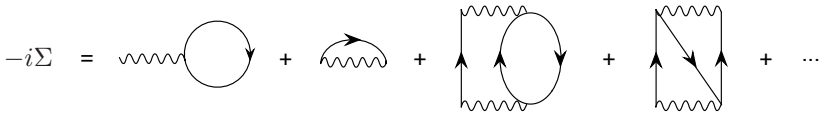

Figure B.4: Diagrammatic expansion of the nucleon self-energy [87].

B.2.3 Hartree propagator

The Hartree propagator is obtained when the interacting propagator is summed to all orders of the second-order tadpole diagram as shown in Figure B.5.

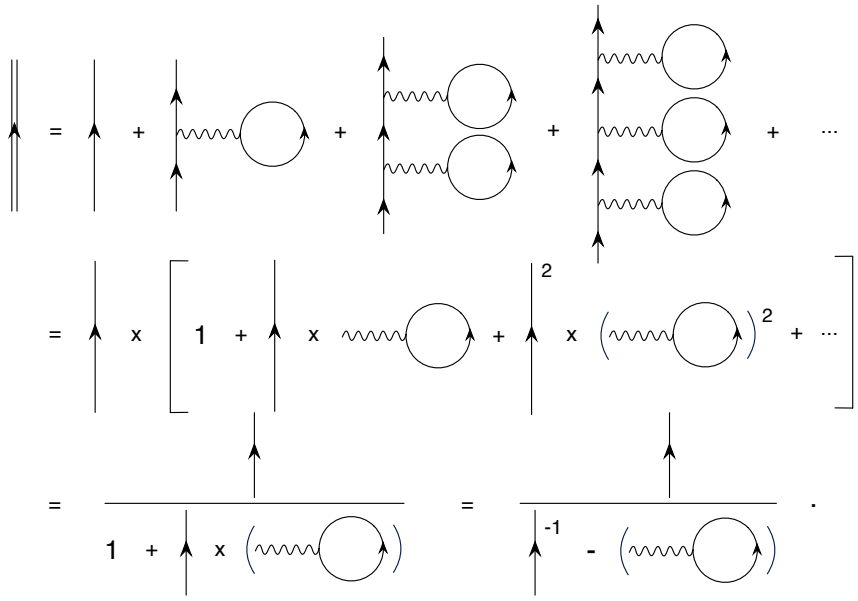

Figure B.5: The Hartree propagator as a sum to all orders of the second-order tadpoles [87].

In the context of QHD-I the the second-order tadpoles consist of scalar en vector meson pieces. Their contribution to the nucleon propagator (Figure B.6) can be written as

$$iG^{(2)}(k) = iG^0(k)\Sigma^{(2)}G^0(k), \tag{B.13}$$

where

$$\Sigma^{(2)} = \Sigma_s^{(2)} - \gamma_\mu \Sigma_v^{(2)\mu}. \tag{B.14}$$

These second-order self-energies are given by

$$\Sigma_s^{(2)} = -ig_s\Delta^0(0)\int \frac{d^4q}{(2\pi)^4}\mathrm{Tr}[G^0(q)]e^{iq_0\eta}, \tag{B.15}$$

$$\Sigma_v^{(2)\mu} = ig_v D^{0\mu\nu}(0)\int \frac{d^4q}{(2\pi)^4}\mathrm{Tr}[G^0(q)\gamma_\nu]e^{iq_0\eta}. \tag{B.16}$$

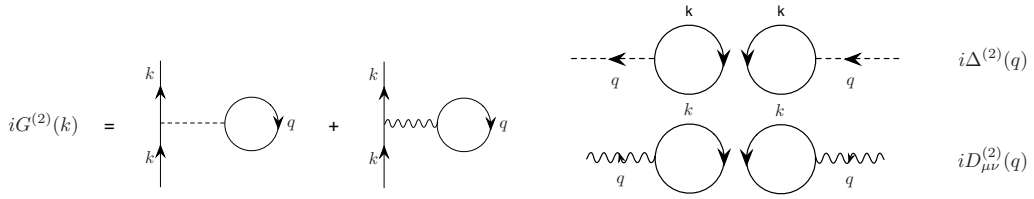

(a) Second-order scalar and vector tadpole contributions.

(b) Meson propagators

Figure B.6: Second-order (tadpole) contributions to the nucleon propagator [31].

The full contribution of the second-order diagrams to the meson propagators are (Figure B.7)

$$i\Delta^{(2)}(q) = i\Delta^0(q)\left[i(2\pi)^4\delta^4(q)\left(g_s\int\frac{d^4k}{(2\pi)^4}\mathrm{Tr}[G^0(k)]\right)^2\right]\Delta^0(q)$$

$$= (2\pi)^4\delta^4(q)\frac{\left[\Sigma_s^{(2)}\right]^2}{g_s^2}, \tag{B.17}$$

$$i\Delta^{(2)}(q) = i\Delta^0(q)\left[-ig_s^2\int\frac{d^4k}{(2\pi)^4}\mathrm{Tr}[G^0(k)G^0(k+q)]\right]\Delta^0(q), \tag{B.18}$$

$$iD^{(2)}_{\mu\nu}(q) = iD^0_{\mu\alpha}(q)\left[-i(2\pi)^4\delta^4(q)g_v^2\int\frac{d^4k}{(2\pi)^4}\mathrm{Tr}[\gamma^\alpha G^0(k)]\int\frac{d^4k}{(2\pi)^4}\mathrm{Tr}[\gamma^\beta G^0(k)]\right]D^0_{\beta\nu}(q)$$

$$= (2\pi)^4\delta^4(q)\frac{\left[\Sigma^{(2)}_{v\mu}\Sigma^{(2)}_{v\nu}\right]}{g_v^2}, \tag{B.19}$$

$$iD^{(2)}_{\mu\nu}(q) = iD^0_{\mu\alpha}(q)\left[-ig_s^2\int\frac{d^4k}{(2\pi)^4}\mathrm{Tr}[\gamma^\alpha G^0(k)\gamma^\beta G^0(k+q)]\right]D^0_{\beta\nu}(q), \tag{B.20}$$

where the quantities in square brackets are known as *polarization insertions* [85]. We also show the mixed scalar-vector propagator

$$i\Delta^0(q)\left[g_sg_v\int\frac{d^4k}{(2\pi)^4}\mathrm{Tr}[G^0(k)\gamma^\mu G^0(k+q)]\right]D^0_{\mu\nu}(q), \tag{B.21}$$

where the quantity in square brackets is known as the *mixed polarization*. Note that this scalar-vector mixing is purely an in-medium effect and vanishes in the vacuum [85].

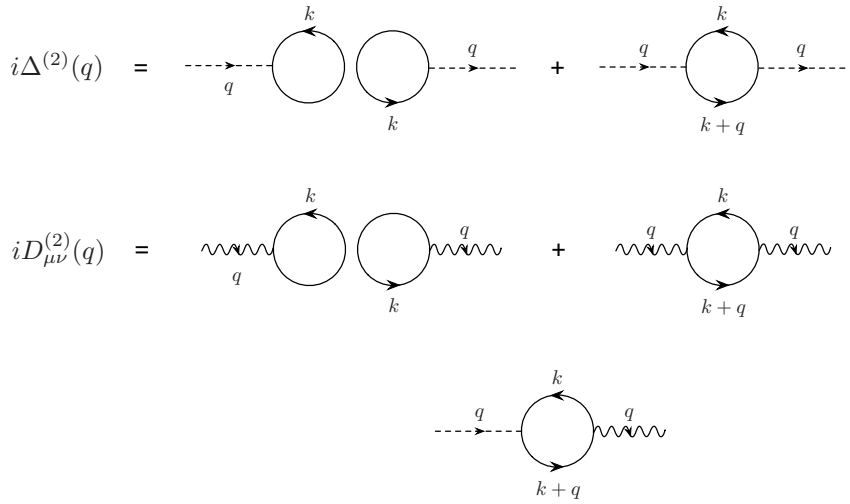

Figure B.7: Second-order contributions to the meson propagators [85].

The resulting Dyson's equation for the nucleon propagator is therefore

$$G(k) = G^0(k) + G^0(k)\Sigma^{(2)}G(k), \tag{B.22}$$

with its solution given by

$$G(k) = \left[1 - G^0(k)\Sigma^{(2)}\right]^{-1} G^0(k). \tag{B.23}$$

As is noted in Ref. [31], this procedure is not self-consistent because of the fact that the non-interacting nucleon propagators have been used to calculate the self-energies which does not allow the background particles to interact. This can be remedied by using the interacting propagator itself to calculate the self-energies and insisting that the self-energies replicate the exact same propagator (the Hartree self-consistency condition). This leads to the so-called relativistic Hartree approximation (RHA) where

$$G^H(k) = G^0(k) + G^0(k)\Sigma^{(2)}_H G^H(k). \tag{B.24}$$

Here

$$\Sigma_H = \Sigma_{Hs} - \gamma_\mu \Sigma^\mu_{Hv}, \tag{B.25}$$

$$\Sigma_{Hs} = i\frac{g_s^2}{m_s^2}\int \frac{d^4q}{(2\pi)^4}\mathrm{Tr}[G^H(q)]e^{iq_0\eta}, \tag{B.26}$$

$$\Sigma^\mu_{Hv} = i\frac{g_v^2}{m_v^2}\int \frac{d^4q}{(2\pi)^4}\mathrm{Tr}[\gamma^\mu G^H(q)]e^{iq_0\eta}. \tag{B.27}$$

The solution of the Dyson's equation can be written as [31]

$$\begin{aligned} G^H(k) &= \left(\gamma_\mu \bar{k}^\mu + M^*\right)\left[\frac{1}{\bar{k}^2 - M^{*2} + i\epsilon} + \frac{i\pi}{E^*(\mathbf{k})}\delta\left(k^0 - E(\mathbf{k})\right)\theta(k_F - |\bar{\mathbf{k}}|)\right] \\ &= G^H_F(k) + G^H_D(k), \end{aligned} \tag{B.28}$$

where

$$\bar{k}^{\mu} = k^{\mu} + \Sigma^{\mu}_{Hv}, \tag{B.29}$$

$$M^{*} = M + \Sigma_{Hs,} \tag{B.30}$$

$$E^{*}(\mathbf{k}) = \left(\mathbf{k}^2 + M^{*2}\right)^{1/2}, \tag{B.31}$$

$$E(\mathbf{k}) = E^{*}(\mathbf{k}) - \Sigma^{0}_{Hv}. \tag{B.32}$$

The propagator therefore looks similar in form to G^0 (see Eq. (B.8)) except that the baryon mass, energy and wave functions are now modified by the self-energy Σ_H.

Since calculation of the self-energy involves an integral over G^H_F and therefore a sum over all the negative energy states, the contribution arising from this factor is divergent. One way to treat this problem is by the addition of suitable counterterms and renormalizable conditions [31, 39, 85] resulting in the Relativisitc Hartree approximation (RHA). These counterterms, however, contribute only to the scalar self-energy affecting the effective mass of the nucleons by changing the energy-density of the vacuum [84, 85]. Another solution is to ommit the terms arising from integrals over G^H_F and to consider only the contributions from G^H_D. This leads to the so-called mean-field theory (MFT) propagator. Since coupling constants and the mass of the σ meson is obtained from fitting to experimental data, it is assumed that the effect of the vacuum (in MFT) is contained in these quantities [88].

B.3 Mean-field theory

In this approximation nucleons propagate through the many-body environment and interact with the self-consistent mean-fields generated by the rest of the nucleons. MFT neglects vacuum effects and the mean-fields are generated exclusively by postive energy baryons in the Fermi sea [31, 41]. The MFT approximation is made by replacing the meson field by their expectation values, which are classical fields

$$\phi \to \langle \phi \rangle \equiv \phi_{0,} \tag{B.33}$$

$$V_{\mu} \to \langle V_{\mu} \rangle \equiv \delta_{\mu 0} V_0, \tag{B.34}$$

where ϕ_0 and V_0 are constants in a static, uniform system (like infinite nuclear matter). This can be done because here the derivatives of the meson fields are zero and the spatial components of the vector meson field vanish which means that Eqs (B.2) and (B.3) can be solved immediately in terms of the scalar and vector baryon densities (ρ_s and ρ_B) yielding

$$\phi_0 = \frac{g_s}{m_s^2} \langle \bar{\psi}\psi \rangle \equiv \frac{g_s}{m_s^2}\rho_s, \tag{B.35}$$

$$V_0 = \frac{g_v}{m_v^2} \langle \psi^{\dagger}\psi \rangle \equiv \frac{g_v}{m_v^2}\rho_B. \tag{B.36}$$

When these meson fields are substituted into Eq. (B.4) it becomes

$$\left[\left(i\gamma^{\mu}\partial_{\mu} - g_v\gamma^0 V_0\right) - (M - g_s\phi_0)\right]\psi = 0. \tag{B.37}$$

Comparison to the equation of motion for the free Dirac field and its solution, reveals that the effect of the meson fields is to shift the energy and mass of the Dirac field [31, 85, 89]. This implies that the MFT ground state consists of filled Fermi and Dirac seas with baryons having an effective mass [31]

$$M^* = M - g_s\phi_0 \tag{B.38}$$

and an effective energy

$$\begin{aligned} E_k^{\pm} &= \sqrt{\mathbf{k}^2 + M^{*2}} \pm g_v V^0 \\ &= E_k^* \pm g_v V^0, \end{aligned} \tag{B.39}$$

where the nucleon wave function is a plain wave and is given by [39]

$$\psi_{k,s}(x) = e^{-iE(k)t}e^{i\mathbf{k}\cdot\mathbf{x}}u(\mathbf{k},s), \tag{B.40}$$

in terms of the four-component Dirac spinor

$$u(\mathbf{k},s) = \sqrt{\frac{E_k^* + M^*}{2E_k^*}}\begin{bmatrix} \chi_s \\ \frac{\boldsymbol{\sigma}\cdot\mathbf{k}}{E_k^*+M^*}\chi_s \end{bmatrix}, \tag{B.41}$$

where χ_s is a Pauli spinor.

Note that the normalization has been chosen as [2]

$$u^{\dagger}(\mathbf{k},s)\, u(\mathbf{k},s') = \delta_{ss'}. \tag{B.42}$$

In the context of propagator formalism, a similar approximation is made if the self-energies of the baryons are calculated using only the density-dependent part of the nucleon propagator, G_D^H. This does not affect the vector self-energy [85] which can be written as

$$\begin{aligned} \Sigma_v^{\mu} &= \frac{g_v^2}{m_v^2}\int \frac{d^4q}{(2\pi)^4}\mathrm{Tr}[\gamma^{\mu}G_D^H(q)] \\ &= -g_v V_0 \delta^{\mu 0}. \end{aligned} \tag{B.43}$$

The divergence that was present in the scalar self-energy due to the integration over G_F^D is now

avoided. The Hartree self-consistency condition applied to Eq. (B.26) results in

$$\Sigma_s = i\frac{g_s^2}{m_s^2}\int \frac{d^4q}{(2\pi)^4}\mathrm{Tr}[G_D^H(q)]$$

$$= -\frac{g_s^2}{m_s^2}\frac{\gamma}{(2\pi)^3}\int_0^{k_F} d^3q\,\frac{M^*}{E^*(q)}, \tag{B.44}$$

$$\implies M^* = M - \frac{g_s^2}{m_s^2}\frac{\gamma}{(2\pi)^3}\int_0^{k_F} d^3q\,\frac{M^*}{E^*(q)} \tag{B.45}$$

$$= M - g_s\phi_0, \tag{B.46}$$

which follows from Eqs (B.30) and (B.35) [31]. Here γ is the spin-isospin degeneracy (4 for nuclear matter). Eq. (B.45) embodies a transcendental self-consistency relation and can be used to solve for M^*.

The baryon propagator in MFT therefore has exactly the same form as Eq. (B.28) where Eqs (B.30) to (B.32) together with Eqs (B.46) and (B.43) now lead to

$$\bar{k}^\mu = (k^0 - g_v V_{0,}\mathbf{k}), \tag{B.47}$$

$$M^* = M - g_s\phi_0, \tag{B.48}$$

$$E^*(\mathbf{k}) = \left(\mathbf{k}^2 + M^{*2}\right)^{1/2}, \tag{B.49}$$

$$E^{\pm}(\mathbf{k}) = E^*(\mathbf{k}) \pm g_v V_0. \tag{B.50}$$

B.4 Relativistic Hartree Approximation

If vacuum effects are included in the self-energies and self-consistency is enforced, the vector self-energy is unaffected [31, 85]. The scalar self-energy, however, needs to be renormalized by the addition of suitable counterterms to the original Langrangian. Different renormalization schemes are discussed in Refs. [85] and [31] but the nett result of this procedure is a new effective mass of the baryons

$$M^* = M - \frac{g_s^2}{m_s^2}\frac{\gamma}{(2\pi)^3}\int_0^{k_F} d^3q\,\frac{M^*}{E^*(q)}$$

$$+ \frac{g_s^2}{m_s^2}\frac{1}{\pi^2}\left[M^{*3}\ln\left(\frac{M^*}{M}\right) - M^2(M^*-M) - \frac{5}{2}M(M^*-M)^2 - \frac{11}{6}(M^*-M)^3\right]. \tag{B.51}$$

Appendix C

Hartree polarizations

C.1 Traces

When evaluating the trace $\mathcal{T}^{LL'}$ we use the SPVAT form of $\hat{F}$ where $\lambda^L \in \left\{I_4, \gamma^5, \gamma^\mu, \gamma^5\gamma^\mu, \sigma^{\mu\nu}\right\}$ (i.e. $L = \{S, P, V, A, T\}$). Note that this implies that $\overline{\lambda^L} = \gamma^0 \left[\lambda^L\right]^\dagger \gamma^0 \in \left\{I_4, -\gamma^5, \gamma^\mu, \gamma^5\gamma^\mu, \sigma^{\mu\nu}\right\}$. The nucleon propagator is given by Eq. (2.118). The traces for all $\mathcal{T}^{LL'}$ are shown in Tables C.1 to C.5.

Table C.1: $\mathcal{T}^{LL'}$ for all different combinations of S and P (0th order tensors).

LL'	$\mathcal{T}(k, k+q)$	$\mathcal{T}(k-q, k)$
SS	$4\left(M^{*2} + k^2 + k\cdot q\right)$	$4\left(M^{*2} + k^2 - k\cdot q\right)$
$SP = PS$	0	0
PP	$4\left(-M^{*2} + k^2 + k\cdot q\right)$	$4\left(-M^{*2} + k^2 - k\cdot q\right)$

Table C.2: $\mathcal{T}^{LL'}$ for all different combinations of L and L' which result in traces containing one Lorentz-index (1st order tensors).

LL'	$\mathcal{T}^\mu(k, k+q)$	$\mathcal{T}^\mu(k-q, k)$
$SV = VS$	$4M^*(2k^\mu + q^\mu)$	$4M^*(2k^\mu - q^\mu)$
$SA = AS$	0	0
$PV = VP$	0	0
$PA = AP$	$4M^*q^\mu$	$4M^*q^\mu$

Table C.3: $\mathcal{T}^{LL'}$ for all different combinations of S, P, V, A and T which result in traces containing two Lorentz-indices (2nd order tensors).

LL'	$\mathcal{T}^{\mu\nu}(k, k+q)$	$\mathcal{T}^{\mu\nu}(k-q, k)$
ST	$4i\left(k^\mu q^\nu - q^\mu k^\nu\right)$	$4i\left(k^\mu q^\nu - q^\mu k^\nu\right)$
TS	$4i\left(-k^\mu q^\nu + q^\mu k^\nu\right)$	$4i\left(-k^\mu q^\nu + q^\mu k^\nu\right)$
$PT = TP$	$4\epsilon^{\mu\nu\alpha\beta}k_\alpha q_\beta$	$4\epsilon^{\mu\nu\alpha\beta}k_\alpha q_\beta$
VV	$4\left[g^{\mu\nu}\left(M^{*2} - k^2 - k\cdot q\right)\right.$	$4\left[g^{\mu\nu}\left(M^{*2} - k^2 + k\cdot q\right)\right.$
	$\left.+2k^\mu k^\nu + q^\mu k^\nu + k^\mu q^\nu\right]$	$\left.+2k^\mu k^\nu - q^\mu k^\nu - k^\mu q^\nu\right]$
$VA = AV$	$4i\epsilon^{\mu\nu\alpha\beta}k_\alpha q_\beta$	$4i\epsilon^{\mu\nu\alpha\beta}k_\alpha q_\beta$
AA	$4\left[-g^{\mu\nu}\left(M^{*2} + k^2 + k\cdot q\right)\right.$	$4\left[-g^{\mu\nu}\left(M^{*2} + k^2 - k\cdot q\right)\right.$
	$\left.+2k^\mu k^\nu + q^\mu k^\nu + k^\mu q^\nu\right]$	$\left.+2k^\mu k^\nu - q^\mu k^\nu - k^\mu q^\nu\right]$

Table C.4: $\mathcal{T}^{LL'}$ for all different combinations of L and L' which result in traces containing three Lorentz-indices (3rd order tensors).

LL'	$\mathcal{T}^{\mu\nu\alpha}(k, k+q)$	$\mathcal{T}^{\mu\nu\alpha}(k-q, k)$
VT	$4iM^*\left(q^\alpha g^{\mu\nu} - q^\nu g^{\alpha\mu}\right)$	$4iM^*\left(q^\alpha g^{\mu\nu} - q^\nu g^{\alpha\mu}\right)$
TV	$4iM^*\left(q^\mu g^{\alpha\nu} - q^\nu g^{\alpha\mu}\right)$	$4iM^*\left(q^\mu g^{\alpha\nu} - q^\nu g^{\alpha\mu}\right)$
$AT = TA$	$4M^*\left(2\epsilon^{\alpha\mu\nu\beta}k_\beta + \epsilon^{\alpha\mu\nu\beta}q_\beta\right)$	$4M^*\left(2\epsilon^{\alpha\mu\nu\beta}k_\beta - \epsilon^{\alpha\mu\nu\beta}q_\beta\right)$

Table C.5: $\mathcal{T}^{LL'}$ for all different combinations of L and L' which result in traces containing four Lorentz-indices (4th order tensors).

LL'	$\mathcal{T}^{\mu\nu\alpha\beta}(k, k+q)$
TT	$4\big(-k^\mu q^\alpha g^{\beta\nu} - k^\alpha q^\mu g^{\beta\nu} + k^\nu q^\alpha g^{\beta\mu}$
	$+k^\alpha q^\nu g^{\beta\mu} - 2k^\alpha k^\mu g^{\beta\nu} + 2k^\alpha k^\nu g^{\beta\mu}$
	$+g^{\alpha\nu}\left(-g^{\beta\mu}\left(k\cdot q + k^2 + M^{*2}\right) + k^\mu\left(2k^\beta + q^\beta\right) + k^\beta q^\mu\right)$
	$+g^{\alpha\mu}\left(g^{\beta\nu}\left(k\cdot q + k^2 + M^{*2}\right) + k^\nu\left(-\left(2k^\beta + q^\beta\right)\right) - k^\beta q^\nu\right)\big)$

LL'	$\mathcal{T}^{\mu\nu\alpha\beta}(k-q, k)$
TT	$4\big(k^\mu q^\alpha g^{\beta\nu} + k^\alpha q^\mu g^{\beta\nu} - k^\nu q^\alpha g^{\beta\mu}$
	$-k^\alpha q^\nu g^{\beta\mu} - 2k^\alpha k^\mu g^{\beta\nu} + 2k^\alpha k^\nu g^{\beta\mu}$
	$-g^{\alpha\nu}\left(g^{\beta\mu}\left(-k\cdot q + k^2 + M^{*2}\right) + k^\mu q^\beta + k^\beta\left(q^\mu - 2k^\mu\right)\right)$
	$+g^{\alpha\mu}\left(g^{\beta\nu}\left(-k\cdot q + k^2 + M^{*2}\right) + k^\nu q^\beta + k^\beta\left(q^\nu - 2k^\nu\right)\right)\big)$

C.2 Symmetries

In addition to the symmetries that exist between the polarization tensors due to equal traces (as shown in Tables C.1 to C.5), symmetries of the traces under integration (see Eqs (2.133) and (2.157)) lead to further symmetries in the lowest-order polarizations themselves in the reference frame where $q^\mu = (q^0, 0, 0, |\mathbf{q}|)$ as is evident in Sections C.3 and C.4.

C.3 Imaginary parts of the polarizations

Expressions for the imaginary parts of the polarizations for $LL' = SS$, PP, VV and AA agree with those derived in Refs [39] and [43]. The expression for $LL' = TT$ has to our knowledge never been published for $\lambda^T = \sigma^{\mu\nu}$ due to the form-factor parametrization ($\lambda^T = {}^{i\sigma^{\mu\nu}q_\mu}/_{2M}$) employed by most authors (see Refs [43] and [47]).

In addition to the imaginary parts discussed above, the expressions for $LL' = SV$, VS, PA and AP agree with those derived in Refs [39] and [43]. Expressions for the imaginary parts for $LL' = VT$, TV, AT and TA have not been published in the form needed here and those for $LL' = ST$, TS, PT and TP have to our knowledge never been published.

The imaginary parts of the density-dependent polarizations are calculated according to Eq. (2.157) using the traces shown in Section C.1. We choose $q^\mu = (q^0, 0, 0, |\mathbf{q}|)$ and define

$$E_n = \frac{E^n_{\text{upper}} - E^n_{\text{lower}}}{n}, \tag{C.1}$$

where $E_{\rm upper}$ and $E_{\rm lower}$ are given by

$$E_{\rm upper} = \sqrt{k_F^2 + M^{*2}}, \tag{C.2}$$

$$E_{\rm max} = \max\left[M^*, E_{\rm upper} - q^0, \frac{|\mathbf{q}|}{2}\left(-q^0 + \sqrt{1 - \frac{4M^{*2}}{q_\mu^2}}\right)\right], \tag{C.3}$$

$$E_{\rm lower} = \min\left[E_{\rm max}, E_{\rm upper}\right], \tag{C.4}$$

C.3.1 0th order

$$\mathrm{Im}(\Pi^{SS}) = -\frac{\left(4M^{*2} - q_\mu^2\right)}{8\pi|\mathbf{q}|}E_1, \tag{C.5}$$

$$\mathrm{Im}(\Pi^{PP}) = \frac{q_\mu^2}{8\pi|\mathbf{q}|}E_1. \tag{C.6}$$

C.3.2 1st order

$\mathrm{Im}(\Pi^{SV})$ and similarly for $\mathrm{Im}(\Pi^{VS})$:

$$\mathrm{Im}(\Pi^{0}) = -\frac{M^*}{4\pi|\mathbf{q}|}\left[2E_2 + q^0E_1\right], \tag{C.7}$$

$$\mathrm{Im}(\Pi^{3}) = -\frac{M^*q^0}{4\pi|\mathbf{q}|^2}\left[2E_2 + q^0E_1\right]. \tag{C.8}$$

$\mathrm{Im}(\Pi^{PA})$ and similarly for $\mathrm{Im}(\Pi^{AP})$:

$$\mathrm{Im}(\Pi^{0}) = -\frac{M^*q^0}{4\pi|\mathbf{q}|}E_1, \tag{C.9}$$

$$\mathrm{Im}(\Pi^{3}) = -\frac{M^*}{4\pi}E_1, \tag{C.10}$$

or in general

$$\mathrm{Im}(\Pi^{PA}) = q^\mu\left[-\frac{M^*}{4\pi|\mathbf{q}|}E_1\right]. \tag{C.11}$$

C.3.3 2nd order

$\mathrm{Im}(\Pi^{ST})$:

$$\mathrm{Im}(\Pi^{03}) = i\frac{q_\mu^2}{8\pi|\mathbf{q}|^2}\left[2E_2 + q^0E_1\right], \tag{C.12}$$

$$\mathrm{Im}(\Pi^{30}) = -\mathrm{Im}(\Pi^{03}). \tag{C.13}$$

$\mathrm{Im}(\Pi^{TS}) = -\mathrm{Im}(\Pi^{ST})$.

$\mathrm{Im}(\Pi^{PT})$ and similarly for $\mathrm{Im}(\Pi^{TP})$:

$$\mathrm{Im}(\Pi^{12}) = \frac{-q_\mu^2}{8\pi|\mathbf{q}|^2}\left[2E_2 + q^0 E_1\right], \tag{C.14}$$

$$\mathrm{Im}(\Pi^{21}) = -\mathrm{Im}(\Pi^{12}). \tag{C.15}$$

$\mathrm{Im}(\Pi^{VV})$:

$$\mathrm{Im}(\Pi^{00}) = -\frac{1}{2\pi|\mathbf{q}|}\left[E_3 + q^0 E_2 + \frac{q_\mu^2}{4}E_1\right], \tag{C.16}$$

$$\mathrm{Im}(\Pi^{03}) = \frac{q^0}{|\mathbf{q}|}\mathrm{Im}(\Pi^{00}), \tag{C.17}$$

$$\mathrm{Im}(\Pi^{30}) = \mathrm{Im}(\Pi^{03}), \tag{C.18}$$

$$\mathrm{Im}(\Pi^{33}) = \left[\frac{q^0}{|\mathbf{q}|}\right]^2 \mathrm{Im}(\Pi^{00}), \tag{C.19}$$

$$\mathrm{Im}(\Pi^{11}) = \frac{q_\mu^2}{4\pi|\mathbf{q}|^3}\left[E_3 + q^0 E_2 + \left(\frac{|\mathbf{q}|^2 M^{*2}}{q_\mu^2} + \frac{q_0^2 + |\mathbf{q}|^2}{4}\right)E_1\right], \tag{C.20}$$

$$\mathrm{Im}(\Pi^{22}) = \mathrm{Im}(\Pi^{11}). \tag{C.21}$$

$\mathrm{Im}(\Pi^{VA})$ and similarly for $\mathrm{Im}(\Pi^{AV})$:

$$\mathrm{Im}(\Pi^{12}) = i\frac{-q_\mu^2}{8\pi|\mathbf{q}|^2}\left[2E_2 + q^0 E_1\right], \tag{C.22}$$

$$\mathrm{Im}(\Pi^{21}) = -\mathrm{Im}(\Pi^{12}). \tag{C.23}$$

$\mathrm{Im}(\Pi^{AA})$:

$$\mathrm{Im}(\Pi^{00}) = -\frac{1}{2\pi|\mathbf{q}|}\left[E_3 + q^0 E_2 + \left(\frac{q_\mu^2}{4} - M^{*2}\right)E_1\right], \tag{C.24}$$

$$\mathrm{Im}(\Pi^{03}) = -\frac{q^0}{2\pi|\mathbf{q}|^2}\left[E_3 + q^0 E_2 + \frac{q_\mu^2}{4}E_1\right], \tag{C.25}$$

$$\mathrm{Im}(\Pi^{30}) = \mathrm{Im}(\Pi^{03}), \tag{C.26}$$

$$\mathrm{Im}(\Pi^{33}) = -\frac{1}{2\pi|\mathbf{q}|}\left[\left(\frac{q^0}{|\mathbf{q}|}\right)^2 E_3 + \left(\frac{q^0}{|\mathbf{q}|}\right)^2 q^0 E_2 + \left(\frac{q^0}{|\mathbf{q}|}\right)^2 \frac{q_\mu^2}{4}E_1 + M^{*2}E_1\right], \tag{C.27}$$

$$\mathrm{Im}(\Pi^{11}) = \frac{q_\mu^2}{4\pi|\mathbf{q}|^3}\left[E_3 + q^0 E_2 + \left(\frac{-|\mathbf{q}|^2 M^{*2}}{q_\mu^2} + \frac{q_0^2 + |\mathbf{q}|^2}{4}\right)E_1\right], \tag{C.28}$$

$$\mathrm{Im}(\Pi^{22}) = \mathrm{Im}(\Pi^{11}), \tag{C.29}$$

or in general

$$\mathrm{Im}(\Pi^{AA}) = \mathrm{Im}(\Pi^{VV}) + g^{\mu\nu}\left[\frac{M^{*2}E_1}{2\pi|\mathbf{q}|}\right]. \tag{C.30}$$

C.3.4 3rd order

$\mathrm{Im}(\Pi^{VT})$:
Two types of terms occur. Listed below are the expression and the corresponding entries in the tensor. If we define

$$A = -i\frac{M^*}{4\pi}E_1, \tag{C.31}$$

$$B = \frac{q^0}{|\mathbf{q}|}A, \tag{C.32}$$

then

$$A = \mathrm{Im}(\Pi^{003}),\ -\mathrm{Im}(\Pi^{030}),\ -\mathrm{Im}(\Pi^{113}),\ \mathrm{Im}(\Pi^{131}),\ -\mathrm{Im}(\Pi^{223}),\ \mathrm{Im}(\Pi^{232}), \tag{C.33}$$

$$B = \mathrm{Im}(\Pi^{101}),\ -\mathrm{Im}(\Pi^{110}),\ \mathrm{Im}(\Pi^{202}),\ -\mathrm{Im}(\Pi^{220}),\ \mathrm{Im}(\Pi^{303}),\ -\mathrm{Im}(\Pi^{330}). \tag{C.34}$$

$\mathrm{Im}(\Pi^{TV})$:

$$A = -\mathrm{Im}(\Pi^{030}),\ \mathrm{Im}(\Pi^{131}),\ \mathrm{Im}(\Pi^{232}),\ \mathrm{Im}(\Pi^{300}),\ -\mathrm{Im}(\Pi^{311}),\ -\mathrm{Im}(\Pi^{322}), \tag{C.35}$$

$$B = -\mathrm{Im}(\Pi^{011}),\ -\mathrm{Im}(\Pi^{022}),\ -\mathrm{Im}(\Pi^{033}),\ \mathrm{Im}(\Pi^{101}),\ \mathrm{Im}(\Pi^{202}),\ \mathrm{Im}(\Pi^{303}). \tag{C.36}$$

$\mathrm{Im}(\Pi^{AT})$ and similarly for $\mathrm{Im}(\Pi^{TA})$:
Two types of terms occur. Listed below are the expression and the corresponding entries in the tensor.

$$\frac{M^*q^0}{4\pi|\mathbf{q}|^2}\left[2E_2 + q^0E_1\right] = \mathrm{Im}(\Pi^{012}),\ -\mathrm{Im}(\Pi^{021}),\ -\mathrm{Im}(\Pi^{102}),\ \mathrm{Im}(\Pi^{120}),\ \mathrm{Im}(\Pi^{201}),$$
$$-\mathrm{Im}(\Pi^{210}), \tag{C.37}$$

$$\frac{|\mathbf{q}|}{q^0}\mathrm{Im}(\Pi^{012}) = \mathrm{Im}(\Pi^{123}),\ -\mathrm{Im}(\Pi^{132}),\ -\mathrm{Im}(\Pi^{213}),\ \mathrm{Im}(\Pi^{231}),\ \mathrm{Im}(\Pi^{312}),$$
$$-\mathrm{Im}(\Pi^{321}). \tag{C.38}$$

C.3.5 4th order

$\mathrm{Im}(\Pi^{TT})$:
Five types of terms occur. Listed below are the expressions and the corresponding entries in the tensor.

- $\frac{-1}{4\pi|\mathbf{q}|^3}\left\{\left[q_0^2+|\mathbf{q}|^2\right]\left[E_3+q^0E_2+\frac{q_\mu^2}{4}E_1\right]-|\mathbf{q}|^2M^{*2}E_1\right\}$
  $\mathrm{Im}(\Pi^{0101}),-\mathrm{Im}(\Pi^{0110}),\mathrm{Im}(\Pi^{0202}),-\mathrm{Im}(\Pi^{0220}),-\mathrm{Im}(\Pi^{1001}),\mathrm{Im}(\Pi^{1010}),-\mathrm{Im}(\Pi^{2002}),\mathrm{Im}(\Pi^{2020})$
- $\frac{q^0}{2\pi|\mathbf{q}|^2}\left[E_3+q^0E_2+\frac{q_\mu^2}{4}E_1\right]$
  $\mathrm{Im}(\Pi^{0113}),-\mathrm{Im}(\Pi^{0131}),\mathrm{Im}(\Pi^{0223}),-\mathrm{Im}(\Pi^{0232}),-\mathrm{Im}(\Pi^{1013}),\mathrm{Im}(\Pi^{1031}),\mathrm{Im}(\Pi^{1301}),-\mathrm{Im}(\Pi^{1310})$
  $-\mathrm{Im}(\Pi^{2023}),\mathrm{Im}(\Pi^{2032}),\mathrm{Im}(\Pi^{2302}),-\mathrm{Im}(\Pi^{2320}),-\mathrm{Im}(\Pi^{3101}),\mathrm{Im}(\Pi^{3110}),-\mathrm{Im}(\Pi^{3202}),\mathrm{Im}(\Pi^{3220})$
- $\frac{q_\mu^2}{2\pi|\mathbf{q}|^3}\left[E_3+q_0E_2+\left(\frac{q_0^2}{4}+\frac{M^{*2}|\mathbf{q}|^2}{q_\mu^2}\right)E_1\right]$
  $\mathrm{Im}(\Pi^{0303}),\ -\mathrm{Im}(\Pi^{0330}),\ -\mathrm{Im}(\Pi^{3003}),\ \mathrm{Im}(\Pi^{3030})$
- $\frac{q_\mu^2}{2\pi|\mathbf{q}|^3}\left\{E_3+q_0E_2+\frac{q_0^2}{4}E_1+\frac{q_0^3}{24}\right\}$
  $\mathrm{Im}(\Pi^{1212}),\ -\mathrm{Im}(\Pi^{1221}),\ -\mathrm{Im}(\Pi^{2112}),\ \mathrm{Im}(\Pi^{2121})$
- $\frac{-1}{4\pi|\mathbf{q}|^3}\left\{\left[q_0^2+|\mathbf{q}|^2\right]\left[E_3+q^0E_2+\frac{q_\mu^2}{4}E_1\right]+|\mathbf{q}|^2M^{*2}E_1\right\}$
  $\mathrm{Im}(\Pi^{1313}),-\mathrm{Im}(\Pi^{1331}),\mathrm{Im}(\Pi^{2323}),-\mathrm{Im}(\Pi^{2332}),-\mathrm{Im}(\Pi^{3113}),\mathrm{Im}(\Pi^{3131}),-\mathrm{Im}(\Pi^{3223}),\mathrm{Im}(\Pi^{3232})$

C.4 Real parts of the polarizations

The necessary real parts of the density-dependent polarizations are calculated according to Eq. (2.133) using the traces shown in Section C.1. The angular integrals are performed analytically and we list the results below. We choose $q^\mu=(q^0,0,0,|\mathbf{q}|)$ and define

$$L_1(k,q)=\log\left|2E_k^*q^0-2|\mathbf{k}||\mathbf{q}|-q_\mu^2\right|, \tag{C.39}$$

$$L_2(k,q)=\log\left|2E_k^*q^0+2|\mathbf{k}||\mathbf{q}|-q_\mu^2\right|, \tag{C.40}$$

$$L_3(k,q)=\log\left|2E_k^*q^0-2|\mathbf{k}||\mathbf{q}|+q_\mu^2\right|, \tag{C.41}$$

$$L_4(k,q)=\log\left|2E_k^*q^0+2|\mathbf{k}||\mathbf{q}|+q_\mu^2\right|, \tag{C.42}$$

$$L_{12}=L_1-L_2, \tag{C.43}$$

$$L_{34}=L_3-L_4, \tag{C.44}$$

$$L_{12-34}=L_{12}-L_{34} \tag{C.45}$$

$$L_{12+34}=L_{12}+L_{34} \tag{C.46}$$

and

$$E_L=\left(2E_k^*-q^0\right)L_{12}-\left(2E_k^*+q^0\right)L_{34}. \tag{C.47}$$

C.4.1 0th order

$$I_\theta^{SS}=\frac{\left(4M^{*2}-q_\mu^2\right)\left(L_{12-34}\right)+8|\mathbf{k}||\mathbf{q}|}{|\mathbf{k}||\mathbf{q}|}. \tag{C.48}$$

C.4.2 1st order

I_θ^{SV} and similarly for I_θ^{VS}:

$$I_\theta^0 = \frac{2M^*}{|\mathbf{k}||\mathbf{q}|} E_L, \tag{C.49}$$

$$I_\theta^3 = \frac{q^0}{|\mathbf{q}|} I_\theta^0. \tag{C.50}$$

I_θ^{PA} and similarly for I_θ^{AP}:

$$I_\theta^0 = \frac{2M^* q^0}{|\mathbf{k}||\mathbf{q}|} L_{12-34}, \tag{C.51}$$

$$I_\theta^3 = \frac{|\mathbf{q}|}{q^0} I_\theta^0. \tag{C.52}$$

C.4.3 2nd order

I_θ^{ST}:

$$I_\theta^{03} = -i \frac{q_\mu^2}{|\mathbf{k}||\mathbf{q}|^2} E_L, \tag{C.53}$$

$$I_\theta^{30} = -I_\theta^{03}. \tag{C.54}$$

$I_\theta^{TS} = -I_\theta^{ST}$.

I_θ^{PT} and similarly for I_θ^{TP}:

$$I_\theta^{12} = \frac{q_\mu^2}{|\mathbf{k}||\mathbf{q}|^2} E_L, \tag{C.55}$$

$$I_\theta^{21} = -I_\theta^{12}. \tag{C.56}$$

I_θ^{VV}:

$$I_\theta^{00} = \frac{1}{|\mathbf{k}||\mathbf{q}|}\left[\left(4E_k^{*2}+q_\mu^2\right)L_{12-34} - 4E_k q^0 L_{12+34} - 8|\mathbf{k}||\mathbf{q}|\right], \tag{C.57}$$

$$I_\theta^{03} = \frac{q^0}{|\mathbf{q}|}I_\theta^{00}, \tag{C.58}$$

$$I_\theta^{30} = I_\theta^{03}, \tag{C.59}$$

$$I_\theta^{33} = \left[\frac{q^0}{|\mathbf{q}|}\right]^2 I_\theta^{00}, \tag{C.60}$$

$$I_\theta^{11} = \frac{1}{2|\mathbf{k}||\mathbf{q}|^3}\left[\left(4|\mathbf{k}|^2|\mathbf{q}|^2 - 4E_k^{*2}q_0^2 - q_\mu^2\left(q_0^2+q^2\right)\right)L_{12-34}\right.$$
$$\left.+4E_k^* q^0 q_\mu^2 L_{12+34} + 8|\mathbf{k}||\mathbf{q}|\left(q_0^2+q^2\right)\right], \tag{C.61}$$

$$I_\theta^{22} = I_\theta^{11}. \tag{C.62}$$

I_θ^{VA} and similarly for I_θ^{AV}:

$$I_\theta^{12} = i\frac{q_\mu^2}{|\mathbf{k}||\mathbf{q}|^2}E_L, \tag{C.63}$$

$$I_\theta^{21} = -I_\theta^{12}. \tag{C.64}$$

C.4.4 3rd order

$\mathrm{Im}(\Pi^{VT})$:
Two types of terms occur. Listed below are the expression and the corresponding entries in the tensor. If we define

$$A = i\frac{2M^*}{|\mathbf{k}|}L_{12-34}, \tag{C.65}$$

$$B = \frac{q^0}{|\mathbf{q}|}A, \tag{C.66}$$

then

$$A = I_\theta^{003},\ -I_\theta^{030},\ -I_\theta^{113},\ I_\theta^{131},\ -I_\theta^{223},\ I_\theta^{232}, \tag{C.67}$$

$$B = I_\theta^{101},\ -I_\theta^{110},\ I_\theta^{202},\ -I_\theta^{220},\ I_\theta^{303},\ -I_\theta^{330}. \tag{C.68}$$

$\mathrm{Im}(\Pi^{TV})$:

$$A = -I_\theta^{030},\ I_\theta^{131},\ I_\theta^{232},\ I_\theta^{300},\ -I_\theta^{311},\ -I_\theta^{322}, \tag{C.69}$$

$$B = -I_\theta^{011},\ -I_\theta^{022},\ -I_\theta^{033},\ I_\theta^{101},\ I_\theta^{202},\ I_\theta^{303}, \tag{C.70}$$

$\mathrm{Im}(\Pi^{AT})$ and similarly for $\mathrm{Im}(\Pi^{TA})$:
Two types of terms occur. Listed below are the expression and the corresponding entries in the tensor.

$$-\frac{2M^* q^0}{|\mathbf{k}||\mathbf{q}|^2} E_L = I_\theta^{012},\ -I_\theta^{021},\ -I_\theta^{102},\ I_\theta{}^{120},\ I_\theta^{201},\ -I_\theta^{210}, \tag{C.71}$$

$$\frac{|\mathbf{q}|}{q^0} I_\theta^{012} = I_\theta^{123},\ -I_\theta^{132},\ -I_\theta^{213},\ I_\theta^{231},\ I_\theta^{312}, -I_\theta^{321}. \tag{C.72}$$

Bibliography

[1] C. J. Horowitz and D. P. Murdock, Phys. Rev. C **37**, 2032 (1988).

[2] C. J. Horowitz and J. Piekarewicz, Phys. Rev. C **50**, 2540 (1994).

[3] G. C. Hillhouse, *Relativistic description of polarization transfer observables for quasielastic proton scattering*, PhD thesis, Stellenbosch University, 1999.

[4] C. J. Horowitz and M. J. Iqbal, Phys. Rev. C **33**, 2059 (1986).

[5] K. Wehrberger and F. Beck, Phys. Lett. B **270**, 1 (1991).

[6] R. D. Smith and S. J. Wallace, Phys. Rev. C **32**, 1654 (1985).

[7] T. A. Carey et al., Phys. Rev. Lett. **53**, 144 (1984).

[8] T. Chen et al., Physics Letters B **103**, 192 (1981).

[9] J. S. Wesick et al., Phys. Rev. C **32**, 1474 (1985).

[10] J. A. McNeil, L. Ray, and S. J. Wallace, Phys. Rev. C **27**, 2123 (1983).

[11] J. A. McNeil, J. R. Shepard, and S. J. Wallace, Phys. Rev. Lett. **50**, 1439 (1983).

[12] J. A. Tjon and S. J. Wallace, Phys. Rev. C **32**, 1667 (1985).

[13] J. A. Tjon and S. J. Wallace, Phys. Rev. C **32**, 267 (1985).

[14] J. A. Tjon and S. J. Wallace, Phys. Rev. Lett. **54**, 1357 (1985).

[15] J. A. Tjon and S. J. Wallace, Phys. Rev. C **35**, 280 (1987).

[16] J. A. Tjon and S. J. Wallace, Phys. Rev. C **36**, 1085 (1987).

[17] C. J. Horowitz, Phys. Rev. C **31**, 1340 (1985).

[18] L. Ray and G. W. Hoffmann, Phys. Rev. C **31**, 538 (1985).

[19] O. Häusser et al., Phys. Rev. C **43**, 230 (1991).

[20] J. C. Caillon and J. Labarsouque, Nucl. Phys. A **595**, 189 (1995).

[21] B. C. Clark, R. L. Mercer, D. G. Ravenhall, and A. M. Saperstein, Phys. Rev. C **7**, 466 (1973).

[22] L. G. Arnold, B. C. Clark, R. L. Mercer, D. G. Ravenhall, and A. M. Saperstein, Phys. Rev. C **14**, 1878 (1976).

[23] L. G. Arnold, B. C. Clark, and R. L. Mercer, Phys. Rev. C **19**, 917 (1979).

[24] L. G. Arnold, B. C. Clark, R. L. Mercer, and P. Schwandt, Phys. Rev. C **23**, 1949 (1981).

[25] B. C. Clark, S. Hamma, and R. L. Mercer, *The interaction between medium energy nucleons in nuclei*, page 260, American Institute of Physics, New York, 1983.

[26] Z. P. Li, G. C. Hillhouse, and J. Meng, Phys. Rev. C **78**, 014603 (2008).

[27] M. V. Hynes, A. Picklesimer, P. C. Tandy, and R. M. Thaler, Phys. Rev. Lett. **52**, 978 (1984).

[28] L. Ray et al., Phys. Rev. Lett. **56**, 2465 (1986).

[29] D. P. Murdock and C. J. Horowitz, Phys. Rev. C **35**, 1442 (1987).

[30] J. Piekarewicz and J. R. Shepard, Phys. Rev. C **51**, 806 (1995).

[31] B. D. Serot and J. D. Walecka, Adv. Nucl. Phys. **16**, 1 (1986).

[32] C. J. Horowitz and J. Piekarewicz, Phys. Lett. B **301**, 321 (1993).

[33] G. C. Hillhouse and P. R. De Kock, Phys. Rev. C **49**, 391 (1994).

[34] E. D. Cooper, S. Hama, B. C. Clark, and R. L. Mercer, Phys. Rev. C **47**, 297 (1993).

[35] O. Häusser et al., Phys. Rev. Lett. **61**, 822 (1988).

[36] M. Ichimura, K. Kawahigashi, T. S. Jørgensen, and C. Gaarde, Phys. Rev. C **39**, 1446 (1989).

[37] C. J. Horowitz and B. D. Serot, Nucl. Phys. A **368**, 503 (1981).

[38] J. F. Dawson and R. J. Furnstahl, Phys. Rev. C **42**, 2009 (1990).

[39] K. Wehrberger, Phys. Rep. **225**, 273 (1993).

[40] B. D. Serot and J. D. Walecka, Int. J. Mod. Phys. **6**, 515 (1997).

[41] C. J. Horowitz and J. Piekarewicz, Nucl. Phys. A **511**, 461 (1990).

[42] C. J. Horowitz and J. Piekarewicz, Phys. Rev. Lett. **62**, 391 (1989).

[43] H. Kim, *Neutrino-nucleus scattering and relativistic nuclear structure effects*, PhD thesis, Indiana University, 1995.

[44] J. Piekarewicz, Phys. Rev. C **64**, 024307 (2001).

[45] R. J. Furnstahl, Lect. Notes Phys. **641**, 1 (2004).

[46] C. J. Horowitz and J. Piekarewicz, Phys. Rev. C **47**, 2924 (1993).

[47] C. J. Horowitz and K. Wehrberger, Nucl. Phys. A **531**, 665 (1991).

[48] H. Kurasawa and T. Suzuki, Nucl. Phys. A **445**, 685 (1985).

[49] A. L. Fetter and J. D. Walecka, *Quantum Theory of many-particle system*, McGraw-Hill Book Company, New York, 1971.

[50] J. Piekarewicz, Phys. Rev. C **62**, 051304 (2000).

[51] H. Kurasawa and T. Suzuki, Phys. Lett. B **173**, 377 (1986).

[52] K. Wehrberger and F. Beck, Phys. Rev. C **35**, 298 (1987).

[53] K. Wehrberger and F. Beck, Phys. Rev. C **37**, 1148 (1988).

[54] G. C. Hillhouse and P. R. De Kock, Phys. Rev. C **52**, 2796 (1995).

[55] G. C. Hillhouse, B. I. S. van der Ventel, S. M. Wyngaardt, and P. R. De Kock, Phys. Rev. C **57**, 448 (1998).

[56] B. I. S. Van der Ventel, G. C. Hillhouse, and P. R. De Kock, in *Proceedings of RCNP International Symposium on Nuclear Responses and Medium Effects*, edited by T. Noro, H. Sakaguchi, H. Sakai, and T. Wakasa, page 183, Osaka, Japan, November 1998, Universal Academy Press Inc.

[57] B. I. S. Van der Ventel, G. C. Hillhouse, P. R. De Kock, and S. J. Wallace, Phys. Rev. C **60**, 064618 (1999).

[58] B. I. S. Van der Ventel, G. C. Hillhouse, and P. R. De Kock, Phys. Rev. C **62**, 024609 (2000).

[59] H. Otsu, *Study of Reaction Mechanisms for (p,n) and (p,p') quasi elastic scatterings*, PhD thesis, University of Tokyo, 1997.

[60] J. D. Bjorken and S. Drell, *Relativistic Quantum Mechanics*, McGraw-Hill, New York, 1964.

[61] W. Greiner and A. Schafer, *Quantum Chromodynamics*, Springer-Verlag, Berlin, 1995.

[62] J. R. Shepard, E. Rost, and J. Piekarewicz, Phys. Rev. C **30**, 1604 (1984).

[63] E. Rost and J. R. Shepard, Phys. Rev. C **35**, 681 (1987).

[64] Y. Ikebata, Phys. Rev. C **52**, 890 (1995).

[65] B. I. S. Van der Ventel, *General Lorentz invariant representations of the NN interaction applied to quasielastic scattering of polarized protons*, PhD thesis, Stellenbosch University, 1999.

[66] D. L. Adams and M. Bleszynski, Phys. Lett. B **136**, 10 (1984).

[67] J. J. Sakurai, *Modern Quantum Mechanics*, Addison-Wesley Publishing Company Inc., Reading, Massachusetts, 1985.

[68] E. Rost, J. R. Shepard, E. R. Siciliano, and J. A. McNeil, Phys. Rev. C **29**, 209 (1984).

[69] H. C. Jean, J. Piekarewicz, and A. G. Williams, Phys. Rev. C **49**, 1981 (1994).

[70] C. J. Horowitz, Nucl. Phys. A **412**, 228 (1984).

[71] K. Lim and C. J. Horowitz, Nucl. Phys. A **501**, 729 (1989).

[72] R. J. Furnstahl and C. J. Horowitz, Nucl. Phys. A **485**, 632 (1988).

[73] P. G. Blunden and P. McCorquodale, Phys. Rev. C **38**, 1861 (1988).

[74] F. Gross, *Relativistic Quantum Mechanics*, John Wiley & Sons Inc., New York, 1993.

[75] W. Press, S. A. Teukolsky, W. Vetterling, and B. P. Flannery, *Numerical Recipes in Fortran*, Cambridge University Press, New York, 2nd edition, 1992.

[76] D. Sebilleau, Journal of Physics A: Mathematical and General **31**, 7157 (1998).

[77] J. Rasch and A. C. H. Yu, SIAM Journal on Scientific Computing **25**, 1416 (2003).

[78] D. Pinchon and P. E. Hoggan, International Journal of Quantum Chemistry **107**, 2186 (2007).

[79] D. Levin, Mathematics of Computation **38**, 531 (1982).

[80] D. Levin, Journal of Computational and Applied Mathematics **67**, 95 (1996).

[81] G. A. Evans and J. R. Webster, J. Comput. Appl. Math. **112**, 55 (1999).

[82] J. Li, X. Wang, T. Wang, and C. Shen, Applied Mathematics and Computation **209**, 327 (2009).

[83] G. R. Satchler, *Direct Nuclear Reactions*, Oxord University Press, New York, 1983.

[84] X. Ji, Phys. Lett. B **208**, 19 (1988).

[85] S. A. Chin, Ann. Phys. **108**, 301 (1977).

[86] J. D. Bjorken and S. Drell, *Relativistic Quantum Fields*, McGraw-Hill, New York, 1965.

[87] R. D. Mattuck, *A guide to Feynman Diagrams in the many-body problem*, McGraw-Hill Publishing Company Ltd, London, 1992.

[88] J. R. Shepard, E. Rost, and J. A. McNeil, Phys. Rev. C **40**, 2320 (1989).

[89] S. A. Chin, Phys. Lett. B **62**, 263 (1976).